CHALMERS

Brake Control for Lateral Vehicle Dynamics

Master's thesis in Automotive Engineering

ANDERS LARSSON
KARA GHASEMIANI

Department of Applied Mechanics
Division of Vehicle Engineering and Autonomous Systems
Group of Vehicle Dynamics
CHALMERS UNIVERSITY OF TECHNOLOGY
Göteborg, Sweden 2015
Master's thesis 2015:18

MASTER'S THESIS IN AUTOMOTIVE ENGINEERING

Brake Control for Lateral Vehicle Dynamics

ANDERS LARSSON
KARA GHASEMIANI

Department of Applied Mechanics
Division of Vehicle Engineering and Autonomous Systems
Group of Vehicle Dynamics
CHALMERS UNIVERSITY OF TECHNOLOGY

Göteborg, Sweden 2015

Brake Control for Lateral Vehicle Dynamics
ANDERS LARSSON
KARA GHASEMIANI

Master's thesis 2015:18
ISSN 1652-8557
Department of Applied Mechanics
Division of Vehicle Engineering and Autonomous Systems
Group of Vehicle Dynamics
Chalmers University of Technology
SE-412 96 Göteborg
Sweden
Telephone: +46 (0)31-772 1000

Cover:
Photograph taken by Kara Ghasemiani showing the front left wheel of the test vehicle

Chalmers Reproservice
Göteborg, Sweden 2015

Brake Control for Lateral Vehicle Dynamics
Master's thesis in Automotive Engineering
ANDERS LARSSON
KARA GHASEMIANI
Department of Applied Mechanics
Division of Vehicle Engineering and Autonomous Systems
Group of Vehicle Dynamics
Chalmers University of Technology

Abstract

This thesis describes the evaluation of the potential in utilizing the brakes on a vehicle to perform a small-overlap avoidance maneuver as a potential future active safety system and is done through both experimental and simulated testing. A strong reason for using brakes instead of steering is the availability of a powerful actuator that can be controlled by-wire while being less intrusive than a mechanically connected steering-actuated system. A 2008 SAAB 9-3 test vehicle is equipped with a separate electronic hydraulic brake system, enabling differential braking that can be implemented in a way to generate a yawing motion of the vehicle similar to turning the steering wheel.

Simulink was used to develop a controller to autonomously perform the avoidance maneuver, requiring only an input describing the desired lateral displacement. In order to verify the functionality of the controller without experimental testing the vehicle dynamic simulation software, CarSim, was used. The developed avoidance maneuver controller was identical in both simulation and in the test vehicle to ensure proper correlation between the two.

In order to evaluate and quantify the differential braking potential, the experimental tests were conducted in different conditions and levels of intervention. Parameters such as velocity, vehicle load, road friction, and lateral displacement were varied to achieve a good performance estimation. To minimize driver intrusiveness during a differential braking avoidance maneuver tests were also conducted with spacers installed between the front wheels and hubs to remove the lateral component of the scrub radius and thereby decrease the torque steer effect during braking. However the results proved that self-aligning moment is more dominant than torque steer and the installed spacers had a negligible effect on both driver intrusiveness and avoidance maneuver performance. To evaluate the potential of differential braking, the maneuvers were compared to corresponding simulated and experimental front wheel steered maneuvers to generate a reliable and quantifiable assessment of the differential braking potential. The experimental steered maneuvers were performed with a steering robot to ensure high accuracy and consistency.

The results show that there is indeed potential in utilizing differential braking to perform an avoidance maneuver. At higher velocities, differential braking has the potential to perform avoidance maneuvers both at a shorter distance as well as duration compared to steering, especially for smaller lateral displacements. Differential braking decelerates the vehicle, shortening the traveled distance while at the same time increasing the duration to perform the maneuver. At lower velocities, a steered maneuver is performed at both a shorter distance as well as duration, compared to differential braking since the vehicle is not as sensitive to steering inputs and larger steering amplitudes can be applied, resulting in more effective lateral movement.

Keywords: Differential braking, Torque vectoring, EHB, Brake system, Vehicle dynamics, Small-overlap, Collision avoidance, Active safety, System safety, Steering robot, Vehicle simulation, CarSim, dSpace

Preface

This thesis work has been conducted as a partial requirement for the Master of Science degree in Automotive Engineering at Chalmers University of Technology, Gothenburg, Sweden in cooperation with LeanNova Engineering AB, Trollhättan and National Electric Vehicle Sweden AB, Trollhättan. The project was conducted between November 2014 and April 2015 at LeanNova Engineering. Functional testing and verification was conducted on the NEVS test track in Trollhättan, experimental differential braking tests were conducted on the Råda airfield outside of Lidköping and steering robot tests were conducted at, and in cooperation with, Astazero outside of Borås.

Acknowledgements

We would like to acknowledge the resourceful guidance of Gunnar Olsson whose rock-solid experience and passion for vehicle dynamics has been highly contagious. We thank Mathias Lidberg for his inspirational and well-founded expertise, steering us in a steady direction throughout the project. The guidance of Johan Hägnander has been resolute and reliable and we thank Oskar Eklund and Erik Harteilus for their highly valued opinions and inputs as well as their company on endless commutes.

From day one, the great people of LeanNova have made us feel like a part of the family and we give a special thanks to Rami Karjalainen for his dependable mechanical assistance and Lennart Eijerstam for his greatly useful knowledge of CAN-signaling. Among many more who have aided in the progress of this thesis we thank Henrik Petersson at Astazero for his indispensible support of our steering robot tests, Krister Lindblom for organizing the much appreciated assistance from the NEVS mechanics, Anders Torge for organizing our test runs on the NEVS track, and finally a deep bow to Olle and Kent for their loyal patience, waiting in their towing truck and car for hours at end while we drove up and down the Råda air strip.

Nomenclature

Symbols

a	= Acceleration $[\frac{\mathrm{m}}{\mathrm{s}^2}]$
A	= Brake piston area $[\mathrm{m}^2]$
B	= Magic Tire Formula stiffness factor
BD	= Ideal braking distance [m]
C	= Magic Tire Formula shape factor
C_f	= Cornering stiffness, front $[\frac{\mathrm{F}}{\mathrm{rad}}]$
C_r	= Cornering stiffness, rear $[\frac{\mathrm{F}}{\mathrm{rad}}]$
d	= Look-ahead distance from rear axle to target point [m]
D	= Magic Tire Formula peak factor
e	= Error [m]
E	= Magic Tire Formula curvature factor
F	= Force [N]
F_b	= Differential braking force [N]
F_{xT}	= Wheel coordinate system longitudinal force [N]
F_{yT}	= Wheel coordinate system lateral force [N]
F_{zT}	= Wheel coordinate system vertical force [N]
F_z	= Normal force [N]
g_x	= Longitudinal target coordinate [m]
g_y	= Lateral target coordinate [m]
I	= Rotational inertia $[\mathrm{kgm}^2]$
K_d	= Derivative PID-coefficient
K_p	= Proportional PID-coefficient
l	= Distance from CoG to wheel axle [m]
n_{bp}	= Number of brake pads
n_k	= Caster trail [m]
p	= Brake pressure [Pa]
r	= Scrub radius (steering axis offset at ground) [m]
r_{disc}	= Brake disc radius [m]
r_k	= Lateral component of scrub radius [m]
r_{wheel}	= Wheel radius [m]
R	= Curve radius [m]
t	= Time [s]
v	= CoG velocity $[\frac{\mathrm{m}}{\mathrm{s}}]$
V_T	= Wheel center velocity $[\frac{\mathrm{m}}{\mathrm{s}}]$
w	= Track width [m]
x	= Longitudinal distance to obstacle [m]
X	= Vehicle coordinate system, longitudinal direction
y	= Lateral distance required to avoid obstacle [m]
Y	= Vehicle coordinate system, lateral direction
Z	= Vehicle coordinate system, vertical direction
α	= Tire lateral slip angle [rad]
δ	= Steer angle [rad]
κ	= Tire longitudinal slip ratio [%]
λ	= Brake distribution front/rear
μ	= Road friction coefficient
μ_{bp}	= Brake pad friction coefficient
φ	= Angle between vehicle direction and target coordinate [rad]
ψ	= Vehicle yaw angle [rad]
$\dot{\psi}$	= Vehicle yaw rate $[\frac{\mathrm{rad}}{\mathrm{s}}]$
$\ddot{\psi}$	= Vehicle yaw acceleration $[\frac{\mathrm{rad}}{\mathrm{s}^2}]$

Subscripts

f	= Front
FL	= Front left
FR	= Front right
r	= Rear
RL	= Rear left
RR	= Rear right
sw	= Steering wheel
w	= Wheel
x	= Longitudinal direction
y	= Lateral direction
z	= Vertical direction
zz	= Around z-axis (yaw direction)

Abbreviations

ABS	= Anti-lock Brake System
CAN	= Controller Area Network
CoG	= Center of Gravity
DBS	= Differential Braking System
eAWD	= Electric All Wheel Drive
EHB	= Electric Hydraulic Braking
EPS	= Electric Power assisted Steering
ESC	= Electronic Stability Control
FMEA	= Failure Mode and Effects Analysis
GPS	= Global Positioning System
IMU	= Internal Measurement Unit
K&C	= Kinematics and Compliance
NEVS	= National Electric Vehicle Sweden
PID	= Proportional Integral Derivative

Contents

1 Introduction

1.1 Background

Safety systems in modern passenger vehicles play an increasingly larger role due to advancements made in vehicle sensors and computational power. These advancements have made it possible for safety systems to work more autonomously, incorporating vehicle motion sensors, cameras, and radars in combination with advanced algorithms. An active safety system available in most modern passenger cars today is Electronic Stability Control (ESC) which utilizes differential braking in combination with motion sensors to detect and reduce loss of stability by braking individual wheels [19], [4]. Other systems involving braking are Adaptive Cruise Control and Forward Collision Warning, that in the event of an imminent forward collision can autonomously apply the brakes [13], [17].

Existing research confirms that brake control for lateral vehicle dynamics is an area worth investigating with regards to evasive maneuvers. The potential safety benefit of torque vectoring has been evaluated on a theoretic basis where a combination of differential braking together with propulsion by the availability of electric motors is implemented. An approach like this can enhance the vehicle transient response, beneficial in an evasive maneuver [1].

A combination of active braking and steering has been evaluated as a collision avoidance driver assistance system. At low velocities, braking is sufficient to avoid or mitigate a collision. At higher velocities, the distance required to bring the vehicle to a halt is larger which is verified with a simulation tool to observe the required distance for collision avoidance when performing braking and steering maneuvers. Combined differential braking and steering has been implemented and tested to quantify the evasive maneuver benefit [3].

Small-overlap collisions are among the most fatal types of incidents and in-depth analyses of crashes indicate that such collisions account for a significant proportion of frontal collisions with seriously injured occupants [8]. In a frontal collision the front of a passenger car is designed to act as a crush-zone to absorb the impact energy. In the case of a small-overlap collision, a large amount of energy has to be absorbed by a small area which means that the crush-zone is less effective, see Figure 1.1. The collision energy will transfer directly into the front wheel, suspension system and firewall, forcing the wheel into the driver or passenger footwell, resulting in serious leg and foot injuries [15].

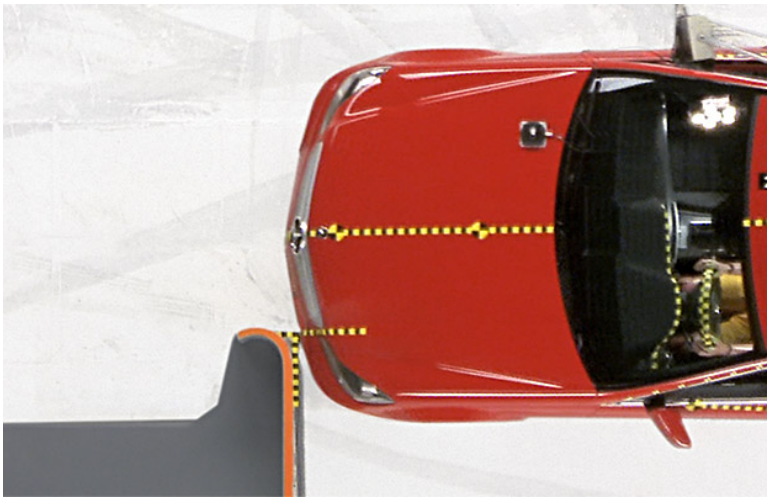

Figure 1.1: *Small-overlap collision test*

There are several safety systems available that utilize brakes while differential braking to perform an avoidance maneuver in the case of a small-overlap frontal collision is an area relatively unexplored. In the scenario where the vehicle velocity is too high to avoid the collision by braking, brakes could be applied to one side of the vehicle in order to create a yawing motion that could avoid the collision by swerving past the obstacle.

1.2 Problem Definition

To control the yaw dynamics and lateral displacement of a vehicle, the steering system is commonly used. There are however scenarios where alternative ways of controlling the lateral displacement of a vehicle could be more effective. Consider the scenario where there is an imminent frontal collision that the driver is either unaware of or too slow to avoid. If an autonomous safety system were in place that utilizes steering to avoid the obstacle, the motion of the steering wheel could be perceived as intrusive by the driver, the worst case scenario being broken thumbs or fingers. This is assuming a mechanical connection between the steering wheel and the front wheels, meaning no steer-by-wire system [10]. A strong reason for using brakes instead of steering is the availability of a powerful actuator that can be controlled by-wire while being less intrusive to the driver than a mechanically connected, steering-actuated system.

1.3 Objective

The objective of this project is to use a test vehicle as well as simulation to study the capacity and evaluate the potential in moving a vehicle sideways through differential braking at varying conditions and levels of intervention. The manner of moving a road vehicle sideways is almost exclusively done by turning the steering wheel. For this reason, the differential braking maneuvers will be compared to corresponding front wheel steered maneuvers since this comparison will produce the best quantifiable assessment of the differential braking potential. The avoidance maneuver is mainly to be evaluated as a small-overlap or obstacle avoidance maneuver, meaning a lateral displacement of up to one meter that should be accomplished in an efficient manner.

Any vehicle system with autonomous control of the brakes will put high demands on functional safety to ensure safe usage of the vehicle. Therefore it also lies within the project objective to determine, quantify and evaluate technical fault scenarios and their consequential safety hazards resulting from a differential braking maneuver.

1.4 Delimitations

- The project will not include combined differential braking and steering maneuvers.
- The project will only include so called torque vectoring based on differential braking. In other words, the avoidance maneuver will only use braking forces and no propulsion forces.
- The project does not include the active safety obstacle detection aspect and the avoidance maneuver will be triggered manually.

2 Theory

To ensure consistency when constructing various vehicle dynamic expressions and free-body diagrams it is important to use coordinate systems based on a widely used and recognized standard. In order to comprehend the concept of differential braking and its vehicle dynamic effects a well-founded theoretic starting-point is required and covered in this chapter.

2.1 Coordinate Systems & Definitions

Throughout this project the ISO 8855 [24] coordinate system has been used as described in Figure 2.1 and 2.2 below.

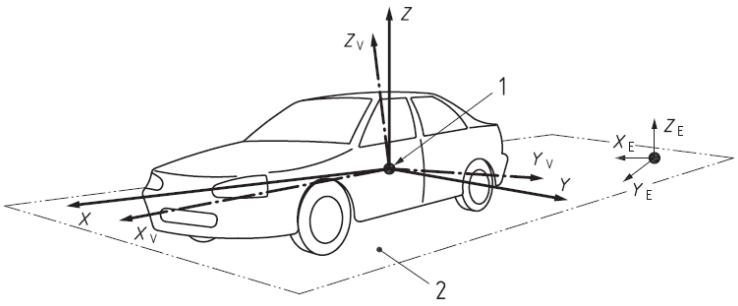

Figure 2.1: *ISO 8855 vehicle coordinate system*

Figure 2.1 illustrates the vehicle coordinate system where the X-direction is forward, the Y-direction to the left, and Z-direction upwards. Roll, pitch, and yaw are applied to the corresponding axes in the same order and are positive in a clockwise direction seen from the vehicle reference point. Point 1 indicates the vehicle reference point and point 2 the ground plane.

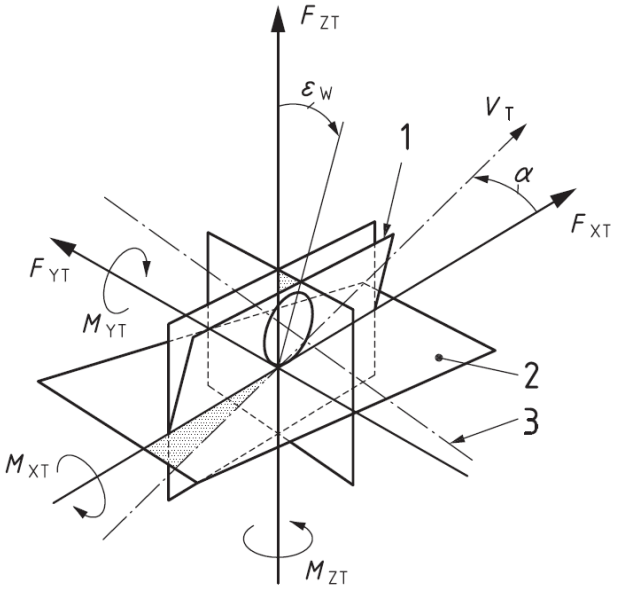

Figure 2.2: *ISO 8855 wheel coordinate system*

Figure 2.2 illustrates the wheel coordinate system. The tire lateral slip angle α describes the angle between a rolling wheel actual direction of travel, here shown as V_T, and the direction to which it is pointing, F_{xt}. Point 1 indicates the wheel plane, point 2 the road plane, and point 3 the wheel spin axis.

2.2 Vehicle Dynamic Theory

The motion of a vehicle is based on the forces generated in the tires by their contact to the ground through vehicle weight, steering, acceleration, and braking. The modern tire is constructed of natural rubber and a core carcass. The natural rubber compound, tire thread, composition and structure of the carcass are parameters that vary significantly between manufacturers and tire applications. This creates difficulties when trying to describe vehicle behavior through computation and simulation. For this reason, different tire models are available with varying complexity. The most well-known tire model is the so called Magic Tire Formula [20]. A simplified expression of the formula is found below that generates curves resembling those acquired from measured tire data for lateral and longitudinal forces .

$$F(\alpha) = D \sin\left(C \arctan\left(B\alpha - E(B\alpha - \arctan B\alpha)\right)\right) \tag{2.1}$$

This expression calculates the forces acting on the tire for a given lateral slip angle α (see Figure 2.2). D is the peak value, C is the shape factor, B is the stiffness factor, and E is the curvature factor. Lateral forces are generated whenever there is a lateral slip angle present and the graphical representation of the Magic Tire Formula with specific coefficients is found in Figure 2.3 which illustrates the normalized force versus slip angle α. The lateral tire force has been normalized by dividing it by the corresponding vertical force. The maximum lateral force that can be achieved is equal to the vertical force at that moment, assuming a friction coefficient of 1. The graph does not include tire load sensitivity which is however implemented in vehicle simulations where more advanced tire models are required (see Section 3.5).

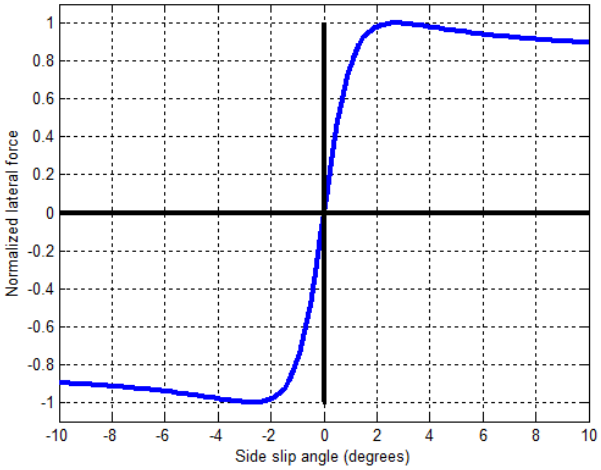

Figure 2.3: *Magic Tire Formula with coefficients* $B = 0.714$, $C = 1.4$, $D = 1.00$, $E = -0.2$

2.2.1 Torque Steer

When braking one wheel on a vehicle the lateral component of the scrub radius described as r_k in Figure 2.4 will cause a so called brake force steer, generating a turning moment of the wheel during braking. When braking one front wheel, the steering wheel might steer in the opposite direction, generating an opposite yaw moment that directly counteracts the differential braking avoidance maneuver. The test vehicle is designed with $r_k < 0$ to improve stability when braking on a split-μ surface. Figure 2.4 describes $r_k > 0$. To overcome the brake force steer effect, the driver could hold on to the steering wheel and not allow the wheels to steer which is still not ideal. Due to compliance in the system, the front wheels would still be subjected to a small steer angle. To reduce the impact of this phenomenon, spacers could be installed between the front wheels and hubs to effectively reduce r_k or even make it positive. This would however decrease the stability when braking on a split-μ surface.

2.2.2 Caster and Pneumatic Trail

Another counteracting phenomenon is caster and pneumatic trail, caster trail being described as n_k in Figure 2.4. While the caster trail is geometrically defined, the pneumatic trail is a varying parameter depending on the physical properties of the tire slip angle and vehicle velocity, either adding or subtracting from the caster trail. Caster trail in combination with pneumatic trail will create a lever arm which when subject to a lateral force will cause a self-aligning moment that will try to stabilize the wheels and align the vehicle towards its longitudinal velocity direction. This self-aligning moment could consequently counteract the desired yawing motion from a differential braking maneuver.

The scrub radius, r, in Figure 2.4 is the distance from the tire contact center at point 2 to the point where the steering axis intersects the road at point 4. Therefore, the tire contact center is not constant which will result in a varying scrub radius.

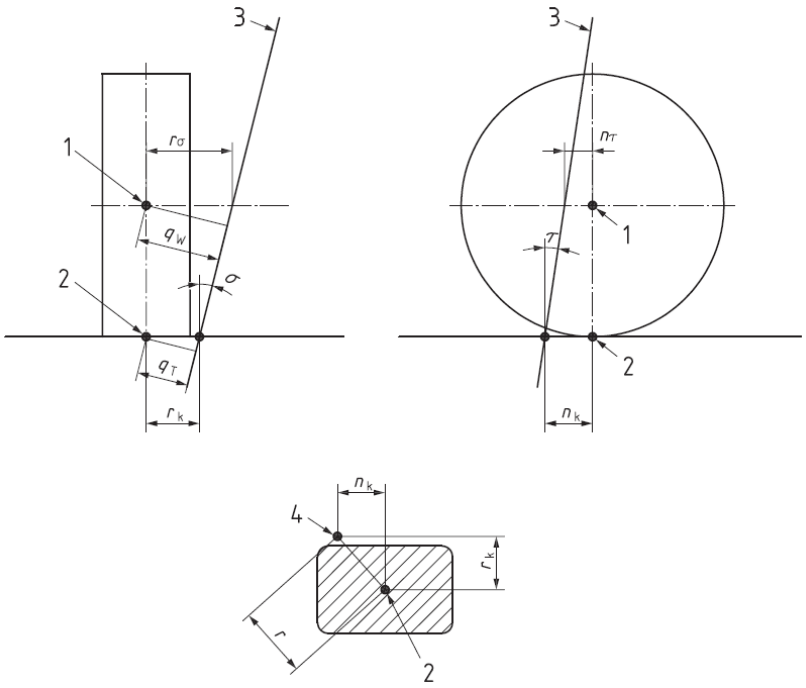

Figure 2.4: *Steering axis geometry [24]*

Figure 2.4 illustrates the steering axis geometry where point 1 indicates the wheel center, point 2 the contact center, point 3 the steering axis, and point 4 where the steering axis intersects the road plane. r is the scrub radius, r_k is the distance in the Y-direction between the XZ-wheel plane and the point where the steering axis intersects the road plane, and n_k is the caster trail, defined as the distance in X-direction from the YZ-wheel plane to the point where the steering axis intersects the road plane.

2.3 Vehicle Modeling

A differential braking force F_b is introduced to a one-track bicycle model in order to construct vehicle equations of motion applicable to the purpose of the project. The equations of motion are meant to describe the vehicle behavior in a real-time processor and for this reason the free-body diagram and corresponding expressions are kept relatively simple to reduce the demand for computational power. The tires are assumed to be within their linear range, the differential braking force F_b is assumed to be small enough not to affect the cornering stiffness' of the vehicle and load transfer is not included in the following expressions.

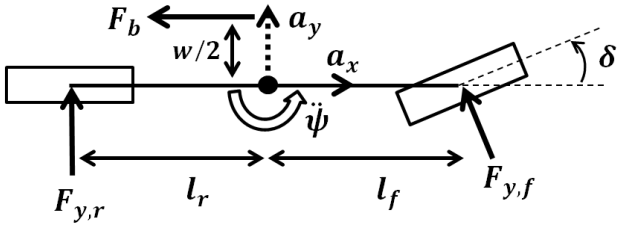

Figure 2.5: *Bicycle model including differential braking force F_b*

Assuming small angles, the free body moment expression becomes as follows:

$$I_{zz}\ddot{\psi} = F_{y,f}l_f - F_{y,r}l_r + F_b\frac{w}{2} \tag{2.2}$$

where w is the vehicle track width. It is also known that [16]:

$$F_{y,f} = C_f \cdot \left(\delta - \frac{v_y + l_f\dot{\psi}}{v_x}\right) \tag{2.3}$$

$$F_{y,r} = -C_r \cdot \left(\frac{v_y - l_r\dot{\psi}}{v_x}\right) \tag{2.4}$$

where C_f and C_r are the front and rear cornering stiffness', δ is the front wheel steer angle, v_x and v_y are longitudinal and lateral velocity, and $\dot{\psi}$ is the vehicle yaw rate. Combining these expressions results in the following expression:

$$\ddot{\psi} = \frac{l_rC_r - l_fC_f}{I_{zz}v_x}v_y - \frac{l_f^2C_f + l_r^2C_r}{I_{zz}v_x}\dot{\psi} + \frac{l_fC_f}{I_{zz}}\delta + \frac{w}{2I_{zz}}F_b \tag{2.5}$$

The pure pursuit method [5] and variations of it is a widely used approach to path tracking problems. It is found to be applicable to the task at hand where an arbitrary target goal is defined at a distance ahead of the vehicle as shown in Figure 2.6.

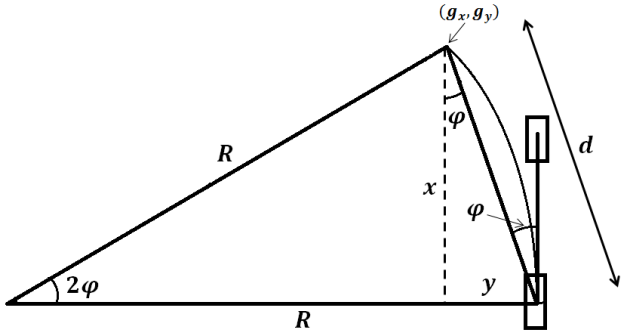

Figure 2.6: *Pure pursuit method*

The pure pursuit method consists of geometrically calculating the curvature of a circular arc that connects the rear axle location to a goal point on a path ahead of the vehicle. The goal point is determined from a look-ahead distance d from the current rear axle position to the desired point. The pure pursuit method in itself assumes steady state conditions and is a strictly geometric algorithm that takes neither vehicle dynamic behavior or slip angles into consideration. In this implementation, the geometric relationships described by the pure pursuit method are used to express the vehicle yaw rate $\dot{\psi}$ in terms of distances x and y as described on the following page. Applying the law of sines to Figure 2.6 results in:

$$\frac{d}{\sin(2\varphi)} = \frac{R}{\sin(\frac{\pi}{2} - \varphi)} \tag{2.6}$$

$$\frac{d}{2\sin(\varphi)\cos(\varphi)} = \frac{R}{\cos(\varphi)} \tag{2.7}$$

$$R = \frac{d}{2\sin(\varphi)} = \left\{\varphi = \arcsin\left(\frac{y}{d}\right)\right\} = \frac{d}{2\sin\left(\arcsin\left(\frac{y}{d}\right)\right)} \tag{2.8}$$

$$R = \frac{d^2}{2y} \tag{2.9}$$

Combining Expression 2.9 with the definition of yaw rate [16] results in:

$$\dot{\psi} = \frac{V}{R} = \frac{\sqrt{v_x^2 + v_y^2}}{R} = \frac{2y\sqrt{v_x^2 + v_y^2}}{d^2} \tag{2.10}$$

$$\dot{\psi} = \frac{2y\sqrt{v_x^2 + v_y^2}}{x^2 + y^2} \tag{2.11}$$

By substituting the yaw rate in Expression 2.5 with its definition in Expression 2.11, the differential brake force, F_b, can be expressed as:

$$F_b = \frac{2\ddot{\psi} I_{zz}}{w} + \frac{l_f C_f - l_r C_r}{w v_x} 2v_y + \left(\frac{l_f^2 C_f + l_r^2 C_r}{w v_x}\right)\left(\frac{4y\sqrt{v_x^2 + v_y^2}}{x^2 + y^2}\right) - \frac{2 l_f C_f}{w}\delta \tag{2.12}$$

If all the motion variables are known, one can input a target goal in the form of the distances x and y from the vehicle and through Expression 2.12 calculate the differential brake force required to reach the target. The reason for deriving this expression is to have a basis for a controller that can perform an avoidance maneuver by only inputting a value for x and y.

The electric hydraulic brake system (EHB) requires a brake pressure input for actuation. Therefore, the force F_b described in Expression 2.12 is converted to brake pressures to the respective brake calipers. A brake distribution between the front and the rear wheels is also implemented and defined as λ, see Expressions 2.14 and 2.16.

$$F_{b,i}\{i = FL, FR\} = p_i \cdot A_f \cdot n_{bp} \cdot \mu_{bp,f} \cdot \frac{r_{disk,f}}{r_{wheel}} \cdot \lambda \tag{2.13}$$

$$p_i\{i = FL, FR\} = \frac{F_{b,i} \cdot r_{wheel,f}}{A_f \cdot n_{bp} \cdot \mu_{bp,f} \cdot r_{disk,f}} \cdot \lambda \tag{2.14}$$

$$F_{b,i}\{i = RL, RR\} = p_i \cdot A_r \cdot n_{bp} \cdot \mu_{bp,r} \cdot \frac{r_{disk,r}}{r_{wheel}} \cdot (1 - \lambda) \tag{2.15}$$

$$p_i\{i = RL, RR\} = \frac{F_{b,i} \cdot r_{wheel}}{A_r \cdot n_{bp} \cdot \mu_{bp,r} \cdot r_{disk,r}} \cdot (1 - \lambda) \tag{2.16}$$

where r_{wheel} = rolling wheel radius [m], r_{disk} = brake disk effective radius [m], A = brake piston area [m^2], n_{bp} = number of brake pads, μ_{bp} = front/rear brake pad to brake disk friction coefficient, p_i= EHB applied brake pressure [Pa].

3 Quantification Methodology

The test vehicle described in Section 3.4 is equipped with an EHB system that enables braking of individual wheels at different levels of intervention. By only braking on one side of the vehicle, the rearward pointing force generated at the wheels will induce a yaw moment on the vehicle. This yaw moment can be utilized to perform an avoidance maneuver and the test procedure to evaluate its potential is presented in this chapter.

A differential braking controller was developed to perform the avoidance maneuver autonomously which also includes a brake limiter to prevent locking of the wheels. The controller utilizes the vehicle motion variables from the CAN-bus and the signals were monitored and logged for comparison with corresponding front wheel steered maneuvers. The test vehicle was modeled in the vehicle simulation software CarSim for development of the controller as well as experimental test verification and correlation.

3.1 Differential Braking System Architecture

An illustration of the differential braking system, hereon called DBS, architecture is found in Figure 3.1. The core of the DBS is the dSPACE MicroAutoBox II described in Section 3.4. The in-vehicle CAN signals as well as the analog signal from the torque-measuring steering wheel described in Section 3.4.2 are interpreted by the dSPACE and imported into the Controldesk PC for monitoring and logging. The DBS-controller is compiled into the dSPACE which utilizes the vehicle CAN signals to calculate and perform the avoidance maneuver. The y-target is set on the Controldesk PC and coded into the dSPACE. The grey blocks inside the dSPACE block illustrate functions. When the maneuver is triggered, a required yaw rate will be calculated based on Expression 2.11 in combination with the PD-controllers described in Section 3.2.

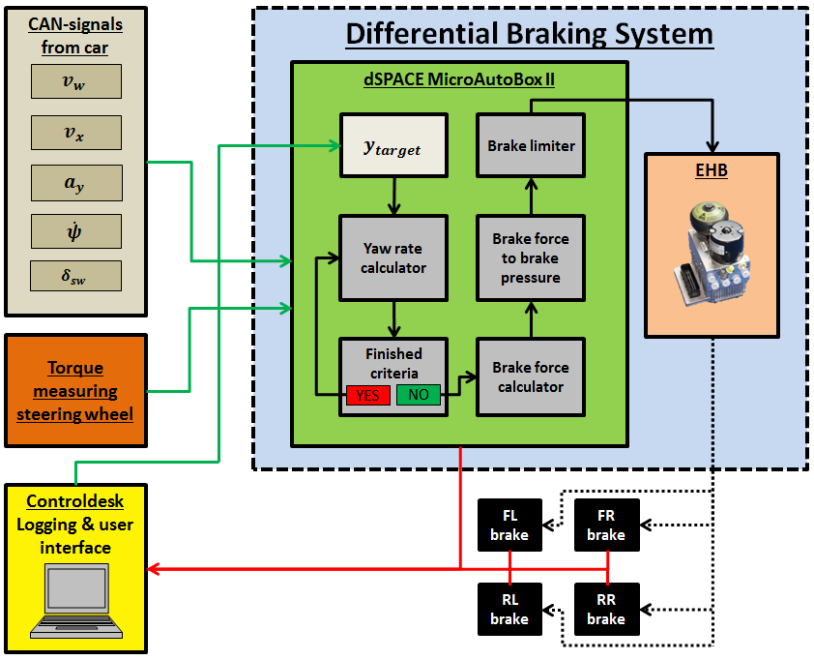

Figure 3.1: *DBS architecture overview*

If the finished maneuver criteria described in Section 3.2 have been fulfilled, a break-signal will set the required yaw rate to zero, thereby disengaging the DBS. If the criteria have not been fulfilled, brake forces will be calculated based on Expression 2.12 and converted to corresponding brake pressures based on Expressions 2.14 and 2.16. The brake limiter will adjust the brake pressures if needed and send a brake pressure demand to the EHB which will finally output the brake pressures to the respective brakes. The red lines illustrate signals for monitoring and logging and the green lines illustrate live variables utilized by the dSPACE to perform the avoidance maneuver.

3.2 Avoidance Maneuver Controller

In order to evaluate the potential of differential braking a controller was developed to perform the avoidance maneuver in the best possible manner while considering parameters such as velocity, vehicle weight, distance to the obstacle, and road friction. In order to do this, the controller has to know where the vehicle is located in relation to the road. Since the vehicle longitudinal velocity, lateral acceleration, and yaw rate are available from the in-vehicle CAN-bus, the following expressions were used to calculate the position of the vehicle in relation to the road:

$$x_{glob} = \int (v_x \cos\psi - v_y \sin\psi)\, dt \tag{3.1}$$

$$y_{glob} = \int (v_y \cos\psi + v_x \sin\psi)\, dt \tag{3.2}$$

where lateral velocity v_y is found by integrating the lateral acceleration and the yaw angle ψ was found by integrating the yaw rate $\dot{\psi}$. When integrating CAN signals such as lateral acceleration and yaw rate, the resulting values will most likely deviate from the actual ones due to signal noise and inaccuracy further discussed in Section 4.4. If the DBS is implemented in a production vehicle, more accurate sensors such as cameras and radars would be used to determine and adjust the vehicle position in relation to the road and the obstacle.

The avoidance maneuver controller inputs are based on Expression 2.12 and are defined as the longitudinal distance x to an obstacle and the lateral displacement y required to avoid it, as described in Figure 3.2. Ideally, the avoidance maneuver should only require two brake sequences; one avoidance sequence and one correction sequence wherein the vehicles initial heading angle is restored, see Figure 3.2. To have a fast responding system at both high and low velocities, dual PD-controllers are implemented, one for low velocity and one for high velocity.

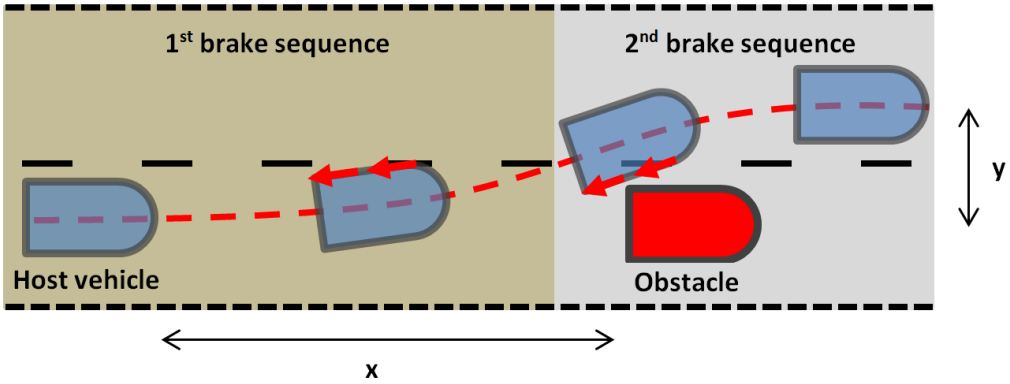

Figure 3.2: *Illustration of differential braking maneuver*

A proportional-integral-derivative controller (PID-controller) involves three separate coefficients, the proportional, integral, and the derivative. Simply put, P depends on the present error, I on the accumulation of past errors, and D is a prediction of future errors. In this implementation, the integral coefficient was ignored since the accumulation of past errors is not of interest, hence a PD-controller. The advantage of using a PD-controller is that it only requires an error value that it will attempt to minimize without overshooting the defined target. This function can be directly applied to a DBS in the way that the controller will attempt to reach a target position without overshooting it, meaning that it will also attempt correct the vehicle to its initial heading angle.

When the avoidance maneuver is triggered, the calculated vehicle global y-coordinate is subtracted from the input desired lateral displacement, thereby generating an error-value as described in Expression 3.3. This value is input to the PD-controller located inside the yaw rate calculator block which will attempt to minimize the error. The output from the PD-controller is input as the y-value in the differential brake force calculation in Expression 2.12 and can be seen as a momentary fictitious lateral target that is adjusted continuously in order to reach the desired lateral target.

$$e(t) = y_{target} - y_{glob} \tag{3.3}$$

Initially, when the difference between the desired lateral target and present lateral displacement is large, the PD-controller will attempt to compensate for this by outputting a large fictitious lateral target. As the vehicle starts approaching the desired lateral target, the PD-controller will instead output a negative fictitious lateral target. The negative fictitious y-value will result in a negative brake force demand which is translated into braking the opposite side of the vehicle, initiating the second brake sequence of the maneuver to restore the initial heading angle of the vehicle. Figure 3.3 illustrates the PD-controller functional structure together with the relevant expressions.

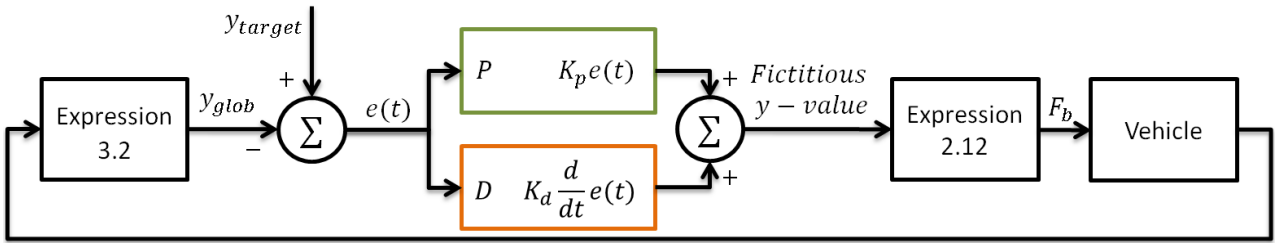

Figure 3.3: *PD-controller functional structure*

Two controller termination criteria were created to determine whether the maneuver has been completed successfully or not:

1. The target lateral displacement has been reached
2. The heading angle is within a range of $-3° < \psi < +3°$ from the original heading

Once these criteria are met, the controller disengages by setting the yaw rate and consequently the brake force to zero at which point the driver will retake control of the vehicle. The controller termination criteria are deliberately designed to allow for a lateral overshoot of the predefined target to ensure that the obstacle is avoided. An illustration of the yaw rate calculator including the dual PD-controllers and maneuver criteria implemented in Simulink is found in Appendix B together with the complete Simulink system overview.

3.2.1 Brake Limiter

The EHB system implements a limited brake pressure restricted to 100bar which in a production vehicle would produce very large brake forces but the brake calipers and pistons in the test vehicle are relatively small which results in smaller brake forces with the same pressure. Within the controller, the front brakes were restricted to 100bar while the rear brakes were restricted to 80bar since larger pressures would only result in locking the rear wheels. This observation was made during the brake test discussed in Section 3.5.

The best assessment of the differential braking potential is done by trying to reach the desired lateral target in as short of a longitudinal distance as possible. By setting $x = 0$, the controller assumes that the obstacle is right in front of the vehicle and will attempt to achieve the lateral target in a step-like manner, instead of at a predefined longitudinal distance ahead of the vehicle. The reason for setting $x = 0$ is to perform the avoidance maneuver as fast as possible by maximizing the time spent utilizing the maximum braking capacity. Any time not spent utilizing the maximum available grip in the tires could be seen as a deficiency since there would be margins left for the maneuver to be conducted faster. This approach could cause stability and/or robustness complications but for the purpose of evaluating differential braking potential it has proven to be an efficient approach.

By setting $x = 0$, the resulting yaw rate and subsequent brake pressure demand is larger than can be achieved with the available brake system. To overcome this problem and at the same time utilize the maximum possible brake force, a brake limiter was developed within the DBS. The brake limiter can be viewed as a simple anti-lock braking system (ABS) that will try to obtain a predefined longitudinal slip ratio $\kappa = 8\%$ by either increasing or decreasing the brake pressure. According to generic tire data 8% longitudinal slip is below the maximum longitudinal force available in the tires. By not utilizing the maximum longitudinal tire force, there will be a lateral force buffer available as defined by the friction circle seen in Figure 3.4. After initiating differential braking, this buffer becomes useful as the vehicle starts yawing and thereby generating lateral tire forces.

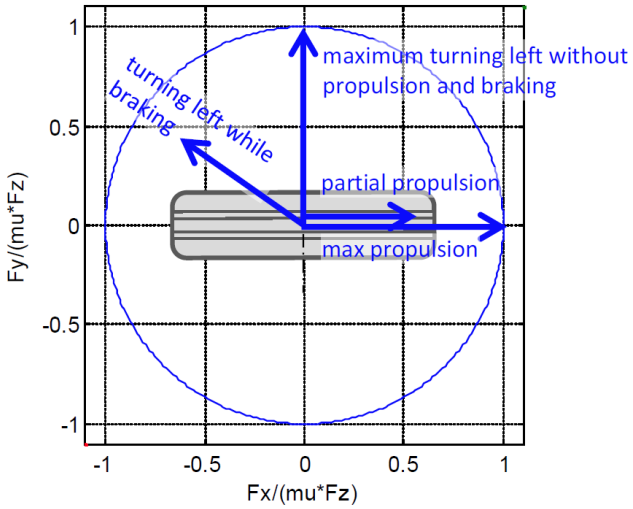

Figure 3.4: *Friction circle [16]*

The longitudinal slip is calculated by comparing vehicle velocity to individual wheel velocities that are available through the in-vehicle CAN-bus, see the expression below.

$$\kappa = \frac{v_x - v_w}{v_x} \tag{3.4}$$

If the slip ratio is too high, the brake limiter reduces the brake pressure demand and if the slip ratio is too low, it will try to increase the pressure until it reaches the brake pressure limit or the brake pressure demand based on Expression 2.12. The brake limiter could be further improved but since it is outside the focus of the project it is considered sufficient. Furthermore, in a production vehicle, the DBS would utilize the existing ABS in the vehicle which would be more advanced than the current brake limiter. An illustration of the brake limiter implemented in Simulink can be found in Appendix B.

3.3 Procedure for Experimental Testing

Experimental testing was conducted in a wide range of different conditions and levels of intervention to accurately capture the vehicle behavior and maneuver performance when performing a differential braking avoidance maneuver. Three different vehicle velocities were included in the test plan to represent common scenarios:

- 50km/h – city driving
- 80km/h – country roads
- 120km/h – highway

The way the vehicle is loaded has a large influence on vehicle dynamics and transient behavior and two load cases were included, one with a driver and front passenger and one with a fully loaded car according to vehicle specification. Road condition is an ever-changing factor and the experiments were performed with varying road conditions to include both high friction and low friction cases, defined as dry and wet road surface.

In order to evaluate the magnitude and influence of the torque steer effect during braking described in Section 2.2.1, test cases were included with spacers installed between the front wheels and hubs to effectively remove the lateral component of the scrub radius and its potential torque steer effect. The avoidance maneuver is focused on small overlap situations of up to one meter and both 0.5m and 1m lateral displacement were tested. The established conditions for the test procedure are summarized in Figure 3.5 below.

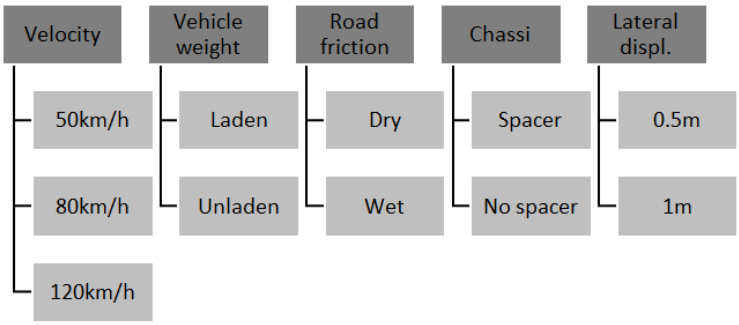

Figure 3.5: *Established testing conditions*

The vehicle weight is defined as unladen with a front seat passenger since a passenger is required to trigger the maneuver and to manage data logging. For the laden setup, an additional 360kg in the form of sand bags were placed in the trunk and rear seat of the vehicle to represent a fully loaded car with 5 passengers and luggage. If the test were to be conducted for the full range of the variable conditions it would result in a total of 48 test cases which would not be an efficient approach. In order to narrow down the range, a default reference case was identified with the most standard conditions as specified below:

- Vehicle velocity: 80km/h
- Vehicle weight: Curb weight + passenger (defined as unladen)
- Road friction: Dry
- Scrub radius: No spacers
- Lateral displacement: 0.5m

From this mode, each condition was varied one at a time while the others were kept in their default mode. This approach resulted in a total of seven test cases. For more comprehensive quantification, additional cases were included and the complete test chart is found in Figure 3.6 below. A full description of the conducted test cases is listed in Appendix D.2.

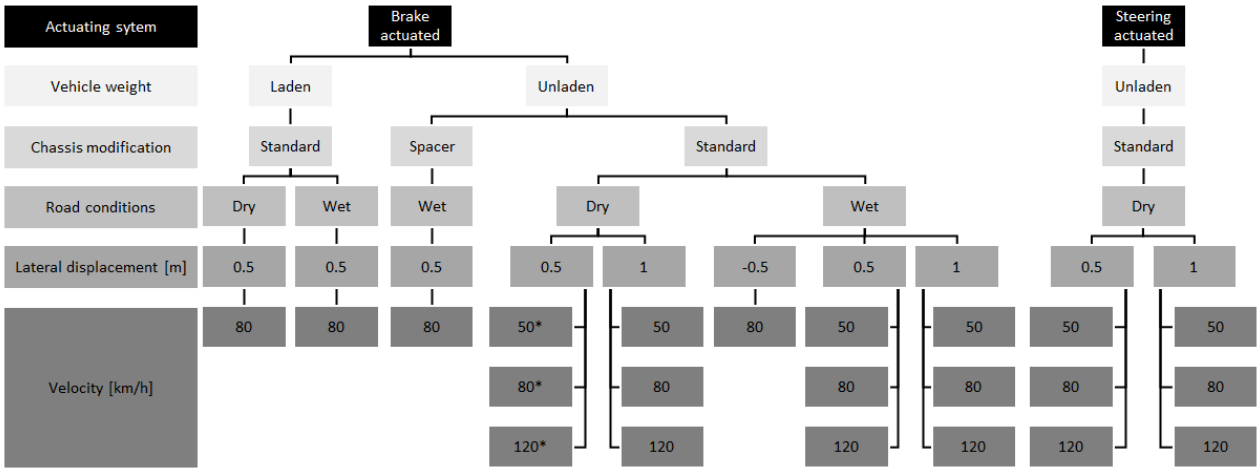

Figure 3.6: *Combinations of test conditions to be evaluated, the *-marked tests are also conducted with the maximum EHB pressure capacity*

One test case was added with a negative lateral displacement to evaluate whether systematic variations were present depending on if the maneuver is executed to the left (positive lateral displacement) or to the right (negative lateral displacement). To ensure precise and consistent data, the mechanical locking function was utilized on the torque-measuring steering wheel described in Section 3.4.2 which was set to a zero-degree steering angle. This was done for three reasons:

- To ensure that the vehicle is traveling with no steer angle or yaw rate before actuating the differential braking maneuver
- For precise quantification of the torque steer effect
- To minimize variations between tests and increase consistency

When the steering wheel was locked in a zero-degree position, the exact amount of torque subjected to the steering wheel could be registered and this way the spacers influence on the torque steer effect could be quantified. A large number of signals were monitored and logged for each test case and the following signals were found most relevant:

- Vehicle and wheel velocities
- Yaw angle and yaw rate
- Longitudinal and lateral acceleration
- Steering wheel angle and torque
- Applied brake pressures
- Distance traveled

The tests were conducted according to the following procedure:

1. Data logging is initiated
2. Vehicle accelerates to a velocity slightly above the specified test velocity
3. Gear is put into neutral
4. Steering wheel is locked at zero-degree angle
5. Controller interface confirms that steering wheel angle and yaw rate are zero
6. Maneuver is initiated by inputting target lateral displacement once the velocity has dropped down to the specified test velocity

All the logged differential braking tests were conducted on Råda airfield outside of Lidköping, Sweden. The field of application for a DBS is assumed be in situations where the brakes are in ambient temperatures. Therefore the full length of the airstrip was used for each test in order to cool the brakes since warm brakes would increase braking performance and produce inconsistent test data. Each test case was carried out six times to ensure consistent data and to identify and reduce effects resulting from stochastic errors. The gathered data was compiled into an observable format, analyzed, and finally compared to corresponding simulated and experimental front wheel steered maneuvers for quantification of the differential braking potential. The steering robot described in Section 3.4.3 was used to perform the experimental steered avoidance maneuvers. A total of six different steered maneuvers were conducted; 0.5m and 1m lateral displacements at velocities of 50, 80 and 120km/h on dry road conditions.

3.4 Test Vehicle and Equipment

The test vehicle is based on a 2008-model SAAB 9-3 Aero with a 2.8L V6 Turbo engine and a manual gearbox. The vehicle was modified as part of a master's thesis work performed by Horace Lai and David Madås for SAAB's hybrid vehicle development program [12]. Various parameters specific for the test vehicle are found in Appendix A.

Figure 3.7: *SAAB 9-3 test vehicle*

The vehicle is equipped with an EHB system with additional brake calipers mounted at each wheel that can be controlled independently. All four steering knuckles have been modified to house the new calipers while retaining the standard calipers. The battery has been moved to the trunk of the vehicle and the EHB unit has been mounted in its place in the engine compartment. The EHB system is actuated by a dSPACE MicroAutoBox II control-board that is located inside the driver compartment. The dSPACE communicates with the EHB, the in-vehicle CAN-bus, and additional sensors. An overview of the EHB system is shown in Figure 3.8.

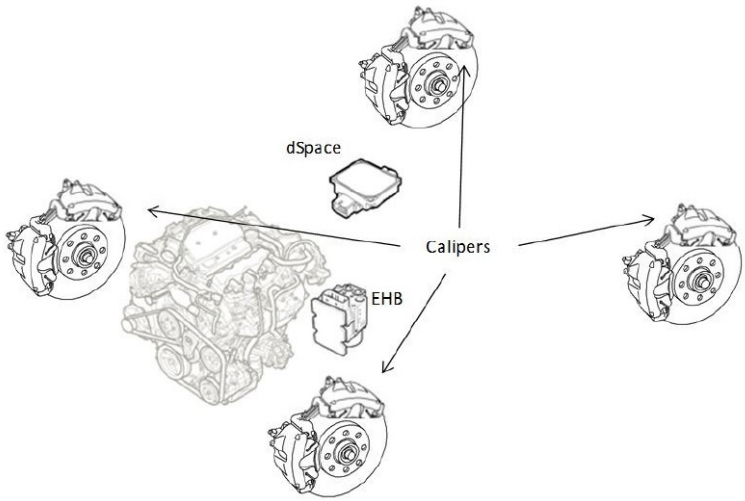

Figure 3.8: *EHB system overview [12]*

The Simulink EHB unit block was provided by TNO, a Dutch technical research institute. The Simulink program is compiled to a format compatible with the dSPACE software Controldesk which in turn controls the EHB unit and when and how it should actuate the brakes.

3.4.1 Data Acquisition

To quantify the vehicle test results, logging of the vehicle motion parameters are required during the experimental tests. The data could be acquired through either the in-vehicle CAN-bus or through a second option, a VBOX 3i Dual Antenna [26] with an additional Inertial Measurement Unit [27]. The VBOX uses dual GPS antennas (see vehicle roof in Figure 3.7) at a logging rate of 100Hz to accurately determine the vehicle motion variables listed above but not specific vehicle parameters as individual wheel speeds. From previous experience it was known that the VBOX is a very accurate and precise tool. Since the accuracy of the in-vehicle CAN-bus was not known, the vehicle motion was monitored with both systems during an avoidance maneuver and a free roam. The data from the VBOX was used as a reference to evaluate the accuracy of the CAN signals.

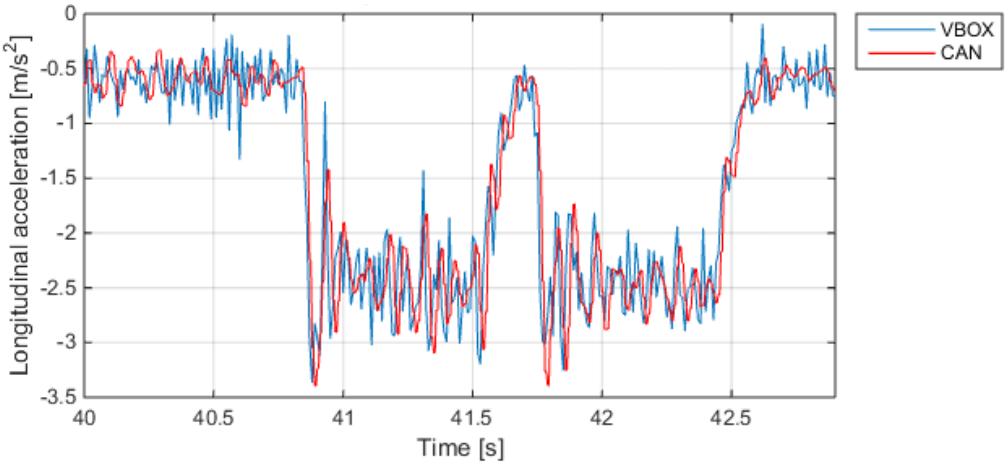

Figure 3.9: *Longitudinal acceleration signal comparison between in-vehicle CAN-bus and VBOX*

Figure 3.9 shows a comparison of the non-filtered longitudinal acceleration between the in-vehicle CAN signal and the VBOX from the same maneuver. It is observed that the in-vehicle CAN-bus signal follows the VBOX signal very well. The remaining signals such as lateral acceleration and yaw rate show the same correlation between the CAN-bus and VBOX data. For the sake of simplicity and practicality, the CAN-bus was used for data acquisition. Further comparisons between the VBOX and CAN-bus data is found in Appendix C.

3.4.2 Torque-measuring Steering Wheel

Due to the torque steer effect described in the Section 2.2.1, an RMS FEL20 [22] torque-measuring steering wheel is installed in order to quantify and evaluate the torque steer intrusiveness to the driver, see Figure 3.10. The lateral component of the scrub radius described as r_k in Figure 2.4 will contribute to a counteracting steering torque and caster and pneumatic trail will contribute to a self-aligning moment on the wheels when performing differential braking. It is of importance to evaluate how these phenomena affect the maneuver performance and how they are perceived by the driver. By installing a torque-measuring steering wheel, the torque steer intrusion at differential braking can be quantified and compared for different test cases. The steering wheel is connected to the dSPACE control board by an analog signal. It has the capacity to monitor steering wheel angle, angular velocity and steering wheel torque. Only the torque signal is registered since the angle is already available from the CAN-bus and the angular velocity is not of interest. The torque-measuring steering wheel also offers mechanical functions such as locking the steering wheel at specific angles as well as setting steer angle limits.

Figure 3.10: *RMS FEL20 torque-measuring steering wheel installed in test vehicle*

3.4.3 Steering Robot

To quantify the differential braking potential, the maneuvers were compared to corresponding front wheel steered maneuvers. If the steered maneuvers were to be performed by a driver, reproducibility would be poor since manually steering the vehicle is difficult to do to exact measures. The AB Dynamics SR60-Orbit steering robot is a lightweight, geared, steering actuator [6]. It was installed in the test vehicle to perform the experimental steered avoidance maneuvers, see Figure 3.11.

Similar to the DBS-controller algorithm described in Section 3.2, the steering robot input is the desired lateral displacement. The longitudinal distance was set to a value below what is achievable which results in that the steering robot will attempt to achieve the lateral displacement as fast as possible, a requirement for an accurate evaluation of the DBS potential. It was not possible to set the longitudinal distance to $x = 0$ on the steering robot due to a restriction in the algorithm designed to prevent the vehicle from losing control. This restriction became more evident at higher velocities when the vehicle is more sensitive to steering inputs. The steering robot path tracking function utilizes a high precision gyroscopic sensor and a GPS base station, resulting in very high position accuracy. The steering robot was connected to separate computers and controller software interface.

Figure 3.11: *Anthony Best Dynamics SR60-Orbit steering robot*

3.5 Calibration of Vehicle Model

A simulated vehicle model was used during the development of the DBS-controller described in Section 3.2. Implementing the controller on a vehicle model allowed for an initial estimation of how the vehicle would behave during a differential braking avoidance maneuver as well as facilitating a structured basis for varying the vehicle test parameters. CarSim is a commercial software designed by Mechanical Simulation. It is a powerful tool that simulates the dynamic behavior of passenger cars, race cars, light trucks, and utility vehicles [18]. The software has been evaluated as a thesis work at Volvo Car Corporation combining assistive braking and steering [2]. Since the objective of this thesis is not model simulation, a generic model D-class sedan was chosen from the CarSim library to conduct the vehicle simulations with.

Of the vehicle segments available in the CarSim library, the D-class sedan was considered to resemble the properties of the test vehicle the most and was therefore used as a starting point. Many vehicle parameters specific to the test vehicle were available from K&C-data and implemented in the model for it to more accurately resemble the behavior of the test vehicle. The modified parameters are specified in Appendix D.1. In CarSim, a generic tire model is used that is based on the Magic Tire Formula described in Section 2.2. CarSim also incorporates dynamic load transfer in vehicle simulations.

3.5.1 Steady State Calibration

A steady state cornering test was conducted with the test vehicle to generate a handling diagram. The test was conducted from 10-100km/h at a constant curve radius of 107m and the additional steering angle required to maintain the curve radius was registered. The same test was simulated and the lateral tire parameters in CarSim were modified to achieve the same behavior as in the test vehicle. The longitudinal tire parameters were left unmodified and instead, the brake parameters were adjusted as described later in this section. The resulting comparative handling diagram is found in Figure 3.12, lateral and longitudinal tire performance graphs are found in Appendix E, and the modified tire parameters are found in Appendix D.1. The red x-marks in Figure 3.12 represent the experimental measuring points upon which the blue curve has been fitted. The black curve illustrates the adjusted CarSim handling diagram and the curves show very good correlation except for at higher lateral accelerations that lie outside of the avoidance maneuver span. The model DBS-controller is identical to the DBS-controller used in the test vehicle so that the CarSim model could be used as a verification tool.

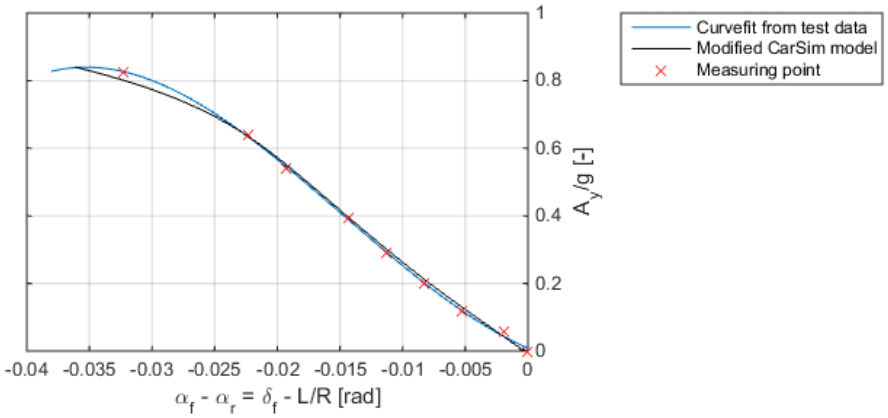

Figure 3.12: *Handling diagram generated from experimental testing vs. corresponding adjusted CarSim data*

3.5.2 Brake Calibration

In order to ensure further correlation between simulated and experimental testing, a deceleration from 80km/h to 30km/h was simulated by applying a constant brake pressure to the front and rear, respectively, as follows:

- 60 bar brake pressure applied only to front brakes
- 40 bar brake pressure applied only to rear brakes

The same braking maneuver was carried out in the test vehicle. The longitudinal acceleration was registered in both simulation and experiment and the data was compared to see the correlation. The simulation model required calibration to reflect the test vehicle properties and behavior, meaning that deceleration and braking distance had to match.

The experimental brake tests consistently resulted in brake pad friction coefficients of $\mu_{bp,f} = 0.15$ and $\mu_{bp,r} = 0.17$ between the brake pads and discs. These values do not correspond to the available friction data available from the brake pad manufacturer. Tests have however previously been conducted [12] to verify the brake pad friction which deviates substantially from the manufacturer specification and shows a better correlation to the above estimated friction as shown in Figure 3.13b. The brake calibration tests were performed in cold conditions and pad temperature were approximated to 0°C which according to the manufacturer friction data should correspond to a friction coefficient of approximately 0.24 corresponding to 0.17 according to the previously conducted friction verification seen in Figure 3.13b. The brake pad friction coefficients in the simulation model were adjusted to match the experimental test results and the resulting longitudinal acceleration graphs are found in Appendix E.

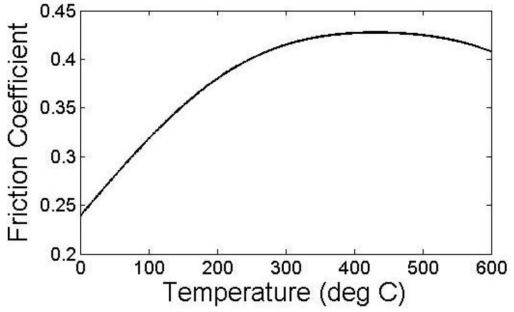

(a) *Manufacturer brake pad friction coefficient specification*

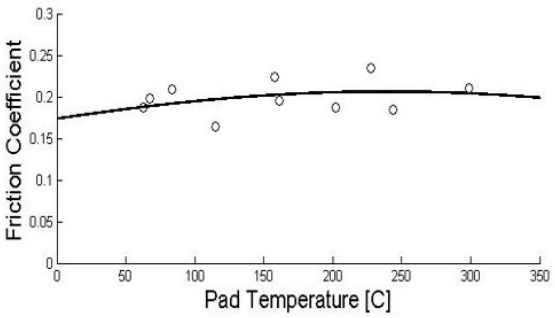

(b) *Measured brake pad friction coefficient [12]*

Figure 3.13: *Brake pad friction coefficient*

3.5.3 Model Verification

If the simulated vehicle model should to be used to conduct front wheel steered maneuvers for quantification of the differential braking performance, the model has to accurately represent the test vehicle. To verify the accuracy of the constructed vehicle model, several simulated front wheel steered avoidance maneuvers were conducted wherein the registered steering wheel angle from the experimental tests with the steering robot were implemented in the simulation. All testing conditions such as velocity and vehicle load were kept the same for both simulation and experimental test in order to accurately verify the correlation.

The results from the simulated tests show good correlation with the experimental tests. The analyzed signals were lateral and longitudinal acceleration, yaw rate, maneuver distance and duration. The simulated signals show a deviation of less than 8% compared to the experimental signals except for the maneuver distance and duration where the deviation was ∼13%. The deviation is explained by the sensor inaccuracy described in Section 4.4 where the trajectory calculated by the DBS deviates from the actual trajectory.

4 Errors, Limitations & Uncertainties

When conducting experimental testing it is likely to encounter errors and variations in the test data that deviate from otherwise unambiguous measurements. It is important to determine whether these errors are stochastic or systematic and to identify uncertainties and limitations within the vehicle and DBS with regards to performing a small overlap avoidance maneuver.

Stochastic Errors

A stochastic error is determined by chance, for example if the vehicle is being tested in a wet condition and there is a puddle of water on the track exactly when the maneuver is triggered. This could cause the wheel to lock when it otherwise would not, which would cause that specific test to deviate from the rest due to a stochastic error. As previously mentioned the majority of the test cases were conducted six times in order to reduce the influence of stochastic errors. Stochastic errors that were identified are listed below.

Varying road friction
: The road surface can vary from one location to another as a result from variations in the paving of the asphalt. If the road surface is wet the road friction variation will increase even further. All experimental tests were conducted on the same location on the test track to minimize the influence from this error.

Uneven road surface
: Road surfaces are rarely completely even and variations in the surface such as bumps or pits which will affect the contact force between the tire and the road surface. The road wetness discussed above will increase the tendency for stochastic errors as water will gather in pits.

EHB error
: In some instances it was noticed that the EHB would momentarily apply brake pressure on all four wheels when the controller only requested brake pressure on two wheels.

Wind gusts
: Gusts of wind could affect the test results depending on the intensity and direction in relation to the vehicle.

Varying velocity
: The vehicle velocity strongly affects the maneuver outcome and it is important to trigger the maneuver at the specified case velocity to ensure consistent results. During the experimental tests the velocity was digitally monitored and triggered at the desired velocity.

Systematic Errors

A systematic error is not determined by chance but by variations or inaccuracy in the system. An example of a systematic error could be that one tire has a lower pressure that the others. This could produce consistent measurement data without any large deviations but where the systematic error is still present which might make it harder to identify. Right & left asymmetry is evaluated separately and discussed in Section 4.1 and additional systematic errors are listed below.

Road banking
: Roads are often banked to allow for water to run off. This will have a large influence on maneuver outcome depending on if the avoidance maneuver is performed against or with the banking. When conducting the experimental tests consideration was taken to perform them on regions where the banking was as small as possible.

Varying brake performance
: If the brakes are not allowed to cool between tests, the brake performance will increase, producing inconsistent results which is also the case if the brake performance differs between individual wheels. Cooling runs were included between tests to minimize the effect from this error.

Uneven tire wear
: Uneven tire wear will affect the maneuver outcome due to varying grip as well as tire radius influencing the effective brake force between the tire and road surface.

Fuel level
Varying fuel levels will change the vehicle weight as well as weight distribution and was compensated for by adding sand bags to the vehicle as the fuel level decreased.

Steady wind
If wind is present with constant intensity and direction it will affect the maneuver outcome.

4.1 Right & Left Asymmetry

All experimental test cases were conducted as an avoidance maneuver to the left except for one that was done to the right. This case was conducted in order to evaluate any presence of possible asymmetric systematic errors. The right maneuver test case was conducted on a wet road surface at a velocity of 80km/h and a lateral displacement of -0.5m. The results are compared to a corresponding test case with the same conditions apart from the lateral displacement which was the standard 0.5m. The right test case data is inverted to match the standard left test case to thereby locate deviations that might suggest a systematic error tendency.

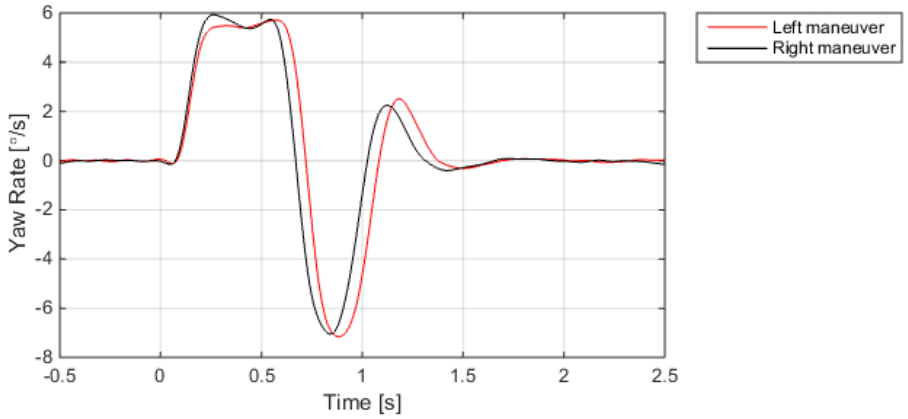

Figure 4.1: *Yaw rate comparison between a maneuver done to the left and to the right*

Figure 4.1 illustrates the yaw rate for the two test cases and a slight mismatch is evident. The right hand maneuver initially shows a slightly larger yaw rate and completes the maneuver after a longitudinal distance of $x = 16.9m$ while the left hand maneuver does it in $x = 18.2m$, a 7.6% increase in longitudinal distance. Additional graphs comparing the right and left avoidance maneuver are found in Appendix F.

The tests were performed on the same strip of road, in the same direction and during the same conditions for both cases. A reason for the mismatch could be because the wetness of the track had changed during testing, resulting in varying grip, or due to varying brake performance between the left and right side of the vehicle. The brake performance was tested by braking one wheel at a time and comparing the longitudinal deceleration and the results proved that there is no difference in brake performance between the two sides. Another reason for the mismatch could because of the banking of the road that had been noticed during testing which is the most likely cause for the mismatch.

4.2 Brake Pressure Build-up & Release Time

Figure 4.2 is a graph over the measured brake pressure at one caliper during a brake sequence. The brake sequence is initiated at $t = 0$ and it is evident that there is a 45ms delay from the activation signal until a pressure increase becomes apparent. There is an additional 75ms until the desired pressure of 100bar is reached, resulting in a total pressure build-up time of 120ms. The activation delay of 45ms is also present when the brake demand is deactivated with an additional 200ms until the brakes are released completely, resulting in a total pressure release time of 245ms. The pressure release time results in a continued yawing motion of the vehicle due to a remaining brake force after the brake demand has been deactivated.

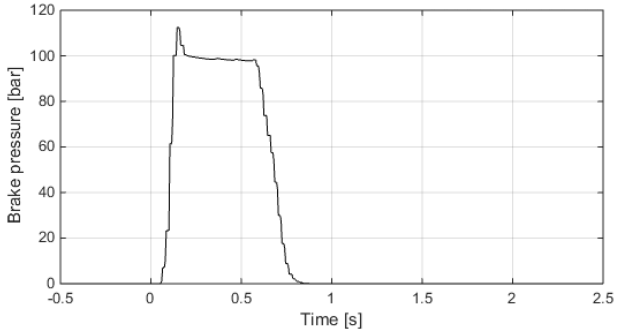

Figure 4.2: *Front left wheel brake pressure during an avoidance maneuver*

The presence of these delays amount to a limitation when performing differential braking avoidance maneuvers. If the avoidance maneuver is performed in two brake sequences, the effect of the brake delay becomes apparent in the overlap between release time on one side of the vehicle and build-up time on the other which results in less efficient yawing motion during the overlap phase. The effects of the delays become more substantial during short braking instances when the overlapping brake sequences become larger in proportion to the total maneuver duration. Another situation where the brake delay becomes a limitation is when longitudinal slip is high. In this scenario, the brake limiter (see Section 3.2.1) will intervene and the release time could result in locked wheels.

4.3 Torque Steer & Self-aligning Moment Influence

A systematic variation rather than an error is the presence of the torque steer effect during braking as well as self-aligning moment discussed in Section 2.2.1. Since the steering wheel was kept in a locked position during all tests, these phenomena are difficult to identify in the vehicle motion test data. The effects do however become apparent in the measured steering wheel torque. Tests were conducted with spacers installed to remove the lateral component of the scrub radius and its potential torque steer effect. The steering wheel torque comparison is found in Figure 4.3 below.

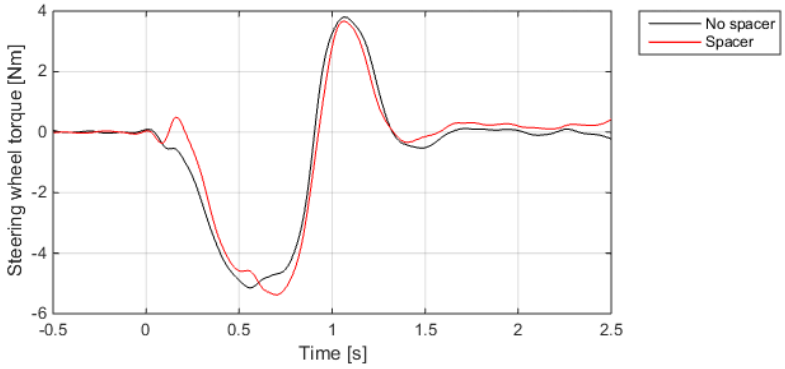

Figure 4.3: *Steering wheel torque when performing a maneuver with and without spacers*

The torque steer effect is noticeable during the initiation of the brake sequences, corresponding to 0.02-0.18s and 0.55-0.75s. When the brakes are engaged the steering wheel is subjected to a torque of 0.5Nm almost instantly without spacers installed. With spacers installed, the same torque is achieved after 0.16 s during which time the torque steer effect during braking is no longer present. The same effect is apparent in the time interval 0.55-0.75s when the second brake sequence is initiated.

Shortly after the brakes are applied, the vehicle starts yawing and producing lateral forces. Once this occurs, the self-aligning moment resulting from pneumatic and mechanical trail (see Section 2.2.1) will overcome the torque steer effect which is why the steering wheel torque is more or less the same for the two cases apart from the brake initiations.

4.3.1 Unrestricted Steering Wheel

As previously mentioned, all experimental tests were performed with the steering wheel locked in a zero-degree position in order to ensure consistent test results and accurate steering wheel torque data. In an actual driving scenario, the steering wheel will not be restricted. For this reason it is important to analyze how the DBS will perform an avoidance maneuver with an unrestricted steering wheel.

The scenario was tested experimentally at a velocity of 80km/h on a wet road surface and a target lateral displacement of 0.5m. Figure 4.4 shows a lateral acceleration comparison of the conducted tests with and without a restricted steering wheel.

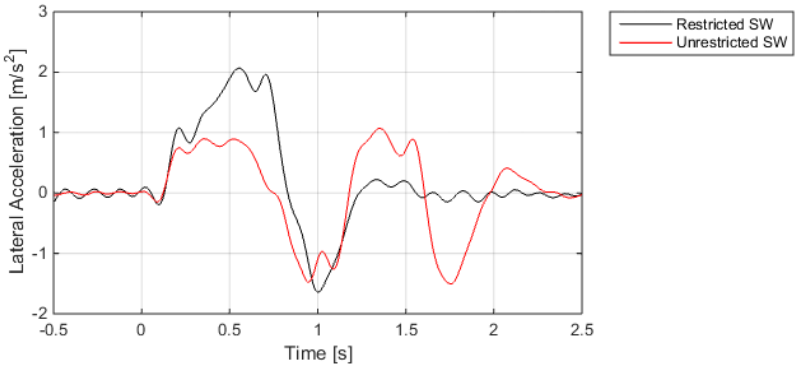

Figure 4.4: *Lateral acceleration comparison with and without a restricted steering wheel*

As the figure illustrates, the maximum achieved lateral acceleration is lower when the steering wheel is unrestricted. With a restricted steering wheel, a maximum lateral acceleration of $a_y = 2.0m/s^2$ is achieved compared to $a_y = 1.3m/s^2$ with the unrestricted steering wheel, a 35% decrease. The reason for the decrease is explained by the torque steer effect and self-aligning moment described in Section 2.2.2. When the steering wheel is unrestricted and the wheels are subject to lateral forces, the front wheels will try to self-align and thereby counteract the yaw motion from the differential braking.

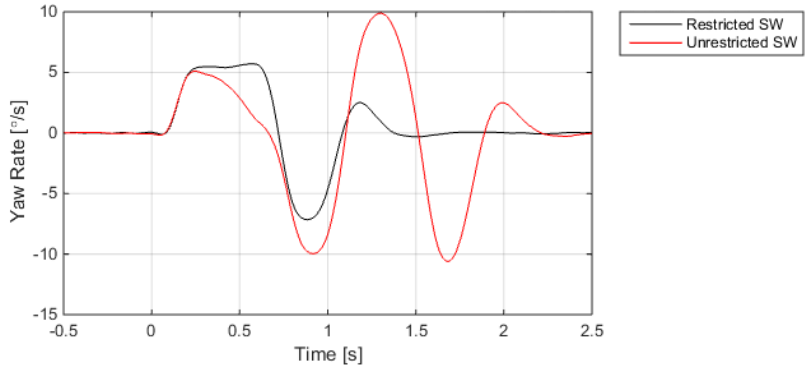

Figure 4.5: *Yaw rate comparison with and without a restricted steering wheel*

The maximum lateral acceleration is decreased with an unrestricted steering wheel while the yaw rate increases as shown in Figure 4.5. Initially, both lateral acceleration and yaw rate remain approximately the same as with the restricted steering wheel. This will cause the PD-controller described in Section 3.2 to assume that the vehicle is approaching the lateral target quickly and therefore switch brake pressure to the other side in order to restore the initial heading angle of the vehicle and not overshoot the lateral target. When the avoidance maneuver is initiated and lateral forces are produced, the front wheels will self-align and turn in the opposite direction of the intended maneuver path. When the second brake sequence is initiated, the self-aligned wheels will point in a more favorable direction compared to a restricted steering wheel and the achieved lateral acceleration and yaw rate during the second brake sequence increase as shown in Figure 4.4 and 4.5.

Since the lateral acceleration and yaw rate decline during the first brake sequence, the lateral target derived from Expression 3.2 is not met and the PD-controller will repeat the brake sequence in order to reach the lateral target. Figure 4.6 illustrates the applied brake pressures during the maneuver for both the restricted and the unrestricted steering wheel.

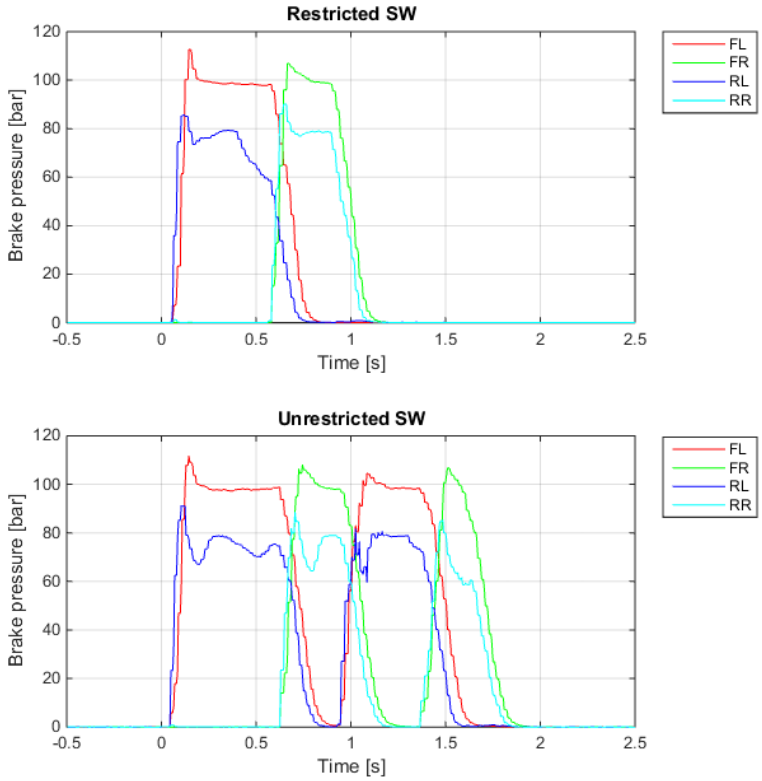

Figure 4.6: *Brake pressure comparison with and without a restricted steering wheel*

The top graph shows the applied brake pressures with the restricted steering wheel and the maneuver is performed in two brake sequences while the same maneuver is performed in four brake sequences when the steering wheel is unrestricted as shown on the bottom graph. An unrestricted steering wheel in combination with the DBS in question results in an ineffective avoidance maneuver. The traveled distance increases by 47%, corresponding to a 50% longer duration required to avoid the obstacle.

4.4 Sensor Inaccuracy

The vehicle position in relation to the road is calculated through Expressions 3.1 and 3.2. The variables ψ and v_y are acquired from integration of yaw rate and lateral acceleration which are available from the in-vehicle CAN-bus. It has been mentioned that integration of live signals could result in deviation from actual values due to signal noise and inaccuracy and since Expressions 3.1 and 3.2 are integrals themselves, this means that the lateral acceleration and yaw rate will be integrated twice in order to acquire the vehicle global coordinates.

An example of signal inaccuracy is if the vehicle is driven on a sloping road or if the gyroscopic sensor is mounted at an angle. Systems in production vehicles compensate for this inaccuracy but in the current controller it could result in for example a lateral acceleration even if the vehicle is driven in a straight line. Integrating this signal which already inherits an inaccuracy will cause the integrated values to be even more inaccurate as time passes. The avoidance maneuver duration is short, around one second, and for this reason the inaccuracy does not have enough time to grow into any substantial deviation.

To verify this assumption, a simple test was conducted as described in Figure 4.7 where the lateral displacement was measured and compared to the calculated lateral displacement. The test was conducted with an unladen vehicle at 80 km/h, in dry conditions, with the lateral target set to one meter. The maneuver was triggered at point 2 at which point position logging was initiated. After the maneuver the lateral displacement was measured at point 1 and point 2 to verify that the vehicle was driven in a straight line. Once this was confirmed, the lateral displacement was measured at point 3 and compared to the logged lateral displacement after 20 m longitudinal travel. The results from the test show that the difference between the calculated and measured lateral displacement was 14.3 %. Data acquisition is carried out using the same logging systems for both differential braking and steered maneuvers which means that the same inaccuracy will be present in both cases and thereby have little influence on comparative results.

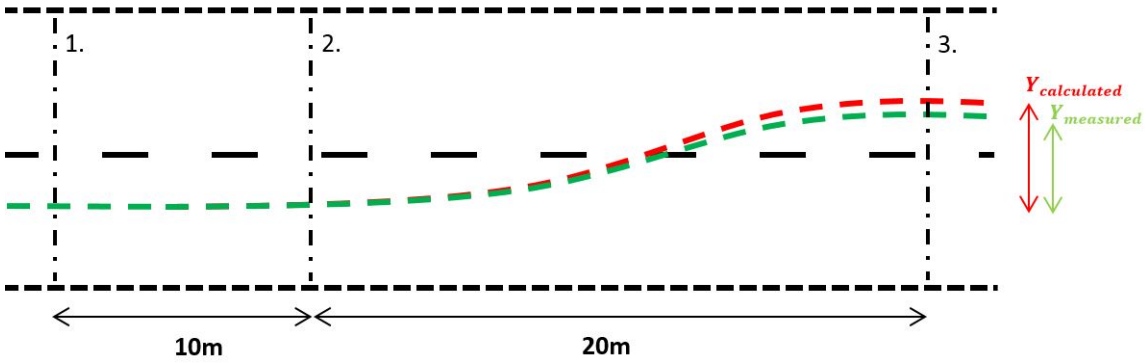

Figure 4.7: *Calculated and measured maneuver trajectory*

4.5 Controller Limitations

As previously mentioned, the DBS-controller will disengage when the following criteria are fulfilled:

1. The target lateral displacement has been reached
2. The heading angle is within a range of $-3° < \psi < +3°$ from the original heading

If the heading angle is within range it does not necessarily mean that a yaw rate is not still present. If the steering wheel is locked in a zero-degree position, a yaw rate might cause the vehicle to drift off further down the path, after the controller has disengaged.

Drifting off the original heading after maneuver completion is however allowed to a certain extent. The goal of the DBS is to avoid an obstacle that the driver is unaware of or unable to avoid in time and afterwards straighten the vehicle back to its original heading so as not to drive off the road. After completion of the maneuver the driver should be alert and retake control of the vehicle. If at that point there is still a yaw angle or yaw rate present, the driver is assumed to compensate for it.

The PD-controllers are tuned and optimized for the test vehicle specifications, braking capacities and experimental test velocities. If any of these parameters should vary to a larger extent, the PD-controllers will no longer be optimized and the avoidance maneuver will not be performed optimally. For the evaluation purposes of this thesis, this limitation is not a problem. If parameters such as braking capacity is changed or if the vehicle velocity lies outside the experimental tests specified in Section 3.3, the PD coefficients have to be adjusted.

5 Quantification of Differential Braking Maneuver

The experimental testing produced extensive data that is compiled and presented in a structured manner to be able to draw conclusions regarding the differential braking potential. Each test case was conducted six times to ensure consistent data and to exclude stochastic errors. The logged data is analyzed and any tests largely deviating from the general trend due to faulty procedure are removed and the remaining data is combined and averaged to produce unambiguous comparisons. The averaged values are also used for quantification purposes when comparing maximum and minimum values regarding for example achieved lateral acceleration or yaw rate during the maneuver.

The main basis for evaluating the potential of a differential braking avoidance maneuver is to compare its performance to corresponding simulated and experimental front wheel steered avoidance maneuvers. A total of 25 experimental avoidance maneuver test cases were conducted by differential braking in order to capture the behavior of the vehicle and the DBS capabilities at varying conditions and loads. Graphs for these test cases illustrating lateral and longitudinal acceleration, yaw rate, and steering wheel torque are found in Appendix G.

Conducting steered maneuver tests corresponding to all of the 25 differential braking maneuvers is unnecessary for the purpose of quantifying the differential braking potential. For this reason, six steered avoidance maneuvers were conducted as described in Section 3.3. Depending on the collision scenario, the maneuver might have to be performed either at a distance or a duration as short as possible as in the case of a stationary obstacle versus a moving one.

The ideal braking distance BD is included in Figure 5.1 and 5.4 to illustrate the ability of the vehicle to decelerate to a complete stop by utilizing all the available traction between the tire and the road surface. This is done by absorbing the vehicle kinetic energy in the form of braking distance as described in Expression 5.1 where the road friction is assumed to be $\mu = 1$.

$$BD = \frac{v_x^2}{2\mu g} \tag{5.1}$$

At higher velocities the longitudinal distance and duration required to avoid an obstacle deviates between simulated and experimental front wheel steered test data as shown in Figures 5.1, 5.2, 5.4, and 5.5. The deviation is explained by the restricting steering robot algorithm described in Section 3.4.3. The simulation software does not implement such restrictions which makes it possible to perform the simulated steered maneuvers more aggressively than the experimental ones, thus reducing the required distance and duration to perform an avoidance maneuver at higher velocities. The simulated maneuvers were manually iterated to obtain a good approximation of how fast the steered maneuver can be performed at different velocities.

The differential braking potential is evaluated by separately analyzing how the following parameters will vary at different vehicle velocities and lateral displacements:

- Longitudinal distance required to achieve the lateral target
- Time required to achieve the lateral target
- Maximum achieved lateral acceleration
- Maximum achieved yaw rate

The controller termination criteria described in Section 3.2 is designed to allow a lateral target overshoot amounting to less than $\sim 15\%$ of the predefined target. The amount of overshoot varies from one test case to another and in order to ensure a fair comparison between the test cases, distance and time required to achieve the lateral target are measured from the point where the DBS is triggered until the point where the lateral target is met rather than when the controller disengages.

A full description of the maneuver performance for the different test cases are listed in Appendix D.3. The figures in Section 5.1 and 5.2 illustrate the maneuvers conducted on wet and dry road conditions with differential braking as well as the corresponding simulated and experimental steered maneuvers conducted on dry road conditions. The green curves illustrating differential braking performance on wet road conditions are included to estimate the road friction influence on the DBS and is not to be compared with the steered maneuver (blue curve) since it is only conducted on dry road conditions.

The curves found in the figures illustrate the varying maneuver potential within the velocity interval 45-125km/h. The curves are approximations based on the data points illustrated by the x-marks which are results from individual tests cases that have been averaged as described in the introduction of this chapter. The three data points on each curve correspond to test velocities 50, 80 and 120km/h. Additional data points would make the curve approximations more accurate but it is not needed for the purpose of comparing and visualizing the trends. As previously mentioned, all the differential braking tests have been conducted with a limited brake pressure of 100bar front and 80bar rear. An additional case was included for the 0.5m lateral displacement wherein the front brake pressure limit was increased to 140bar which is the maximum pressure that the EHB can deliver. This test was conducted to get an estimation of the DBS potential if a larger EHB were to be used. The maximum pressure tests were conducted a limited number of times to lower the risk of damaging the EHB.

When conducting the maximum pressure tests, both front and rear wheels were close to the defined longitudinal slip limit of 8% which indicates that it is in this region that the optimum differential braking performance can be obtained as explained in Section 3.2.1. Confidence intervals are a statistical method to indicate the probability of a random experiment sample to fall within a certain interval [14]. A 95-percentile confidence interval is included in the graphs, meaning that if a test is conducted at the specified test condition, the result will, with a 95% probability, fall within the depicted confidence interval illustrated by the T-bars.

5.1 0.5m Avoidance Maneuver

5.1.1 Required Longitudinal Distance to Avoid Obstacle

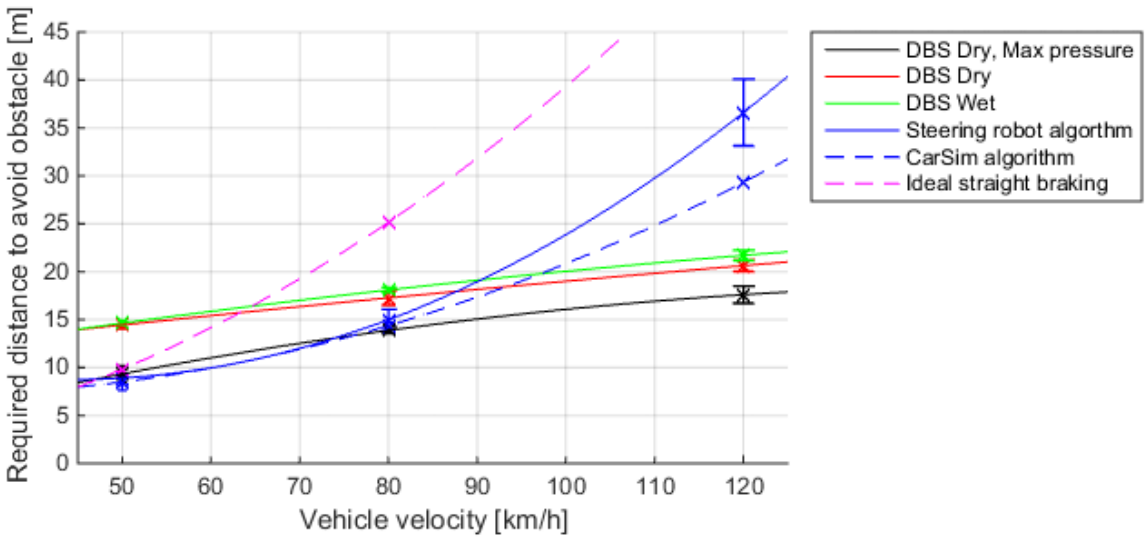

Figure 5.1: *Longitudinal distance required to avoid an obstacle with 0.5m lateral displacement*

When performing a 0.5m displacement maneuver, Figure 5.1 indicates that at velocities above ∼90km/h, differential braking with restricted brake pressure requires a shorter distance to avoid the obstacle than a steered maneuver, regardless of dry or wet road condition. When applying maximum available brake pressure, differential braking is promising even at lower velocities and it becomes distinctly advantageous at velocities above ∼74km/h. The main reason for differential braking performing the maneuver at a shorter distance is due to the fact that the brakes are utilized, resulting in a deceleration of the vehicle during the maneuver which ultimately shortens the traveled distance.

Appendix G.1 to G.3 shows that the lateral acceleration increases rapidly and to larger amplitudes for a steered maneuver compared to a differential braking maneuver, especially at lower velocities. The yaw rate however increases almost identically for both steering and differential braking at all the tested velocities. When initiating a steered maneuver, the front wheels will start producing lateral forces which will cause the vehicle to yaw, causing a delay between producing lateral forces and yaw motion of the vehicle. When initiating a differential braking maneuver the sequence is reversed. The vehicle will first start yawing and since the velocity direction is initially constant, lateral forces will subsequently be produced in the tires.

At higher velocities a small steering input can produce large lateral displacements and the steering amplitude has to be smaller in order not to overshoot the lateral target displacement or lose control of the vehicle. The delay between producing lateral forces and yaw motion of the vehicle combined with the smaller steering amplitude results in that the required distance to avoid the obstacle increases significantly for the steered maneuver at higher velocities. At lower velocities, the vehicle is not as sensitive to steering inputs and steering the vehicle is more advantageous since larger steering amplitudes can be applied, resulting in larger lateral accelerations and a shorter distance to avoid the obstacle.

5.1.2 Required Time to Avoid Obstacle

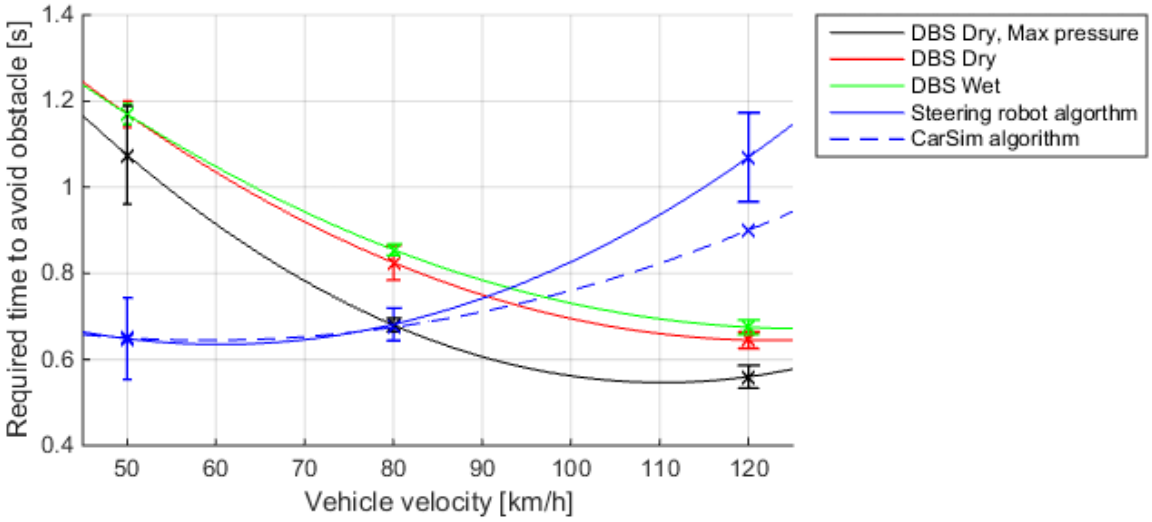

Figure 5.2: *Time required to avoid an obstacle with 0.5m lateral displacement*

Figure 5.2 indicates that conducting an avoidance maneuver by differential braking at low velocities requires almost double the time compared to steering. When traveling at lower velocities, the resulting deceleration from a differential braking maneuver is large and steering the vehicle is more advantageous. The maximum brake pressure DBS performs the maneuver at a shorter duration compared to steering at velocities above ∼80km/h. It is ∼12% more beneficial than the limited brake pressure DBS that is advantageous at velocities above ∼92km/h.

If taking both distance and duration into consideration, the maximum brake pressure DBS is a better solution compared to steering at velocities above ∼80km/h while the limited brake pressure DBS is advantageous above velocities of ∼92km/h.

As indicated by the confidence intervals, DBS testing has proven to produce relatively consistent results except for the maximum pressure case at 50km/h. One reason for this is that the maximum pressure tests were only conducted a limited number of times as previously explained. Another reason is that the DBS-controller brake limiter requires more intervention at lower velocities which is amplified by the higher pressure. The low velocity combined with the limited number of tests results in the larger confidence interval for the 50km/h differential braking maneuver with maximum pressure. The confidence intervals for the steered tests are observably larger since the steered tests were conducted three to four times per case instead of the standard six tests per case for the differential braking maneuvers.

Due to the steering sensitivity at higher velocities it is difficult to achieve an exact lateral displacement of 0.5m which is why the confidence intervals for the steered maneuvers are large at 120km/h, also noticable in Figure 5.1. This inconsistency is also observable in the required duration to perform a 0.5m steered maneuver at 50km/h since large and rapid steering amplitudes are applied to perform the maneuver quickly, resulting in varying duration to complete the maneuver.

5.1.3 Maximum Achieved Lateral Acceleration & Yaw Rate

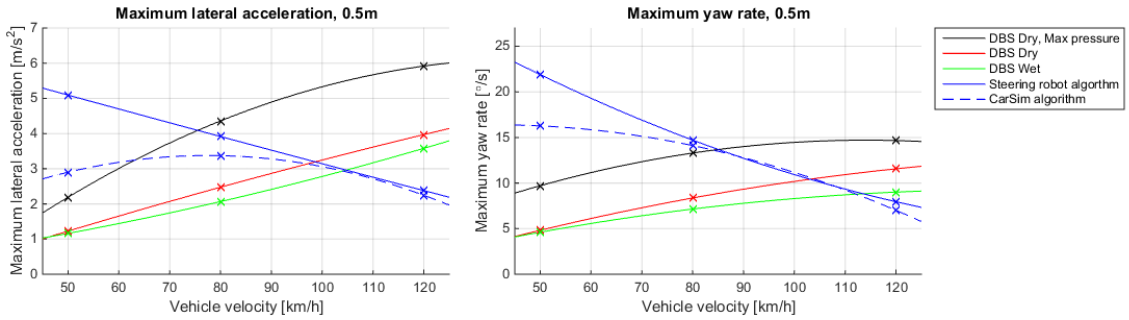

Figure 5.3: *Maximum achieved lateral acceleration and yaw rate during a 0.5m avoidance maneuver*

For a 0.5m avoidance maneuver, longitudinal distance and duration to avoid an obstacle diverges between simulated and experimental steered maneuvers at higher velocities as shown in Figures 5.1 and 5.2. Maximum achieved lateral acceleration and yaw rate show the opposite trend and correlate well at higher velocities while diverging at lower velocities. As discussed in Section 3.5 the simulation model has been verified and correlates well with the test vehicle when performing maneuvers with the same steering input and in the introduction of this chapter it is established that the simulated steered maneuvers can be performed differently from the experimental maneuvers. It is important to keep in mind that the experimental maneuvers, both steered and braked, inherit a sensor inaccuracy that is not present in the simulation and even though correlations are apparent in the figures, the actual experimental values might deviate.

A conclusion that can be drawn from Figure 5.3 is that a maneuver can be performed in many different ways and still achieve the same outcome by for example implementing different steering amplitudes, velocities and accelerations. The steering robot and simulation software use different algorithms to perform the maneuvers and at lower velocities the same maneuver distance and duration is achieved while the lateral acceleration and yaw rate is lower for the simulated maneuvers. Lateral acceleration and yaw rate converge at higher velocities since the vehicle is more sensitive to steering inputs and the margin to perform the maneuver in different ways is smaller.

5.2 1m Avoidance Maneuver

5.2.1 Required Longitudinal Distance to Avoid Obstacle

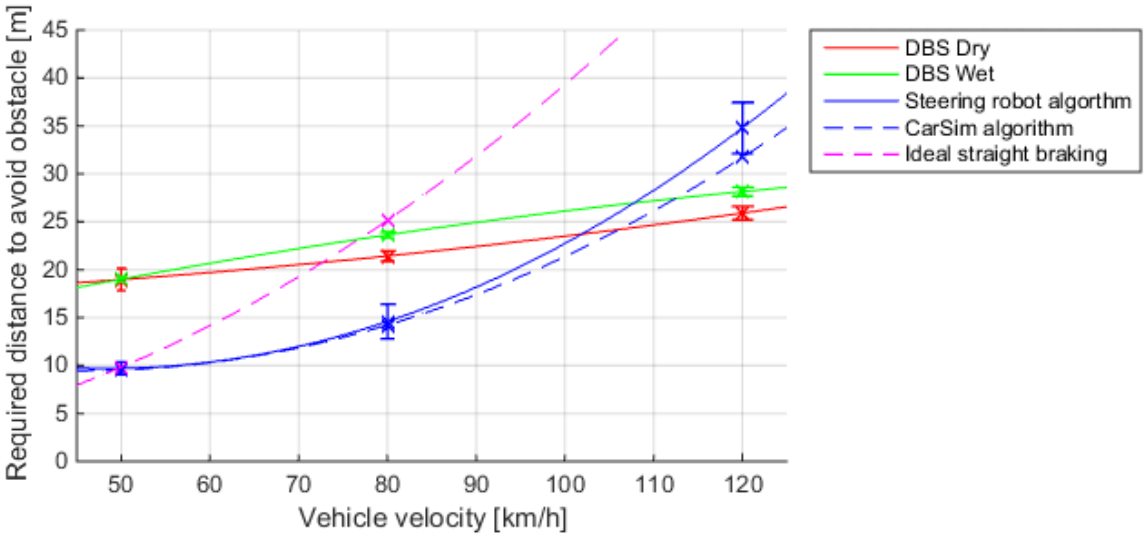

Figure 5.4: *Longitudinal distance required to avoid an obstacle with 1m lateral displacement*

An important distinction for Figures 5.4 and 5.5 is that maximum brake pressure has not been tested for the 1m lateral displacement cases as previously mentioned. When performing a 1m avoidance maneuver, differential braking is less advantageous compared to the 0.5m test cases in Figure 5.1 and 5.2 and the road friction has a larger influence on the differential braking performance. The road friction influence is due to the fact that the larger lateral displacement will require a longer brake duration, resulting in warmer brakes and increased brake performance as well as a more developed elastic load transfer. The effect of these factors become more apparent on wet road conditions as the available grip decreases.

Differential braking performs the 1m avoidance maneuver at a shorter distance compared to the steered maneuver at velocities above ∼104km/h, a 14km/h increase compared to the 0.5m maneuvers. The larger the lateral displacement is, the easier it is to perform a steered maneuver since the steering amplitude can be increased, resulting in larger lateral accelerations and yaw rates while these parameters are limited on the DBS due to the brake pressure limitations. A steered 1m avoidance maneuver at 50km/h requires an ∼8% longer distance compared to a 0.5m maneuver while the DBS requires a total of ∼23% longer distance to perform a 1m maneuver compared to a 0.5m maneuver. At higher velocities the steering sensitivity previously mentioned will eventually cause the steered maneuvers to require a longer distance to avoid the obstacle compared to the differential braking maneuvers.

5.2.2 Required Time to Avoid Obstacle

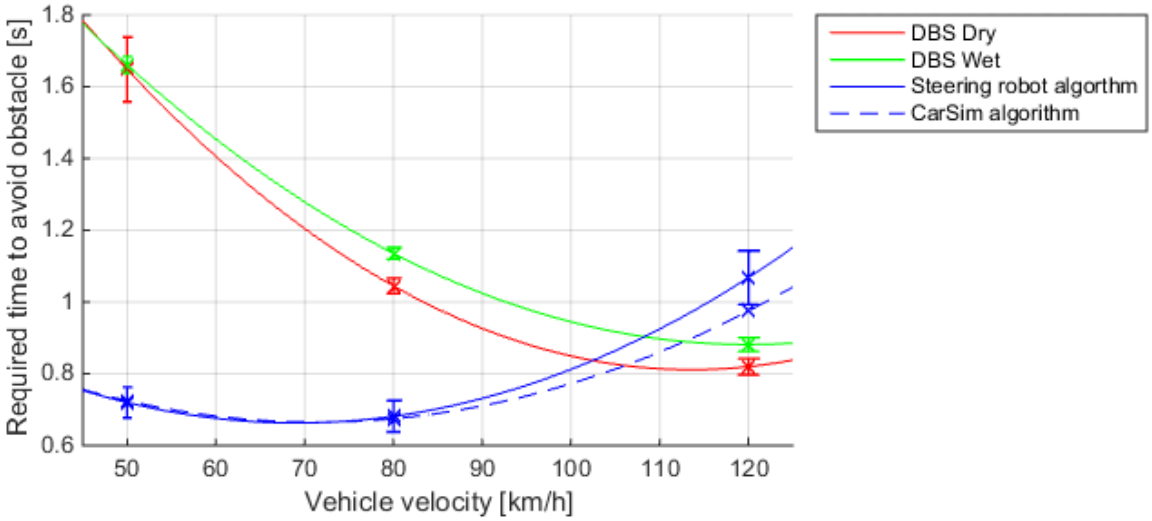

Figure 5.5: *Time required to avoid an obstacle with 1m lateral displacement*

In Figure 5.5, the time difference between the steered and differential braked maneuver at 50km/h is larger than for the 0.5m maneuver in Figure 5.2. A steered 1m maneuver at 50km/h requires a ∼10% longer duration compared to the 0.5m maneuver while differential braking requires a total of ∼29% longer duration to perform a 1m maneuver compared to the 0.5m maneuver. As previously explained, the differential braking maneuvers will generally require a shorter distance to avoid the obstacle due to the deceleration caused by braking which at the same time will increase the required time to avoid the obstacle. When performing a 1m avoidance maneuver with the DBS, the brakes will have to be applied for a longer duration, additionally decelerating the vehicle which will shorten the maneuver distance but ultimately increase the maneuver duration as indicated in Figure 5.5. At velocities above ∼104km/h, differential braking will perform a 1m avoidance maneuver at a both shorter distance and duration compared to a steered maneuver with the restricted EHB.

5.2.3 Maximum Achieved Lateral Acceleration & Yaw Rate

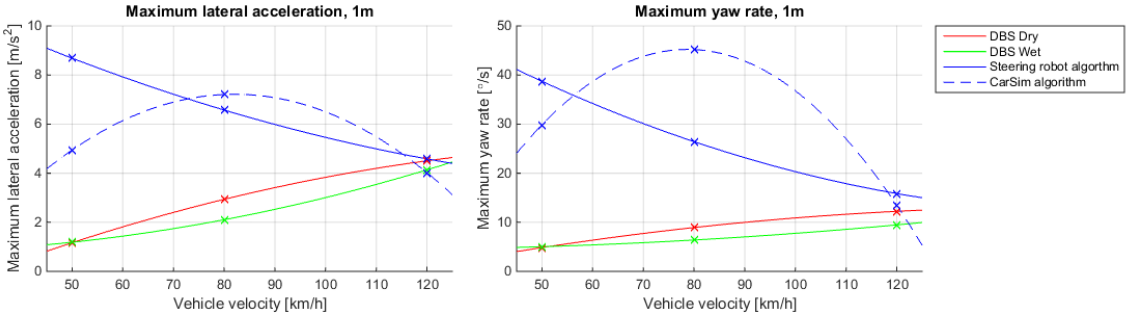

Figure 5.6: *Maximum achieved lateral acceleration and yaw rate during a 1m avoidance maneuver*

The same trends are observed for the 1m and 0.5m avoidance maneuver where the difference between the control algorithms in the steering robot and simulation software produce similar outcomes despite different maneuver executions. For the 1m avoidance maneuver, larger steering inputs can be applied to achieve the desired lateral displacement and the simulated and experimental steered maneuvers show a large yaw rate divergence at 80km/h compared to the 0.5m maneuver where they correlate relatively well. The reason for the deviation is that the simulated vehicle oversteers in the correction sequence of the maneuver, resulting in a large yaw rate. The phenomenon is similar to the so called Scandinavian flick where the vehicle oversteers in the correction sequence of the maneuver due to a pendulum effect generated in the initial avoidance sequence [11].

5.3 Additional Maneuvers

5.3.1 DBS Performance with Laden Vehicle

Tire load sensitivity dictates that the grip decreases with increasing vertical load [28]. Loading a passenger car will increase the load transfer which in combination with the tire load sensitivity will result in a decreased capacity for the tires to develop both lateral and longitudinal forces. Another factor influencing the avoidance maneuver performance is that the vehicle inertia is increased with increasing load, resulting in slower dynamic transient response. When conducting the differential braking test at 80km/h and 0.5m lateral displacement with a fully laden vehicle, the maximum achieved lateral acceleration is ∼10% lower than the for unladen vehicle. The longitudinal distance as well as maneuver duration is increased by ∼3.6% for the laden vehicle. Graphs comparing the laden and unladen test cases are found in Appendix G.2 as well as detailed performance data in Appendix D.3.

5.3.2 DBS Performance with Spacers

Tests were conducted at 80km/h with 0.5m lateral displacement on wet road conditions with spacers installed to evaluate how torque steer and self-aligning moment influences differential braking performance as described in Section 4.3. Installing spacers on the front wheels resulted in a ∼6% decrease in travel distance to avoid the obstacle of as well as a ∼6% decrease in maneuver duration. The maximum achieved lateral acceleration is increased by ∼9% with spacers installed. After conducting the tests with spacers installed it was determined that the torque steer effect at braking has very little influence on the differential braking performance and it is rather the self-aligning moment that is the factor to consider. Installing spacers increases the front wheel track-width which results in a larger lever arm that acts on the vehicle. The increased track-width will effectively increase the yawing capacity of the vehicle as described in Expression 2.2, resulting in an increased avoidance maneuver performance. Graphs describing the test case with mounted spacers are found in Appendix G.2 as well as detailed performance data in Appendix D.3.

5.3.3 Differential Braking Step Input vs. Step Steer

Two additional test cases were conducted at 80km/h on dry road conditions. In the first test a constant step brake input was applied to the left side wheels with the same brake pressures as in the quantification tests, 100bar front and 80bar rear. In the second test a step steer input of 45° to the left was applied at a rise time of $350°/s$. These tests were conducted in order to determine the vehicle response from a maximum pressure step brake input compared to a step steer input. Since constant brake pressure is applied for a longer duration of time, the brake temperature increases, improving brake performance while the the vehicle is decelerating with fully developed load transfer. As a result, the rear left wheel exceeded the specified longitudinal slip target of 8% at which point the brake limiter intervened to keep the wheel from locking. From the achieved yaw rate shown in the right graph in Figure 5.7 it is evident that the yaw rate increases faster with the step brake input compared to the step steer input. This is due to the fact that the yaw rate is a result from lateral acceleration when steering while it is the opposite when braking as discussed in Section 5.1. Graphs illustrating the achieved lateral acceleration and yaw rate during these tests are found in the figure below and additional graphs are found in Appendix G.7.

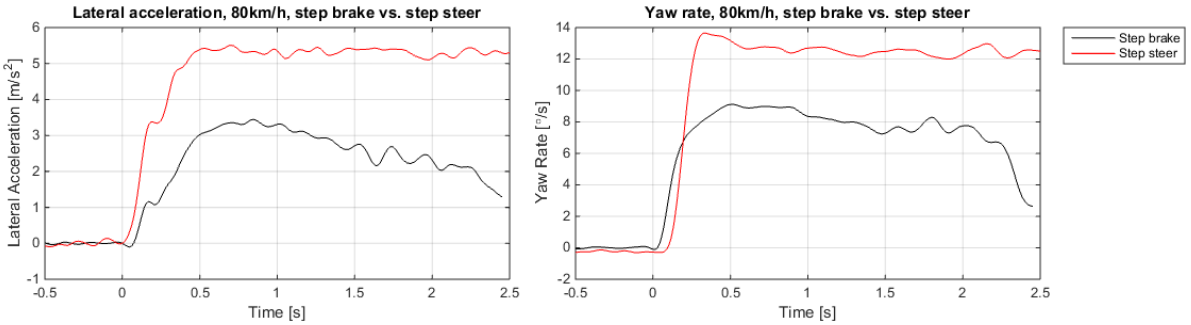

Figure 5.7: *Lateral acceleration (left) and yaw rate (right) resulting from left side step brake input with 100bar front and 80bar rear compared to a 45° step steer input*

6 System Safety Hazard Analysis

Passenger vehicle manufacturers are under constant pressure to ensure that their products are safe and secure. In recent years, as computer and electronic integration within vehicles continue to expand, the task of ensuring driver safety has become more complex. Manufacturers are liable and need to consider any and all possible fault scenarios, what their consequences could be, and what the procedure should be in such a situation. This is especially significant when discussing systems involving safety-critical components such as brakes.

The main focus of this project is to evaluate the potential in moving a vehicle laterally by implementing differential braking. For this reason the safety aspect of a DBS will not be analyzed extensively but rather as a general overview.

A widely used systematic technique for failure analysis is the failure mode and effects analysis (FMEA) developed by reliability engineers in the late 1940s [7]. For the purposes of this project, the FMEA-technique requires too large of an effort. Instead, a so called hazard analysis is implemented [9] to assess the risks of a differential braking system, consequential hazards, and evaluate means of controlling or eliminating them.

6.1 System Failure Analysis

One can never guarantee that a system will not fail and consideration needs to be taken to the hazards that might result from a failure and possible solutions. In this section, worst case fault scenarios from faulty actuation are identified and discussed.

One worst case scenario is if the DBS were to apply a constant, maximum brake pressure on all four wheels. This scenario was tested experimentally on dry road conditions at a velocity of 80km/h. In the test vehicle, maximum brake pressure is defined as 100bar front and 80bar rear. When maximum brake pressure is applied to all four wheels, the longitudinal acceleration within a timeframe of 0-500ms was registered and is presented in the figure below.

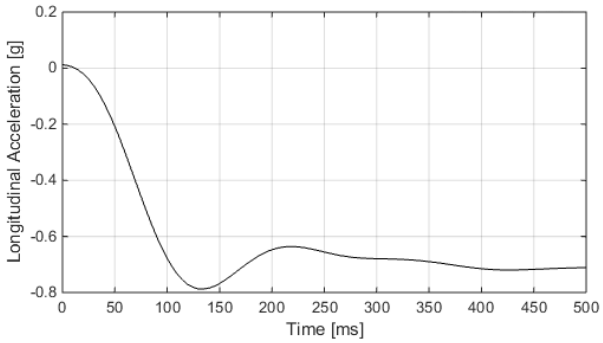

Figure 6.1: *Longitudinal acceleration resulting from maximum brake pressure on all four wheels*

When braking all four wheels the deceleration is substantial. After 100ms, a longitudinal acceleration $a_x = -0.68g$ is achieved and maintained. The large deceleration is considered a hazard and in this scenario the vehicle will decelerate drastically and if there would be traffic behind the host vehicle, there is a large risk of being rear-ended. If the vehicle is in a turn when the brakes are applied there is also the risk of driving off the road or into oncoming traffic, depending on the turn direction. A flow chart illustrating the hazard scenario sequence is found in Figure 6.2 below.

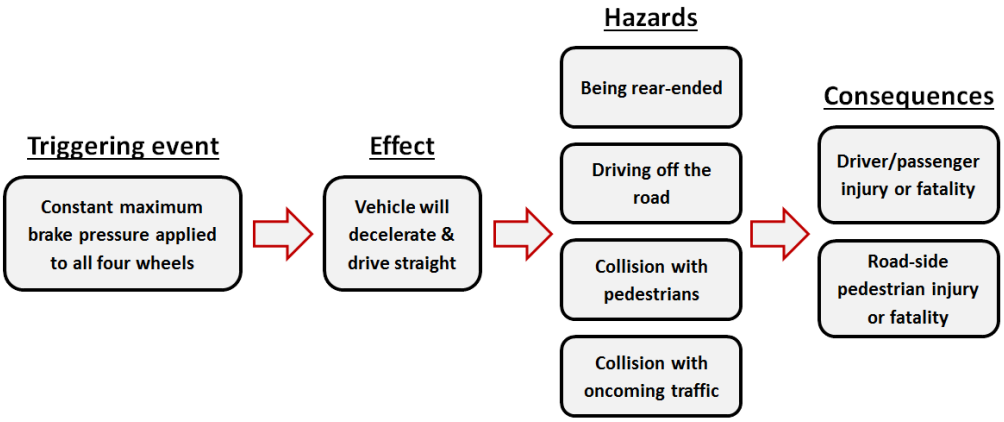

Figure 6.2: *Hazard scenario sequence when maximum brake pressure is applied to all four wheels*

Another worst case scenario is if the DBS were to apply a constant, maximum brake pressure to one side of the vehicle. This scenario was also tested experimentally on dry road conditions at a velocity of 80km/h with brake pressures of 100bar front and 80bar rear. When applying maximum brake pressure to one side of the vehicle, the longitudinal and lateral acceleration within a timeframe of 0-500ms was registered and is presented in the figures below.

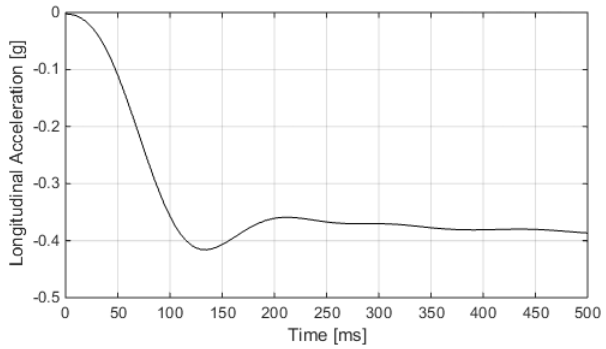

Figure 6.3: *Longitudinal acceleration resulting from maximum brake pressure on left side wheels*

After 100ms, a longitudinal acceleration $a_x = -0.36g$ is achieved and maintained. Even though this is approximately half the deceleration compared to when braking all four wheels, the unintended lateral acceleration may be difficult for the driver to control and is therefore considered a hazard and the fault scenario in Figure 6.2 is still applicable.

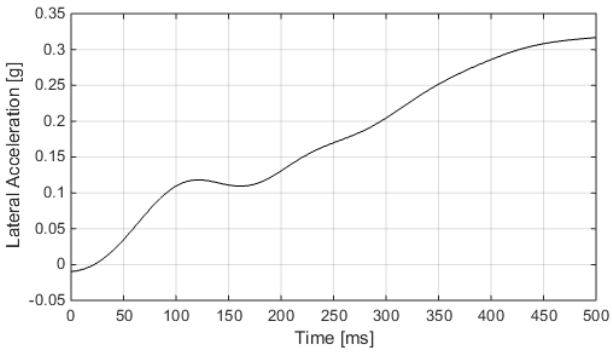

Figure 6.4: *Lateral acceleration resulting from maximum brake pressure on left side wheels*

Figure 6.4 shows the registered lateral acceleration within the same timeframe. After 100ms, a lateral acceleration $a_y = 0.11g$ is achieved. At 200ms the lateral acceleration $a_y = 0.13g$ and increases almost linearly from there. By applying a maximum brake pressure to one side of the vehicle, the subjective impression of the lateral motion felt intrusive and was considered a hazard. When brakes are applied to one side of the vehicle it will not only decelerate but also yaw. Assuming a non-interfering driver, the vehicle will either drive off the road or into oncoming traffic, resulting in a possible head on collision and subsequent injuries or even fatalities. Since the vehicle is also decelerating, the risk of a rear-end collision onto the host vehicle is still plausible. A flowchart illustrating the hazard scenario sequence is found in the figure below. There is a possibility for the driver to manage the vehicle motion caused by the unintended actuation that is discussed in Section 6.2.

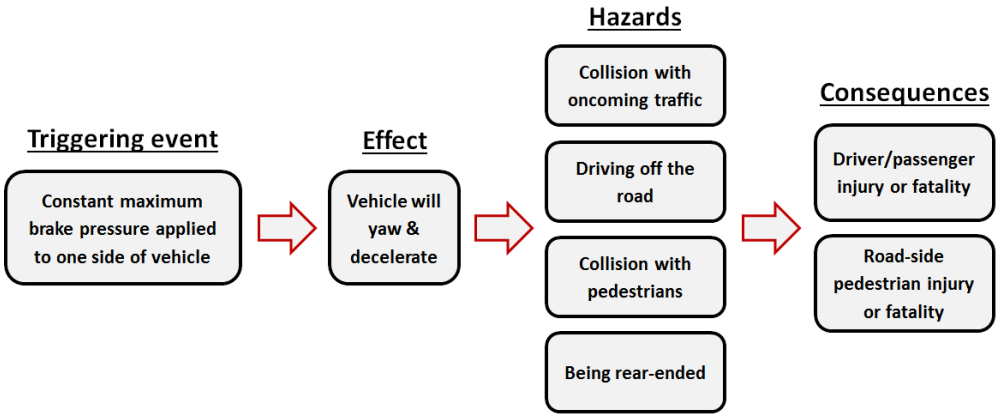

Figure 6.5: *Hazard scenario sequence when maximum brake pressure is applied to left side wheels*

6.2 Steering to Overcome The DBS

If the driver is assumed to intervene with the faulty actuated DBS, one reaction could be to steer against the yawing motion resulting from the differential braking. Such a scenario is illustrated in the free-body diagram below and in this section it is estimated whether the differential braking yawing motion can be overcome by steering.

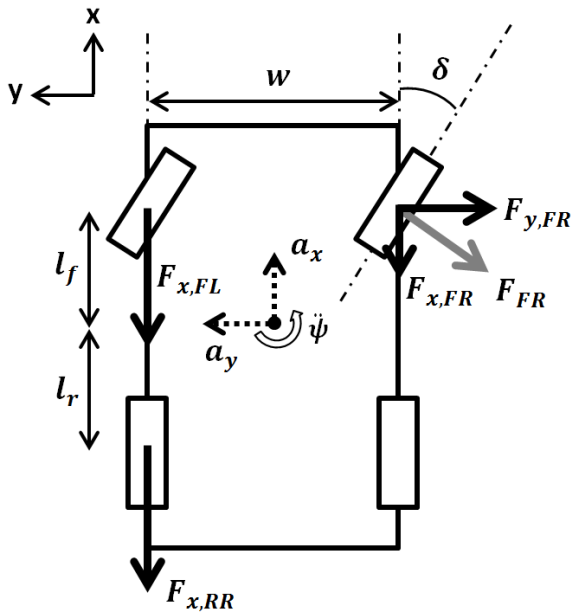

Figure 6.6: *Free-body diagram with brake pressure applied to left wheels while steering to the right*

In the free-body diagram, the left wheels are assumed to be braked until the point of locking. The longitudinal forces available in a tire are illustrated in Figure E.2 in Appendix E. When the wheels are locked, the friction circle in Figure 3.4 is fully utilized and friction forces are counter-directed the sliding motion of the locked wheels, leaving no margin for lateral forces on the left wheels [16]. In Figure E.2, the modified Pacejka curve is approximately $F_x/F_z = 0.8$ when the wheels are locked ($\kappa = 1$). Assuming no load transfer, the forces $F_{x,FL}$ and $F_{x,RL}$ can be determined by the following expressions:

$$F_{x,FL} = 0.8\frac{F_{z,f}}{2} \tag{6.1}$$

$$F_{x,RL} = 0.8\frac{F_{z,r}}{2} \tag{6.2}$$

where $F_{z,f}$ and $F_{z,r}$ are the front and rear axle static vertical forces. From the expressions, the longitudinal forces are found to be $F_{x,FL} = 3849N$ and $F_{x,RL} = 2357N$.

By steering the vehicle in the opposite direction of the yawing motion, a force F_{FR} will be generated at the front right wheel which will counteract the yawing motion caused by the differential braking. There are no longitudinal or lateral forces in the right rear wheel since there is neither propulsion nor braking force present. The force F_{FR} is described in Expression 2.3. Since the vehicle is assumed to be traveling straight , the lateral velocity v_y and yaw rate $\dot{\psi}$ in the expression are zero and the front wheel steering angle δ effectively becomes the front slip angle α_f. The resulting expression becomes:

$$F_{FR} = \{\alpha_f = \delta\} = \alpha_f C_{fw} \tag{6.3}$$

where

$$C_{fw} = C_f/2 \tag{6.4}$$

which is the cornering stiffness for one front wheel instead of for the entire front axle. According to the free-body diagram in Figure 6.6, the forces $F_{x,fr}$ and $F_{y,fr}$ are expressed as follows:

$$F_{x,FR} = \alpha_f C_{fw} sin(\delta) \tag{6.5}$$

$$F_{y,FR} = \alpha_f C_{fw} cos(\delta) \tag{6.6}$$

A moment equation around CoG results in the following expression:

$$(F_{x,FL} + F_{x,RR} - F_{x,FR})\frac{w}{2} - F_{y,FR}l_f = I_{zz}\ddot{\psi} = 0 \tag{6.7}$$

Solving Expression 6.7 numerically results in a wheel angle of $\alpha_f = \delta = 2.8°$, which with a steering ratio of 15.9 corresponds to a steering wheel angle of $\delta_{sw} = 43.8°$ that is required to overcome the yawing motion resulting from the differential braking. Note that these calculations are estimations based on theoretic assumptions to give an indication of the forces involved. The theory confirms that, in terms of yawing motion, steering the vehicle is a more powerful actuator than differential braking. If a faulty DBS actuation should occur where brake pressure is applied to one side of the vehicle to the point of locked wheels, the resulting yawing motion can be canceled out by counter steering. This scenario was tested experimentally with brake pressures of 100bar front and 80bar rear which is not enough to lock the wheels. In this scenario it was however fully possible to overcome the yaw moment generated from differential braking by steering the front wheels. The resulting hazard scenario sequence becomes:

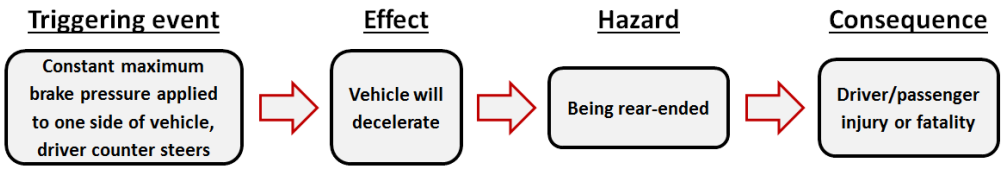

Figure 6.7: *Hazard scenario sequence with one-sided braking of the vehicle and the driver counter steers*

7 Conclusions & Future Work

7.1 Conclusions

The result analysis and evaluation shows that there is indeed potential in utilizing differential braking to perform an avoidance maneuver. At velocities above ∼80km/h, differential braking has the potential to perform a 0.5m lateral displacement avoidance maneuver at both a shorter distance as well as duration compared to steering. Differential braking will always cause the vehicle to decelerate, shortening the traveled distance while at the same time increasing the duration to perform the maneuver. At lower velocities, the vehicle is not as sensitive to steering inputs and larger steering amplitudes can be applied, resulting in more effective lateral movement. For this reason, a steered maneuver is performed at both a shorter distance as well as duration, compared to differential braking.

The larger the desired lateral displacement is, the less advantageous differential braking becomes. Brake duration increases, resulting in additional deceleration and load transfer which decreases the effectiveness of the applied brakes. The 1m lateral displacement maneuver was not tested with maximum brake pressure but with the limited brake pressure and dry road conditions, the DBS performs the 1m maneuver at a shorter distance and duration above velocities of ∼103km/h compared to steering. Should the 1m maneuver be performed with maximum brake pressure it would be more effective and further increase the potential in utilizing differential braking for a 1m lateral displacement maneuver.

Differential braking is most advantageous when longitudinal distance is the critical aspect due to the deceleration resulting from applying the brakes. Translating this aspect into a collision scenario could be if the obstacle to be avoided is stationary and there is no risk of colliding with oncoming traffic. Since the vehicle will both attempt to avoid the obstacle while at the same time decelerating, the obstacle could be detected closer to impact compared to avoiding it by steering. If however the obstacle is moving towards the vehicle, the time to perform the maneuver is more critical at which point using the steering wheel could be more advantageous at lower velocities.

An accident scenario that has not been discussed in which a DBS would be very advantageous is lane keeping assistance/heading correction [25]. Lane keeping systems are already available in passenger vehicles where various sensors in combination with electric power steering (EPS) [23] are used to keep the vehicle from departing from its course. Utilizing a DBS in this scenario could be a very promising solution since the braking intervention to correct the heading will be very fast without being perceived as intrusive by the driver.

A number of differential braking tests were conducted by several different drivers without a restricted steering wheel. The unanimous subjective perception of the differential braking intervention was that it did not feel intrusive. The 0.5m and 1m avoidance maneuvers duration are short and the driver is barely able to react to the differential braking intervention and by the time he/she does, the maneuver is already completed and the driver is able to retake control of the vehicle. With this in mind, letting go of the steering wheel as discussed in Section 4.3.1 is an unlikely driver reaction to a DBS intervention. An unobservant driver could however be holding on to the steering wheel very lightly which could more or less be equal to an unrestricted steering wheel. As discussed in Section 5.3.2 the torque steer effect has a negligible effect on avoidance maneuver performance and it is rather the self-aligning moment that is the factor to consider when performing a differential braking avoidance maneuver with an unrestricted steering wheel. The avoidance maneuver performance in such a scenario proved to be poor and as a result the conclusion is drawn that for this DBS, the steering wheel requires restriction in order optimize the avoidance maneuver performance. This could be implemented if the vehicle is equipped with an EPS which could restrict the steering wheel momentarily when the DBS is engaged.

7.2 Future Work

The developed DBS is relatively simple in its nature and has potential for improvement. The current DBS-controller determines the position and heading angle of the vehicle through equations based on integrated signals. If more accurate positioning systems were to be used such as radars, cameras or GPS, the controller could determine the vehicle position and heading more accurately and thereby allow the DBS to perform more effective and precise maneuvers by narrowing down the required margins. If the DBS is used as an active safety system, these position systems would be required to evaluate the collision scenario and if and how the maneuver should be performed. An example of such a scenario could be if there is oncoming traffic and whether the maneuver can be performed fast enough to return to the initial course. An important aspect to consider is that a collision scenario is not always constant. This is especially the case for moving obstacles which the sensors described above would be able to compensate for by continuously updating the collision scenario and the subsequent DBS intervention.

Another area for improvement of the DBS could be to investigate the potential of implementing variable brake distribution λ to optimize traction and maneuver performance. When the differential braking is initiated the available grip in the rear tires is relatively large but when load transfer starts to develop the available grip decreases at which point the brake distribution could be shifted forwards.

The current DBS utilizes a separate and restricted brake system. If a more powerful brake system were to be used the DBS has the potential to perform avoidance maneuvers more efficiently which was confirmed by testing the EHB at maximum pressure. In a production vehicle the DBS could be integrated with the standard brake system which would have better braking performance than the current EHB system. By using the standard brakes, the existing ABS would be integrated with the DBS-controller which would be much more advanced than the developed brake limiter, allowing a more optimal brake pressure to be applied. More advanced brakes could also decrease the brake pressure build-up and release time discussed in Section 4.2, further optimizing the differential braking performance.

If the DBS applies maximum brake pressure and the wheels are close to locking, an ABS will intervene and adjust the brake pressure. Low road friction will result in continuous intervention from the ABS which is less optimal than if the brake pressure could be adjusted to the road friction and thereby keep it at an optimal level. If a friction estimation system were available this would be possible. Furthermore, the current PD-controller is optimized for a predefined range. If the PD-coefficients were variable, they could be adjusted continuously depending on for example the velocity and road friction, improving the DBS performance.

The results generated in this project have proven that velocity and brake pressure has the largest influence on the differential braking performance compared to a steered maneuver. By testing the differential braking performance at additional and higher velocities as well as higher brake pressures, the potential of differential braking can be further evaluated with a better understanding of the regions where it is advantageous. The experimental steered maneuvers were restricted by the steering robot control algorithm, not allowing the avoidance maneuvers to be performed at the full capacity of the vehicle. If a different algorithm is developed, differential braking potential can be more accurately evaluated. The steering robot algorithm could also be adjusted to reproduce the avoidance maneuver to the capabilities of both a steer-by-wire system as well as a normal driver.

The system safety analysis covered in Chapter 6 is a simplified evaluation. If a DBS is to be considered an active safety system, this analysis has to be much more comprehensive, taking into account all possible system failures, experimental testing of them, consequential actions, and so on. Subjective and objective driver behavior studies have to be conducted and all possible aspects wherein the DBS could be perceived as dangerous have to be evaluated.

Using a DBS as an autonomous active safety system brings up ethical dilemmas as it does with many autonomous systems in development today. The vehicle will more or less have a mind of its own and have to make decisions to save lives, a decision that might be simple on an empty road. If the scenario instead is an imminent collision that cannot be avoided by the DBS without risking pedestrian lives, the dilemma becomes much more complex.

References

[1] A. Arikere, M. Klomp, M. Lidberg, G. Olsson. "The Potential Safety Benefit of Propulsion in Obstacle Avoidance Manoeuvres with Oncoming Traffic". *12th International Symposium on Advanced Vehicle Control (AVEC '14), Tokyo, Japan*. 2014.

[2] A. Gurov, A. Sengupta. *Evaluating the effectiveness of collision avoidance functions using state-of-the-art simulation tools for vehicle dynamics. Master's thesis in Vehicle Engineering*. Royal Institute of Technology, 2013.

[3] A. Gurov, A. Sengupta, M. Jonasson, L. Drugge. "Collision Avoidance Driver Assistance System Using Combined Active Braking and Steering". *12th International Symposium on Advanced Vehicle Control (AVEC '14), Tokyo, Japan*. 2014.

[4] A. T. Van Zanten. *Bosch ESP Systems: 5 Years of Experience*. 2000.

[5] O. Amidi. *Integrated Mobile Robot Control*. 1990.

[6] Anthony Best Dynamics. *Steering Robot Systems*. Mar. 30, 2015. URL: `http://www.abd.uk.com/en/driving_robots/steering_robots`.

[7] ASQ. *Failure Mode Effects Analysis (FMEA)*. Mar. 16, 2015. URL: `http://asq.org/learn-about-quality/process-analysis-tools/overview/fmea.html`.

[8] C. Sherwood, B. Mueller, J. Nolan, D. Zuby, A. Lund. *Traffic Injury Prevention. Development of a Frontal Small Overlap Crashworthiness Evaluation Test, pp 128-135*. Taylor & Francis, 2013.

[9] CA Software in practice. *Hazard Analysis*. Mar. 16, 2015. URL: `http://www.chambers.com.au/glossary/hazard_analysis.php`.

[10] J. Dittmer. *Are You Ready for Drive-by-Wire?* 2001.

[11] E.Velenis, P. Tsiotras, J. Lu. "Modeling Aggressive Maneuvers on Loose Surfaces: The Cases of Trail-Braking and Pendulum-Turn". *European Control Conference, Kos, Greece*. 2007.

[12] H. Lai, D. Madås. *Test Vehicle for Regenerative Braking Emulation. Master's thesis in Automotive Engineering*. Chalmers University of Technology, 2011.

[13] H. Winner. *Handbook of Intelligent Vehicles. Adaptive Cruise Control, pp 613-656*. Springer-Verlag London, 2012.

[14] D. B. Hinkley. *Theoretical Statistics*. Chapman & Hall, 1974.

[15] Insurance Institute for Highway Safety. *Frontal crash tests*. Feb. 23, 2015. URL: `http://www.iihs.org/iihs/ratings/ratings-info/frontal-crash-tests`.

[16] B. Jacobson. *Vehicle Dynamics. Compendium for Course MMF062*. Chalmers University of Technology, 2012.

[17] M. Maurer. *Handbook of Intelligent Vehicles. Forward Collision Warning and Avoidance, pp 657-687*. Springer-Verlag London, 2012.

[18] Mechanical Simulation. *CarSim, Mechanical Simulation*. Mar. 16, 2015. URL: `http://www.carsim.com/products/carsim/index.php`.

[19] L. Morais. *Active Safety Technology Advances*. 2005.

[20] H. B. Pacejka. *Tyre and Vehicle Dynamics*. Elsevier Butterworth-Heinemann, 2002.

[21] M. Persson. *Volvo Car Group's first self-driving Autopilot cars test on public roads around Gothenburg*. Apr. 29, 2014. URL: `https://www.media.volvocars.com/global/en-gb/media/pressreleases/145619/volvo-car-groups-first-self-driving-autopilot-cars-test-on-public-roads-around-gothenburg`.

[22] RMS, Dynamic Test Systems. *Steering Wheel FEL20*. Feb. 25, 2015. URL: `http://www.rms-testsystems.de/index.php/en/vehicle-test-systems/steering-wheel-fel20`.

[23] D. Sherman. Are We Losing Touch? A Comprehensive Comparison Test of Electric and Hydraulic Steering Assist. *Car and Driver* (2012).

[24] Swedish Standard Institute. *SS-ISO 8855:2011. Road vehicles - Vehicle dynamics and road-holding ability - Vocabulary*. 2012.

[25] Toyota Motor Corporation. *Lane Keeping Assist*. Feb. 27, 2015. URL: `http://www.toyota-global.com/innovation/safety_technology/safety_technology/technology_file/active/lka.html`.

[26] VBOX Automotive. *VBOX 3i Dual Antenna — 100Hz*. Feb. 25, 2015. URL: `https://www.vboxautomotive.co.uk/index.php/en/products/data-loggers/vbox-3i-dual-antenna`.

[27] VBOX Automotive. *VBOX Internal Measurement Unit*. Feb. 25, 2015.

[28] W. F. Milliken, D. L. Milliken. *Race Car Vehicle Dynammics*. SAE International, 1994.

Appendices

A Test Vehicle Parameters

c_λ = 51% front, Roll stiffness distribution
c_Φ = 70,000 $\frac{\text{N}}{\text{rad}}$, Total roll stiffness
h = 0.543 m, CoG height from ground
h_0 = 0.4755 m, Height of CoG above roll axis
h_1 = 0.045 m, Front roll center height
h_2 = 0.101 m, Rear roll center height
$I_{w_{yy}}$ = 1.2 kgm^2, Wheel moment of inertia about y-axis
I_{xx} = 800 kgm^2, Vehicle moment of inertia about x-axis
I_{zz} = 2617 kgm^2, Vehicle moment of inertia about z-axis
m = 1675 kg, Vehicle total mass
m_s = 1533 kg, Vehicle sprung mass
m_w = 22.5 kg, Wheel mass
l_f = 1.093 m, Distance from CoG to front axle
l_r = 1.582 m, Distance from CoG to rear axle
L = 2.675 m, Wheelbase
k_λ = 0.56% front, Roll damping distribution
k_Φ = 8000 $\frac{\text{N}}{\text{rad/s}}$, Total roll damping
K_u = 0.00529, Understeer gradient
n_{st} = 15.9, Steering ratio
$r_{disc,f}$ = 0.133 m, Front brake disc effective radius
$r_{disc,r}$ = 0.121 m, Rear brake disc effective radius
R = 0.307 m, Wheel radius
w_f = 1.515 m, Front trackwidth
w_r = 1.508 m, Rear trackwidth

B Simulink Controller

This appendix gives an overview of the Simulink architecture where Figure B.2 illustrates the yaw rate calculator described in Section 3.2. Figure B.1 illustrates the DBS in its entirety as described in Section 3.1. The system in Figure B.1 is implemented in CarSim and the only way it differs from the test vehicle version is that the block to the right named *CarSim S-Function* would instead be the EHB unit block provided by TNO as described in Section 3.4. Figure B.3 illustrates the brake limiter described in Section 3.2.1.

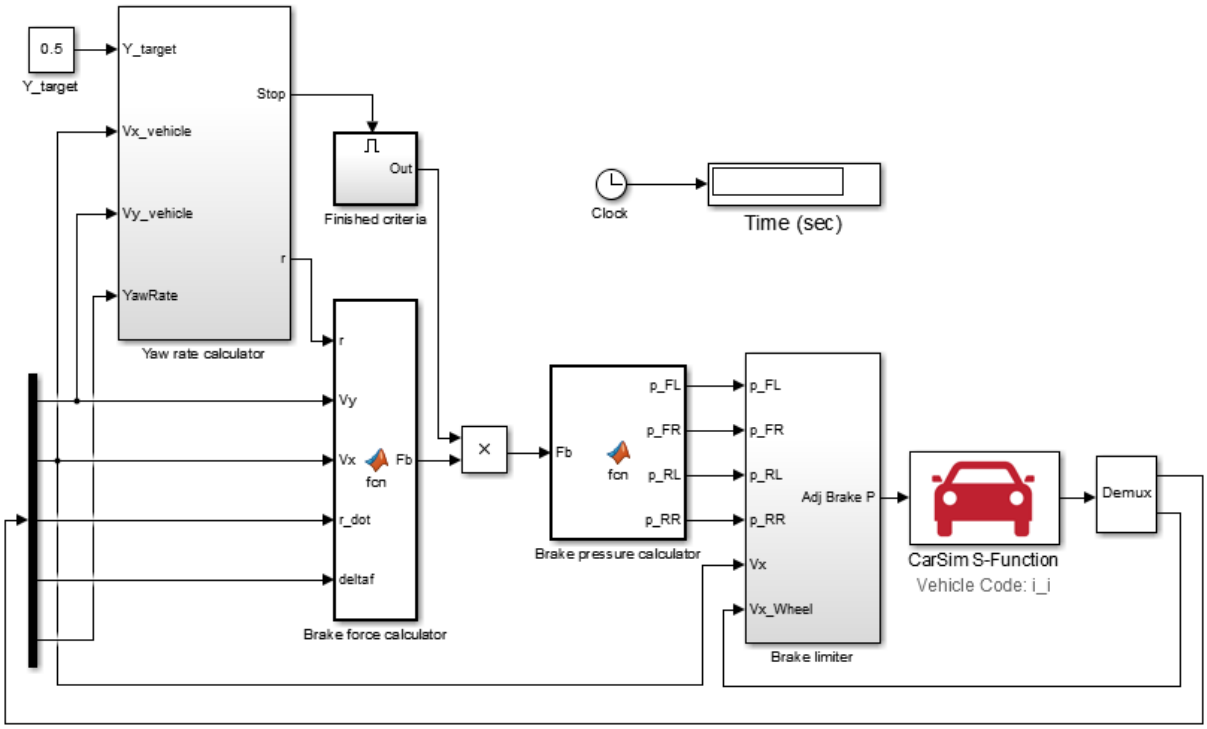

Figure B.1: *Simulink differential braking system overview*

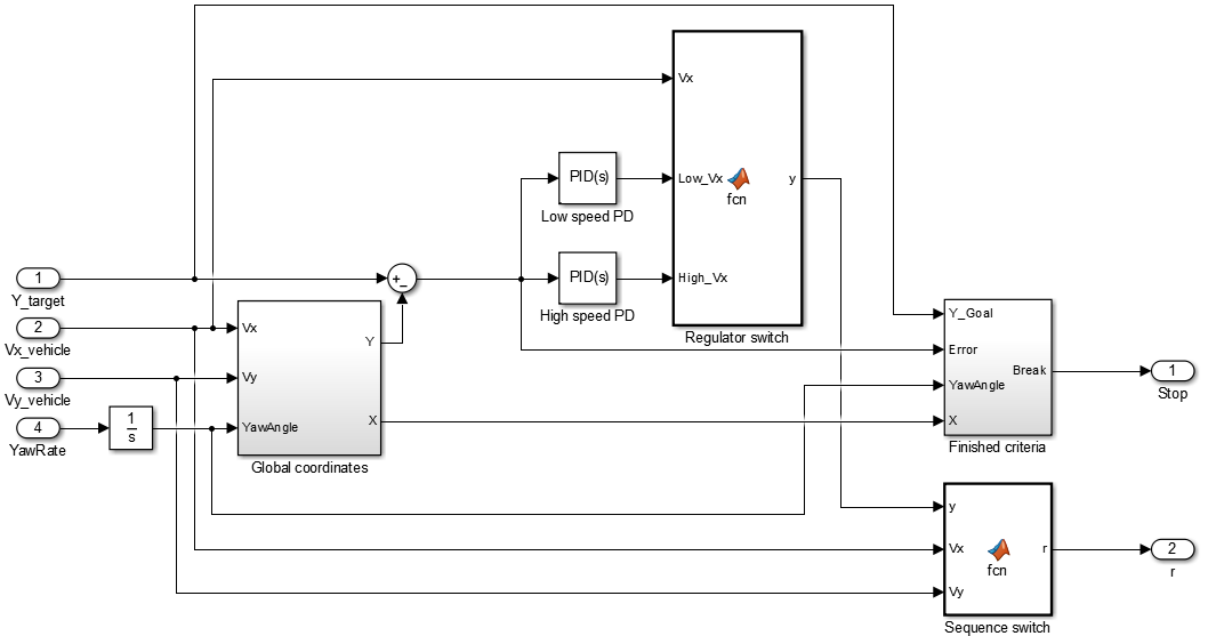

Figure B.2: *Simulink yaw rate calculcator*

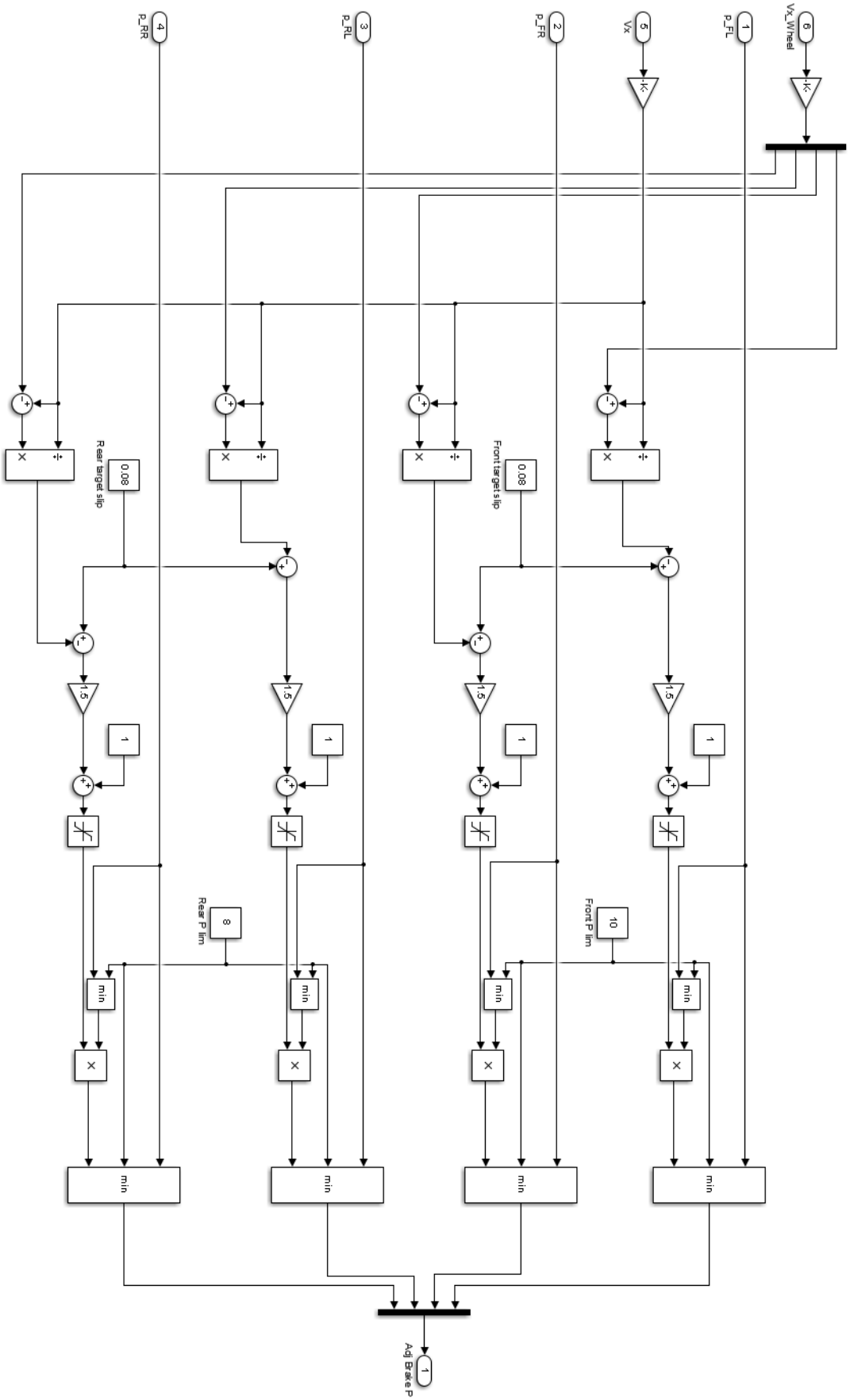

Figure B.3: *Simulink brake limiter*

C Sensor Verification

In Section 3.4.1 the precision and accuracy of the in-vehicle CAN-signals were not known and several tests were conducted where the CAN-signals were compared to corresponding VBOX signals to determine the accuracy of the CAN-signals. The comparative graphs of these two systems are found in this appendix.

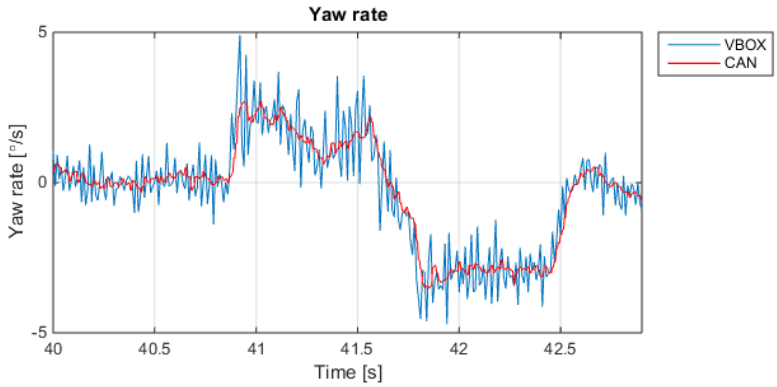

Figure C.1: *Yaw rate comparison between in-vehicle CAN-bus and VBOX*

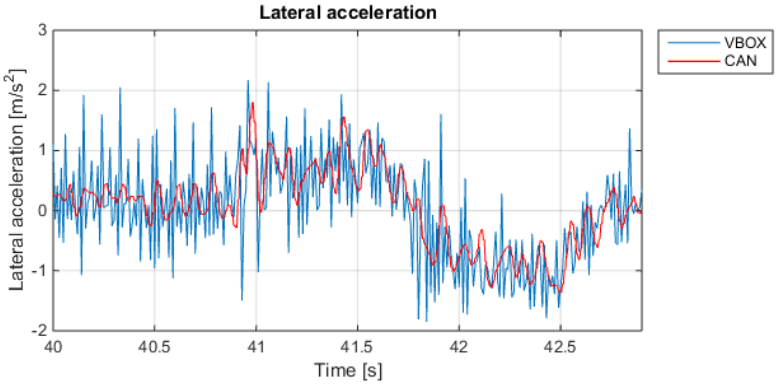

Figure C.2: *Lateral acceleration comparison between in-vehicle CAN-bus and VBOX*

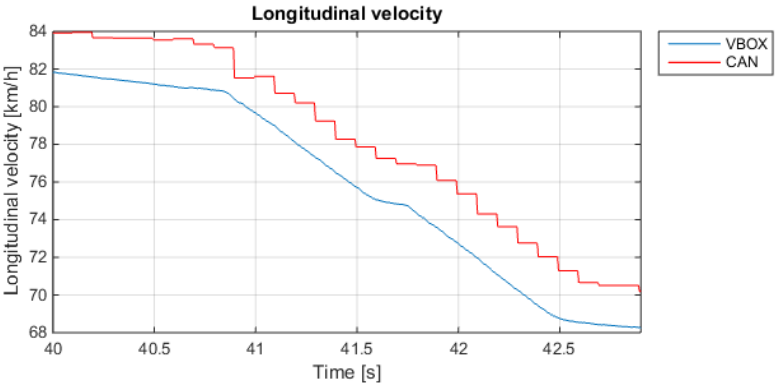

Figure C.3: *Longitudinal velocity comparison between in-vehicle CAN-bus and VBOX*

D Vehicle Parameters & Result Tables

D.1 CarSim Vehicle Parameters

In this appendix, modified CarSim vehicle parameters are shown that have been adjusted for the simulated vehicle model to accurately represent the test vehicle as described in Section 3.5.

Table D.1: Vehicle parameters used in CarSim

Parameter	current	original	unit
Sprung mass			
Height for animation	1450	1471	mm
Width for animation	1750	1795	mm
Distance from x axis to center of LF wheel	320	340	mm
Distance from x axis to center of RF wheel	320	340	mm
Distance from x axis to center of LR wheel	320	325	mm
Distance from x axis to center of RR wheel	320	325	mm
Lf	1093	1110	mm
CoG height	543	520	mm
Wheel base	2677	2780	mm
Sprung mass	1533	1370	kg
Ixx	800	671.3	kg*m^2
Izz	2617	2315.3	kg*m^2
Iyy	1972.8	1972.8	kg*m^2
Aero			
Frontal area	2.17	2.3	m^2
Reference length	2775	2775	mm
Drag coefficient	0.3	0.3	-
Vehicle animation			
Length	4650	4300	mm
Height	1450	1433	mm
Width	1750	1753	mm
Wheel center spacing Front Axle	1515	1600	mm
Wheel center spacing Rear Axle	1502	1600	mm
Wheel center height	320	280	mm
Powertrain FWD			
Internal engine model	200	150	Kw
Internal torque converter model	200	150	kW
Internal transmission model	6 speed transmission	6 speed transmission	
Drive shaft roll effect	Ignore	Cause positive roll	
Steering system			
Lateral offset @ center FL	60.6	77	mm
Kingpin inclination FL	11.8	12.5	deg
X coord. Of KP @ center FL	0	5	mm
Caster angle FL	3.3	9.5	deg
Lateral offset @ center FR	60.6	77	mm
Kingpin inclination FR	11.8	12.5	deg
X coord. Of KP @ center FR	0	5	mm
Caster angle FR	3.3	9.5	deg
Steering rack ratio	51	40	mm/rev
Rack to front wheels	Graph from KNC data	Graph	deg/mm
Front steering compliance	No steer compliance	0.001	deg/N-m

Table D.2: Vehicle parameters used in CarSim

Front suspension kinematics				
Track width		1515	1550	mm
Unspring mass (both sides)		115	80	kg
Static Camber		-0.9	0	deg
Static Toe		0.12	0	deg
Camber as a nonlinear function of bump	Graph from KNC data	Graph		deg/mm
Toe as a nonlinear function of bump	Graph from KNC data	Graph		deg/mm

Rear suspension kinematics				
Track width		1502	1550	mm
Unspring mass (both sides)		100	80	kg
Static Camber		0	0	deg
Static Toe		0	0	deg
Camber as a nonlinear function of bump	Graph from KNC data	Graph		deg/mm
Toe as a nonlinear function of bump	Graph from KNC data	Graph		deg/mm

Front Springs, Dampers and Compliance				
Spring stiffness FL		35.3	153	N/mm
Friction		0	20	N
Jounce/Rebound stops FL		66/-101	Graph	mm
Damping	Graph from KNC data	Graph		N/mm*s
Steer / Fx		-1.32E-03	0	deg/N
Steer / Fy		3.80E-05	-2.70E-07	deg/N
Auxiliary Roll moment/roll relative to axle		970	384	Nm/deg

Rear Springs, Dampers and Compliance				
Spring stiffness RL		31	82	N/mm
Friction		0	20	N
Jounce/Rebound stops RL		98/-98	Graph	mm
Damping	Graph from KNC data	Graph		N/mm*s
Steer / Fx		1.20E-05	0	deg/N
Steer / Fy		2.40E-05	-1.00E-07	deg/N
Auxiliary Roll moment/roll relative to axle		418	344	Nm/deg

Brake System, 4wd sytem				
Brake torque at wheel FL		108	65.86	Nm/Mpa
Brake torque at wheel FR		108	65.85	Nm/Mpa
Brake torque at wheel RL		94	62.768	Nm/Mpa
Brake torque at wheel RR		94	62.768	Nm/Mpa
Fluid dynamics transport delay FL		0.1	0	s
Fluid dynamics transport delay FR		0.1	0	s
Fluid dynamics transport delay RL		0.1	0	s
Fluid dynamics transport delay RR		0.1	0	s
Front ABS	Disabled		-	
Rear ABS	Disabled		-	

Table D.3: Tire parameters used in CarSim

Tires, Pacejka 5.2			
PKY1	-12	-12.95	-
PKY2	0.7	1.72	-
PKY3	0.3	0.22	-
Mu X	0.3	1	-
Mu Y	0.3	1	-
R0	0.307	0.298	-
FZ0	4900	4100	-
Contact patch length	70	90	mm
Contact patch width	225	215	mm

D.2 Description of Conducted Tests

This appendix describes the varying test conditions for all the conducted experimental tests.

Table D.4: Test case conditions

Case	Actuating system	Vehicle weight	Chassis modification	Road condition	y [m]	Vx [km/h]	Comment
1	DBS	Unladen	Standard	DRY	0.5	50	
2	DBS	Unladen	Standard	***WET***	0.5	50	
3	***Steering***	Unladen	Standard	DRY	0.5	50	
4	DBS	Unladen	Standard	DRY	0.5	50	***Maximum brake pressure***
5	*Simulation*	Unladen	Standard	Dry	0.5	50	
6	DBS	Unladen	Standard	DRY	0.5	80	
7	DBS	Unladen	Standard	***WET***	0.5	80	
8	DBS	Unladen	***Spacer***	***WET***	0.5	80	
9	DBS	***Laden***	Standard	DRY	0.5	80	
10	DBS	***Laden***	Standard	***WET***	0.5	80	
11	***Steering***	Unladen	Standard	DRY	0.5	80	
12	DBS	Unladen	Standard	DRY	0.5	80	***Maximum brake pressure***
13	DBS	Unladen	Standard	***WET***	-0.5	80	
14	*Simulation*	Unladen	Standard	DRY	0.5	80	
15	DBS	Unladen	Standard	DRY	0.5	120	
16	DBS	Unladen	Standard	***WET***	0.5	120	
17	***Steering***	Unladen	Standard	DRY	0.5	120	
18	DBS	Unladen	Standard	DRY	0.5	120	***Maximum brake pressure***
19	*Simulation*	Unladen	Standard	DRY	0.5	120	
20	DBS	Unladen	Standard	DRY	1	50	
21	DBS	Unladen	Standard	***WET***	1	50	
22	***Steering***	Unladen	Standard	DRY	1	50	
23	*Simulation*	Unladen	Standard	DRY	1	50	
24	DBS	Unladen	Standard	DRY	1	80	
25	DBS	Unladen	Standard	***WET***	1	80	
26	***Steering***	Unladen	Standard	DRY	1	80	
27	*Simulation*	Unladen	Standard	DRY	1	80	
28	DBS	Unladen	Standard	DRY	1	120	
29	DBS	Unladen	Standard	***WET***	1	120	
30	***Steering***	Unladen	Standard	DRY	1	120	
31	*Simulation*	Unladen	Standard	DRY	1	120	

D.3 Performance Results From Conducted Tests

Performance results from the conducted experimental tests described in Table D.4.

Table D.5: Performance results

Case	y [m]	Vx [km/h]	Max Ay [m/s^2]	Max Ax [m/s^2]	Max Yaw rate [deg/s]	Max SW torque [Nm]	x [m]	Duration [s]	Road condition	Comment
1	0.5	50	1.2267	5.387	4.8236	3.7714	14.4487	1.17	DRY	
2	0.5	50	1.1623	4.3001	4.6112	2.6296	14.641	1.17	WET	
3	0.5	50	5.094	0.6117	21.8984	N/A	8.9119	0.6483	DRY	Steered maneuver
4	0.5	50	2.19	8.1248	9.7106	6.3868	9.3387	1.075	DRY	Maximum brake pressure
5	0.5	50	2.9012	0.6095	16.27	17.598	8.504	0.65	DRY	Simulated maneuver
6	0.5	80	2.4751	5.4472	8.3666	6.2192	17.2721	0.825	DRY	
7	0.5	80	2.0676	5.1903	7.1532	5.1441	18.0977	0.855	WET	
8	0.5	80	2.2487	4.9351	7.4337	5.3746	16.9998	0.8	WET	Spacer
9	0.5	80	2.2202	4.6686	7.8112	5.224	17.9115	0.855	DRY	Laden
10	0.5	80	1.4765	3.9871	5.5162	4.1845	21.2525	1.01	WET	Laden
11	0.5	80	3.9162	0.3853	14.7117	N/A	14.9941	0.6817	DRY	Steered maneuver
12	0.5	80	4.36	6.9751	13.2943	6.7357	13.8795	0.68	DRY	Maximum brake pressure
13	-0.5	80	2.0535	5.0208	7.0471	5.1506	17.0667	0.8	WET	Right maneuver
14	0.5	80	3.3721	0.4971	14.111	15	14.381	0.675	DRY	Simulated maneuver
15	0.5	120	3.9711	6.6011	11.5626	8.0923	20.6364	0.645	DRY	
16	0.5	120	3.5804	5.3223	9.0101	6.006	21.708	0.675	WET	
17	0.5	120	2.379	0.4031	7.9546	N/A	36.61	1.07	DRY	Steered maneuver
18	0.5	120	5.9188	7.947	14.6614	7.906	17.6102	0.56	DRY	Maximum brake pressure
19	0.5	120	2.2455	0.4331	7.0117	10	29.333	0.9	DRY	Simulated maneuver
20	1	50	1.1696	4.9271	4.851	3.475	18.9777	1.6483	DRY	
21	1	50	1.1895	4.8671	4.8671	N/A	19.018	1.661	WET	
22	1	50	8.6873	1.633	38.7222	N/A	9.7107	0.72	DRY	Steered maneuver
23	1	50	4.944	1.052	29.87	29.791	9.554	0.725	DRY	Simulated maneuver
24	1	80	2.9369	6.1514	8.9359	7.1266	21.4353	1.045	DRY	
25	1	80	2.1073	4.678	6.3974	4.9512	23.6325	1.1358	WET	
26	1	80	6.5743	0.8315	26.4357	N/A	14.5986	0.6817	DRY	Steered maneuver
27	1	80	7.2082	1.6514	45.191	46.656	14.235	0.675	DRY	Simulated maneuver
28	1	120	4.5066	7.146	12.2405	8.5912	25.9101	0.82	DRY	
29	1	120	4.1385	5.3976	9.4751	6.1592	28.1515	0.8817	WET	
30	1	120	4.5838	0.9478	15.8634	N/A	34.79	1.0683	DRY	Steered maneuver
31	1	120	4.0219	0.5114	13.468	10	31.719	0.975	DRY	Simulated maneuver

E Carsim Calibration Graphs

For the vehicle model to correspond to the test vehicle in the handling diagram in Section 3.5.1, the lateral tire parameters in CarSim were adjusted. The tire performance from the adjusted tires compared to the standard tires in CarSim are found in Figures E.1 and E.2 below.

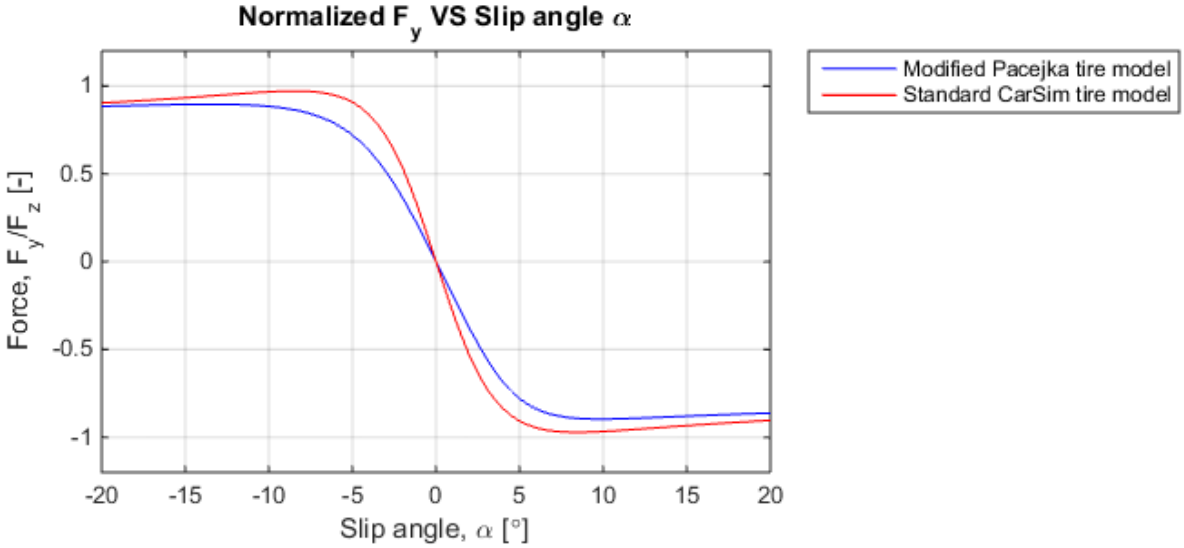

Figure E.1: *Adjusted CarSim vs. standard Pacejka lateral tire performance*

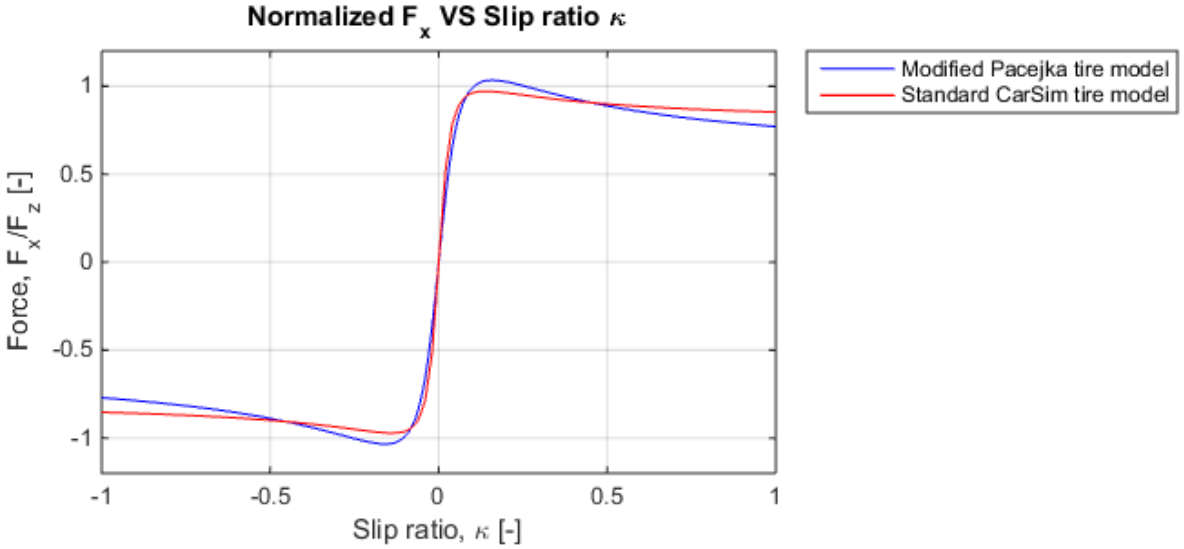

Figure E.2: *Adjusted CarSim vs. standard Pacejka longitudinal tire performance*

Both experimental and simulated brake tests were conducted as described in Section 3.5.2 to calibrate the brake performance to correlate between test vehicle and vehicle model. The resulting longitudinal acceleration from these tests are found in figures E.3 and E.4 below where the friction between brake pad and disc have been adjusted in CarSim to correlate to the test vehicle.

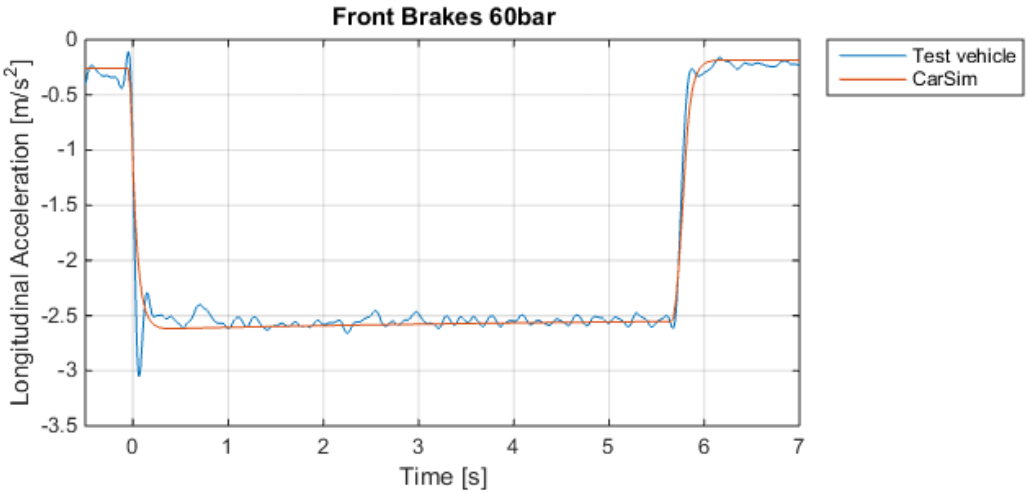

Figure E.3: *Deceleration from test vehicle vs. CarSim with adjusted brake pad friction coefficients. Front wheel braking with 60 bar brake pressure.*

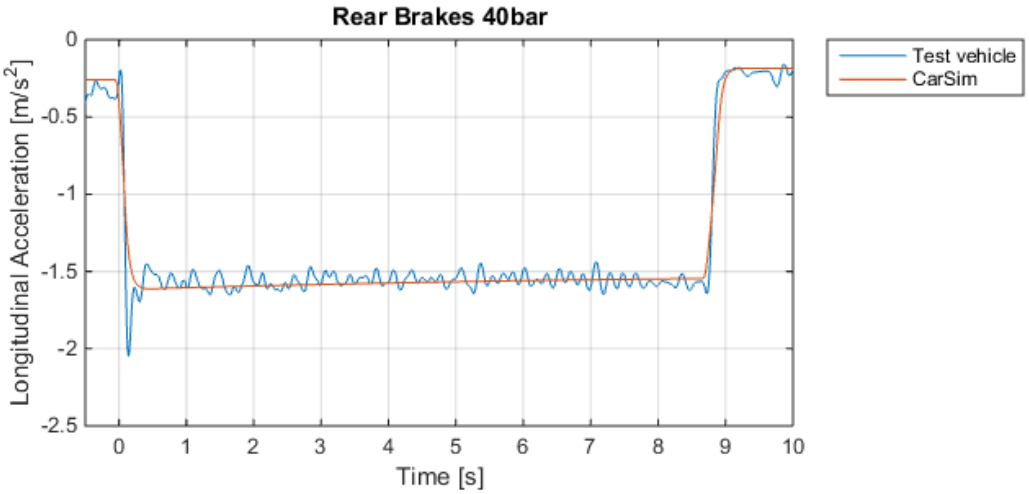

Figure E.4: *Deceleration from test vehicle vs. CarSim with adjusted brake pad friction coefficients. Rear wheel braking with 40 bar brake pressure.*

F Systematic Errors

F.1 0.5m, 80km/h, Right/Left Asymmetry

This appendix shows comparisons between a differential braking avoidance maneuver conducted to the left and to the right to analyze any possible asymmetry that could be defined as a systematic error as discussed in Section 4.1

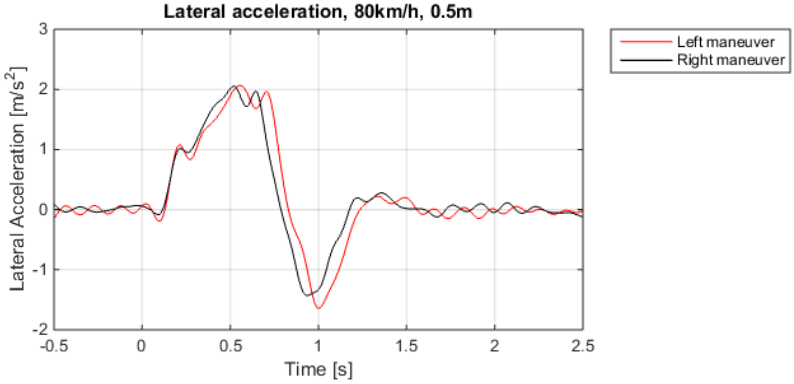

Figure F.1: *Lateral acceleration comparison between right and left maneuver*

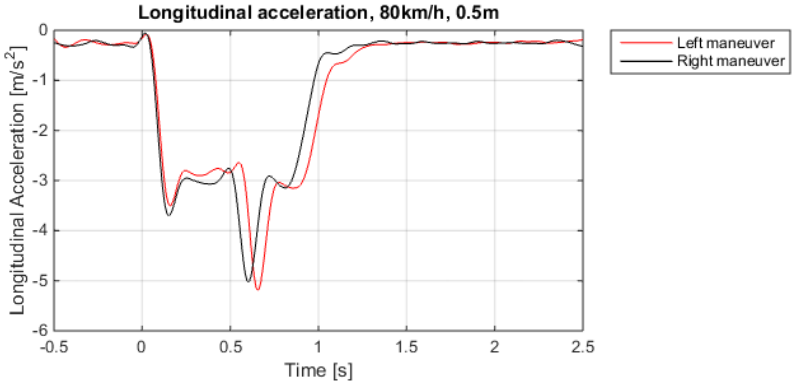

Figure F.2: *Longitudinal acceleration comparison between right and left maneuver*

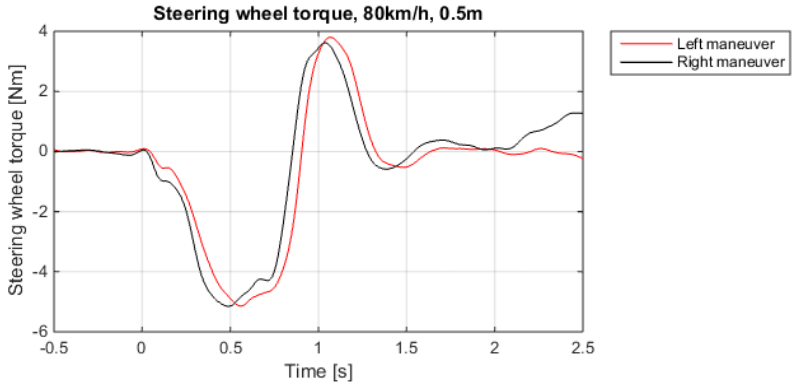

Figure F.3: *Steering wheel torque comparison between right and left maneuver*

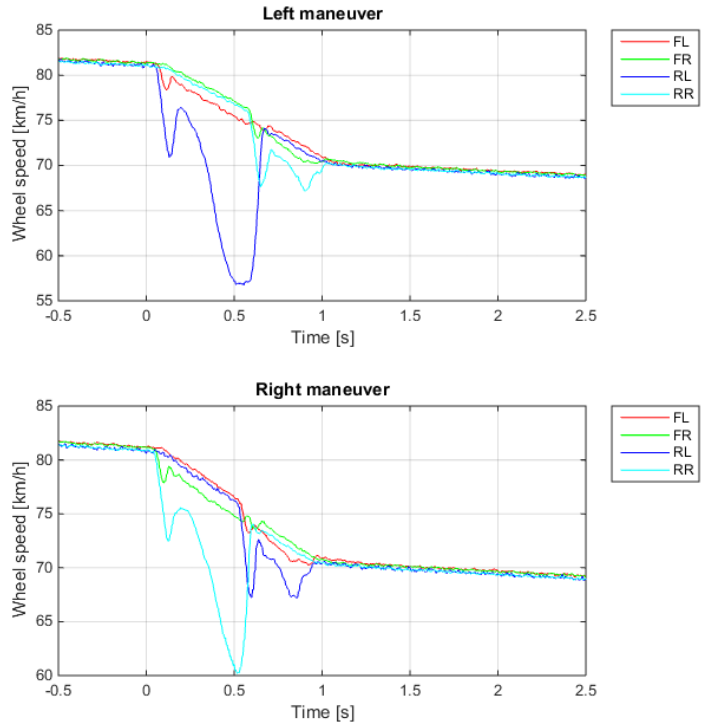

Figure F.4: *Wheel speed comparison between right and left maneuver*

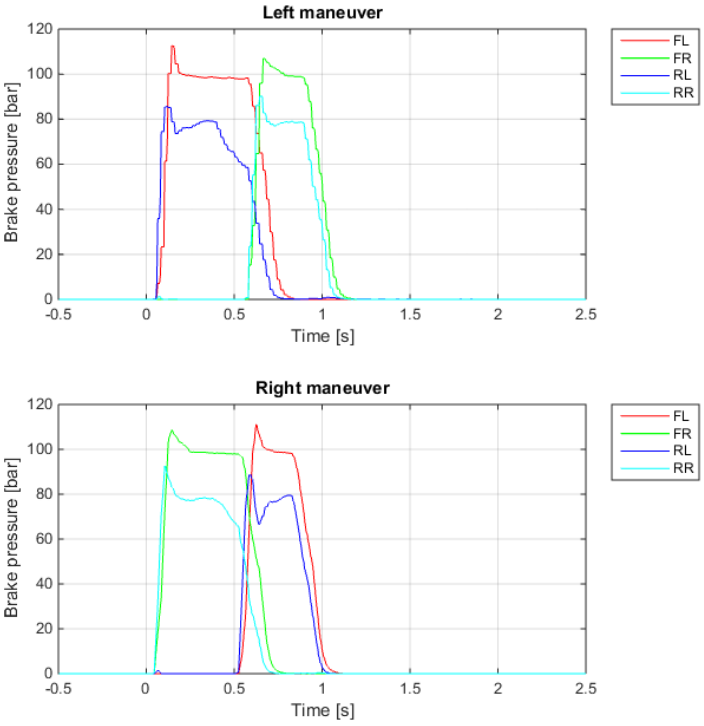

Figure F.5: *Brake pressure comparison between right and left maneuver*

G Experimental Avoidance Maneuver Results

This appendix shows the results from the experimental avoidance maneuver tests for all the various conditions and parameters specified in the test chart in Section 3.3.

G.1 0.5m, 50km/h Avoidance Maneuver

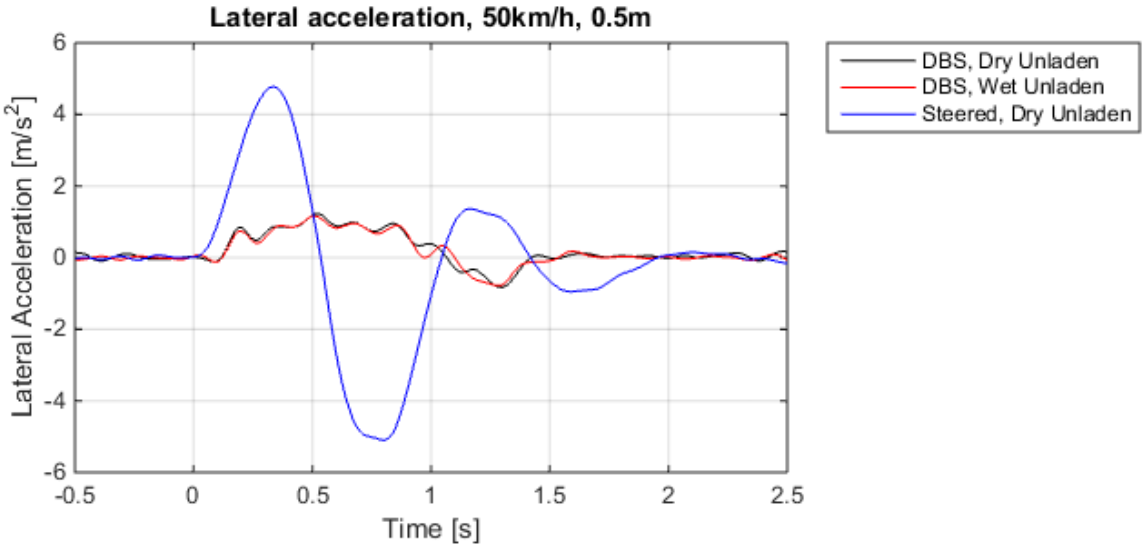

Figure G.1: *Lateral acceleration comparison*

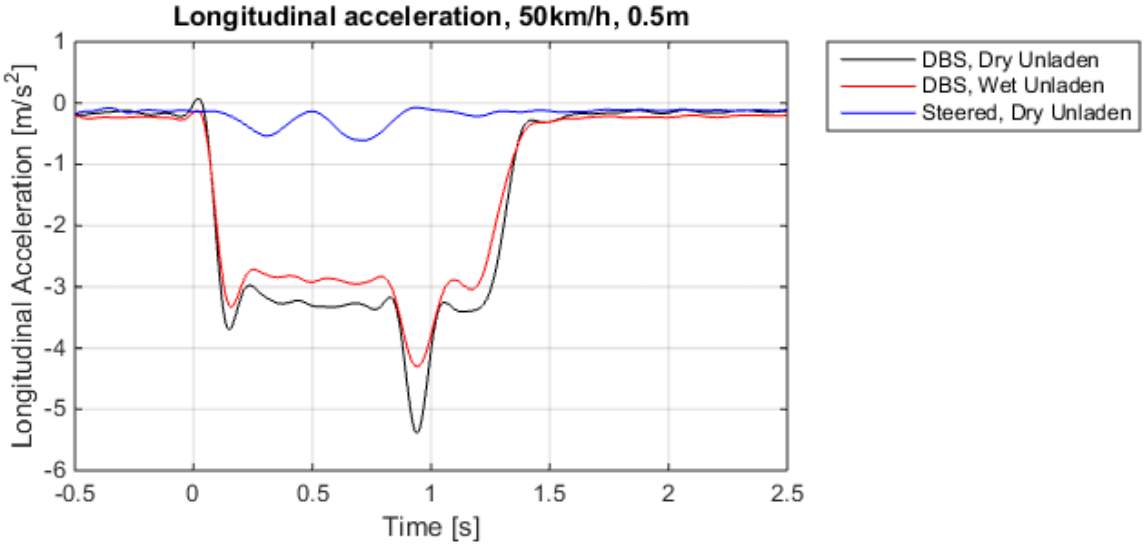

Figure G.2: *Longitudinal acceleration comparison*

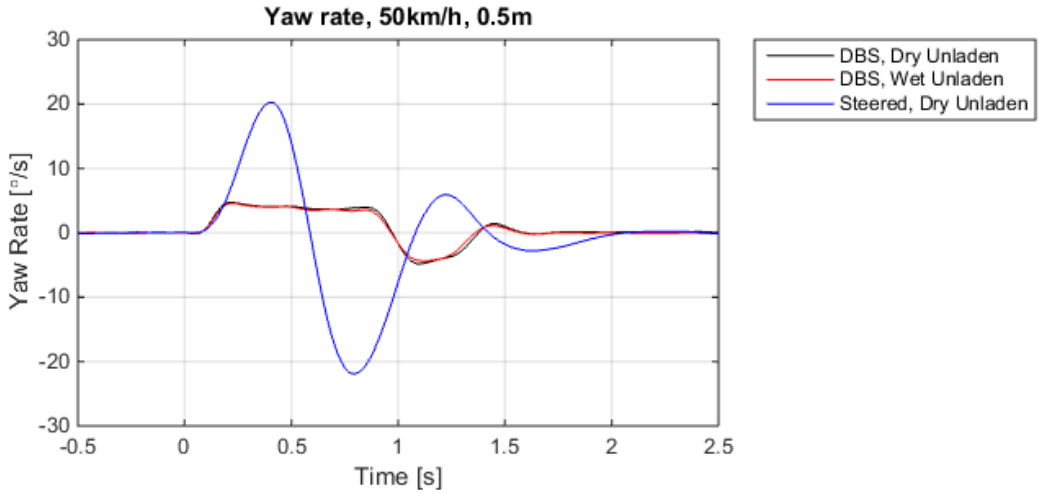

Figure G.3: *Yaw rate comparison*

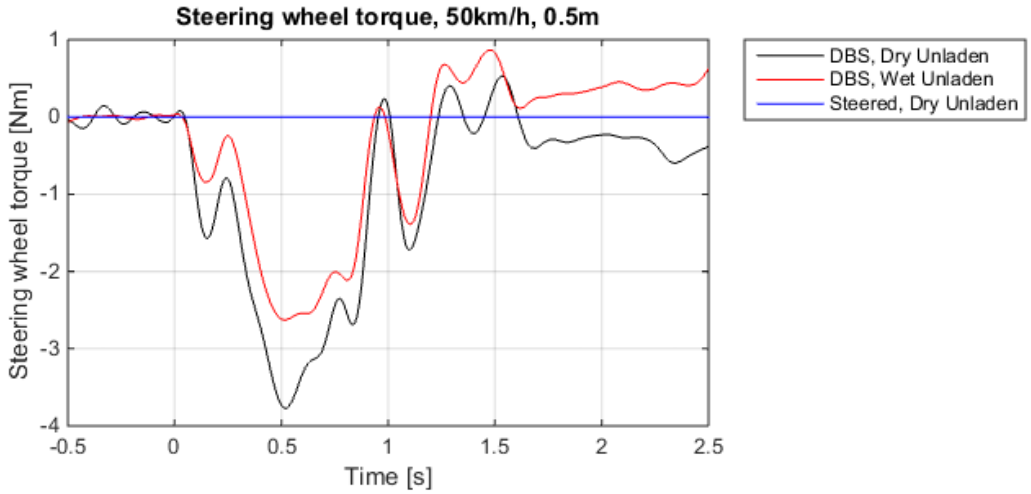

Figure G.4: *Steering wheel torque (steered maneuver not logged)*

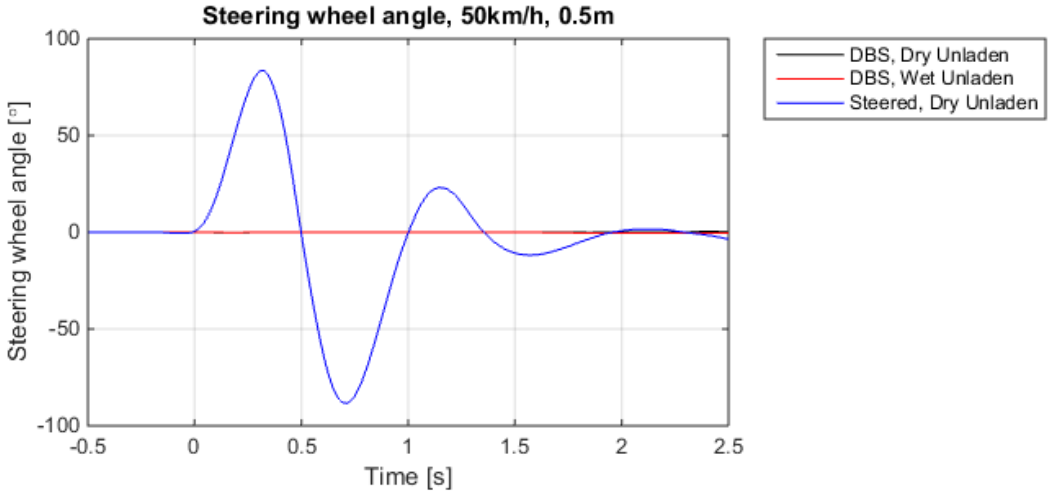

Figure G.5: *Steering wheel angle*

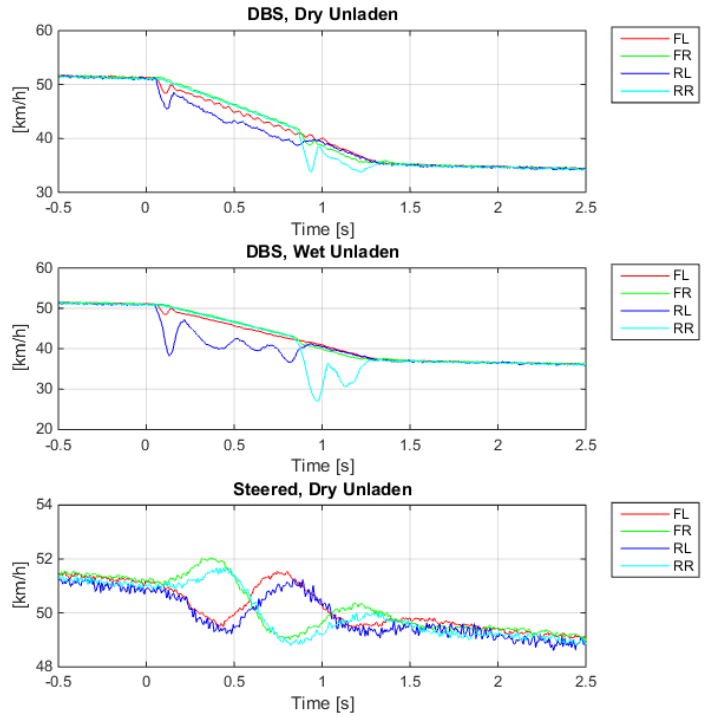

Figure G.6: *Wheel speed comparison*

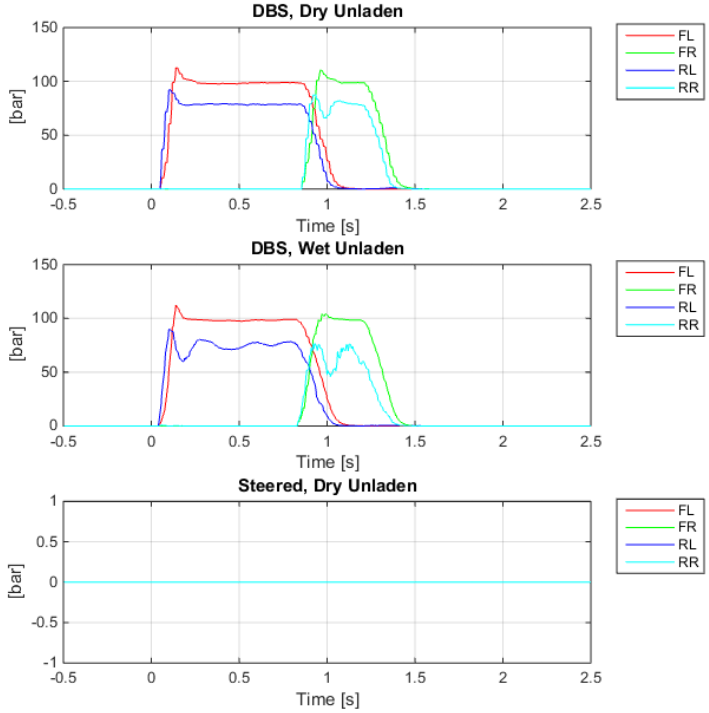

Figure G.7: *Brake pressure comparison*

G.2 0.5m, 80km/h Avoidance Maneuver

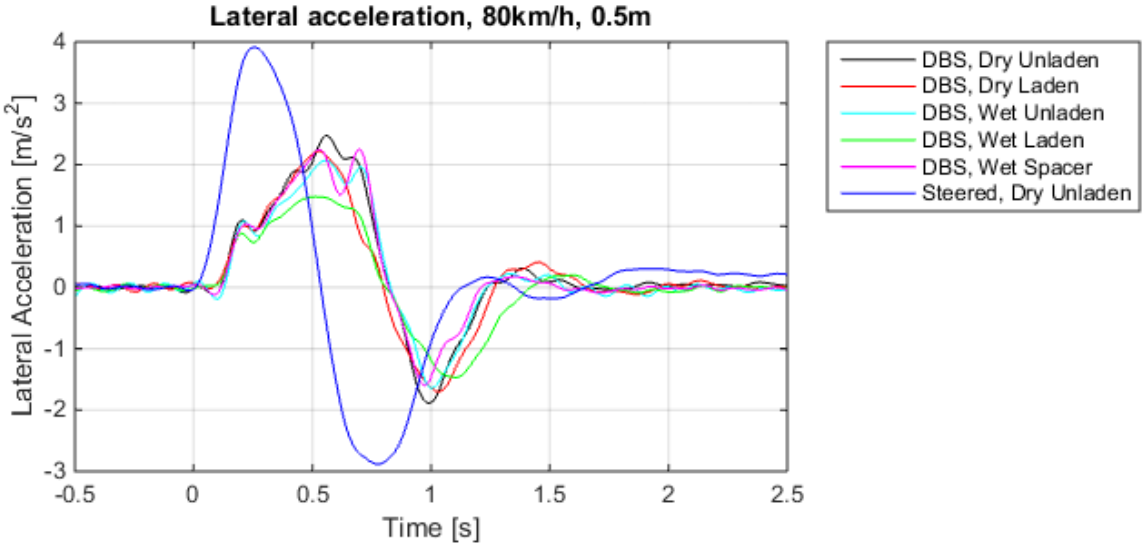

Figure G.8: *Lateral acceleration comparison*

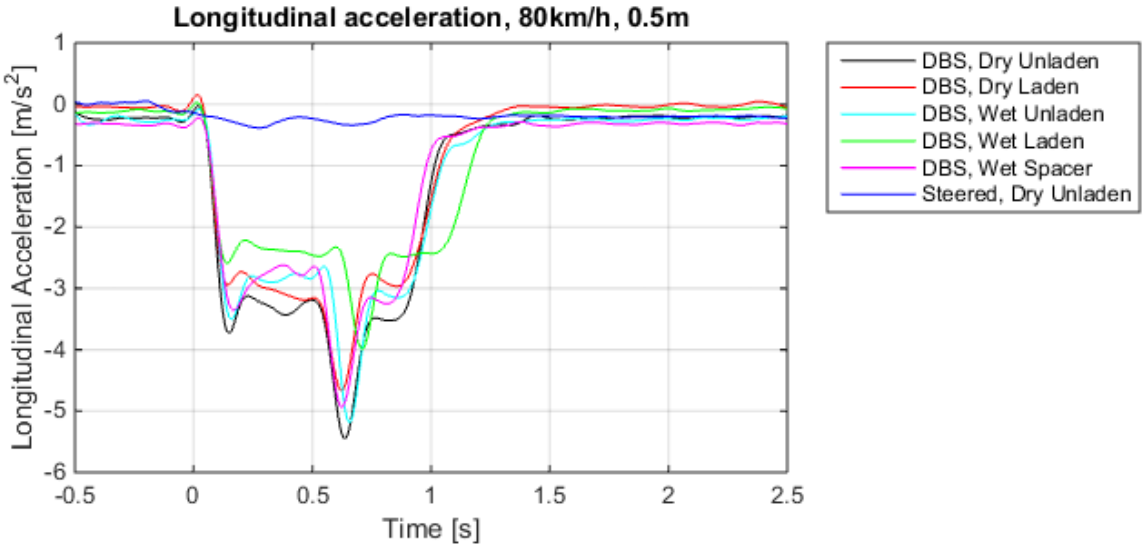

Figure G.9: *Longitudinal acceleration comparison*

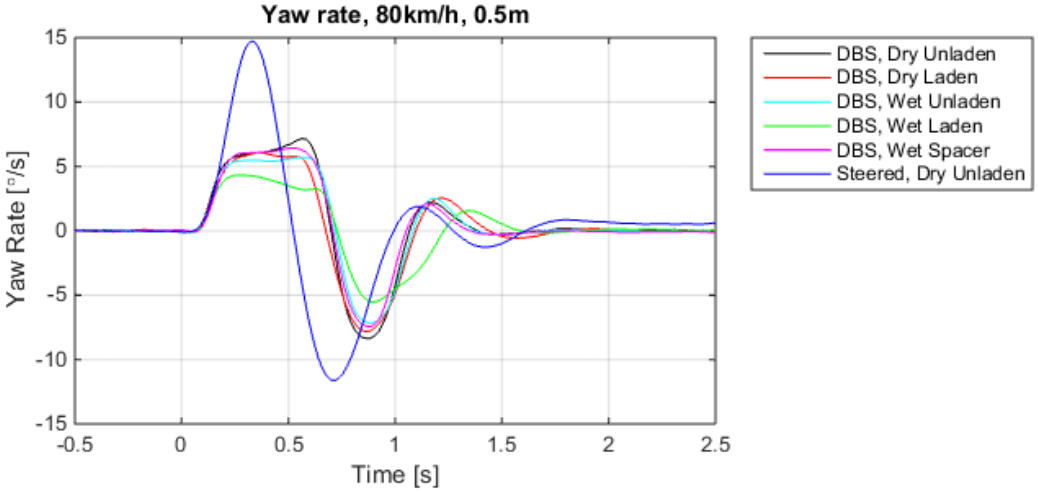

Figure G.10: *Yaw rate comparison*

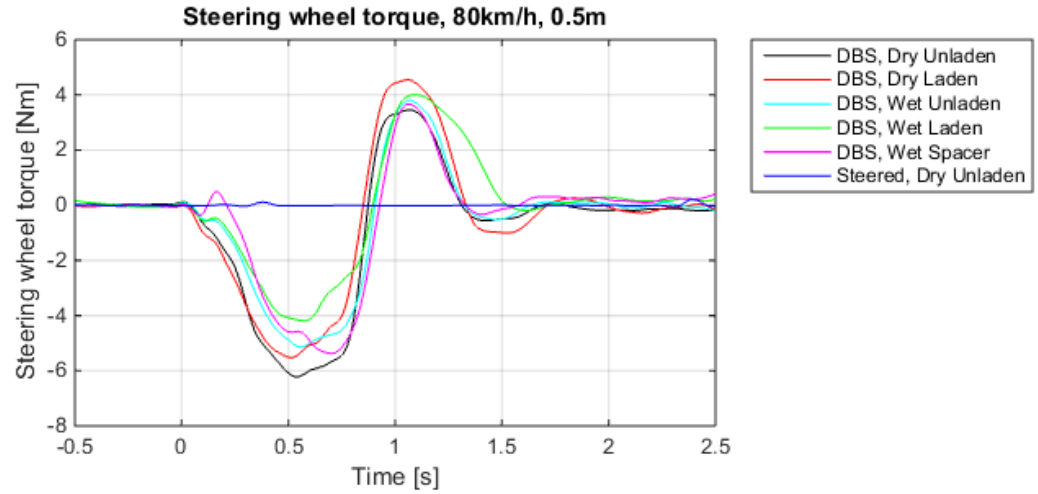

Figure G.11: *Steering wheel torque comparison (steered maneuver not logged)*

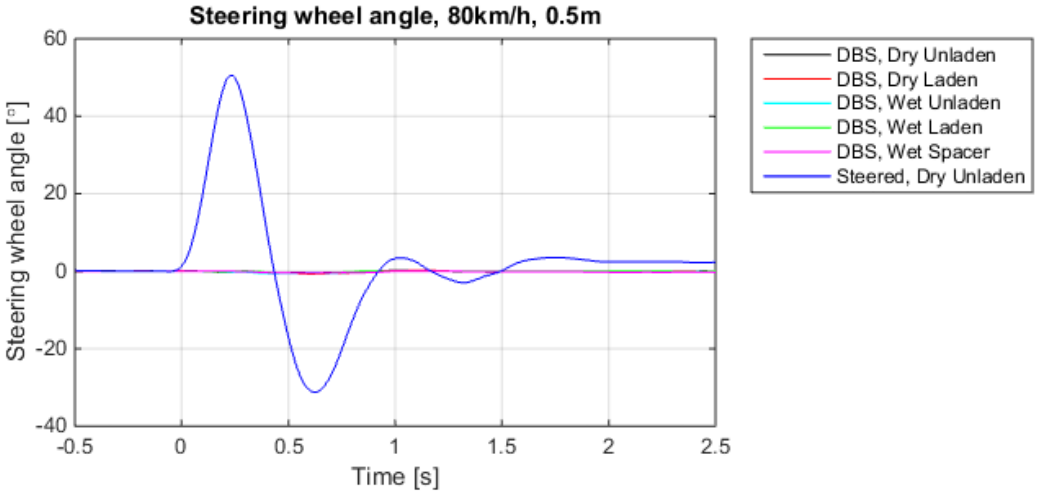

Figure G.12: *Steering wheel angle*

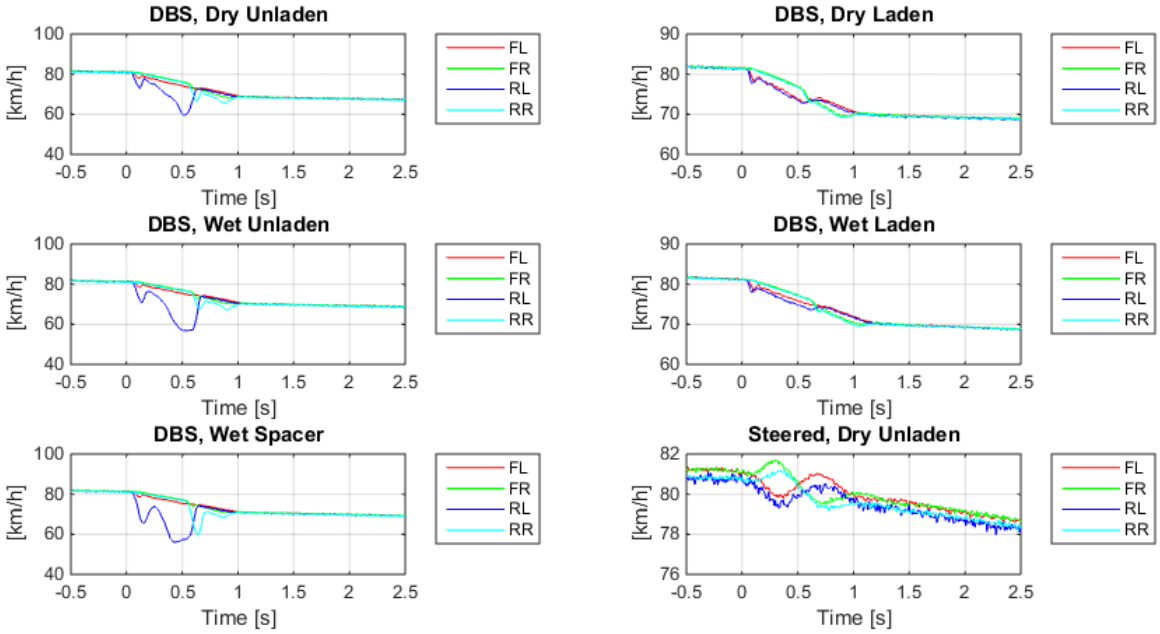

Figure G.13: *Wheel speed comparison*

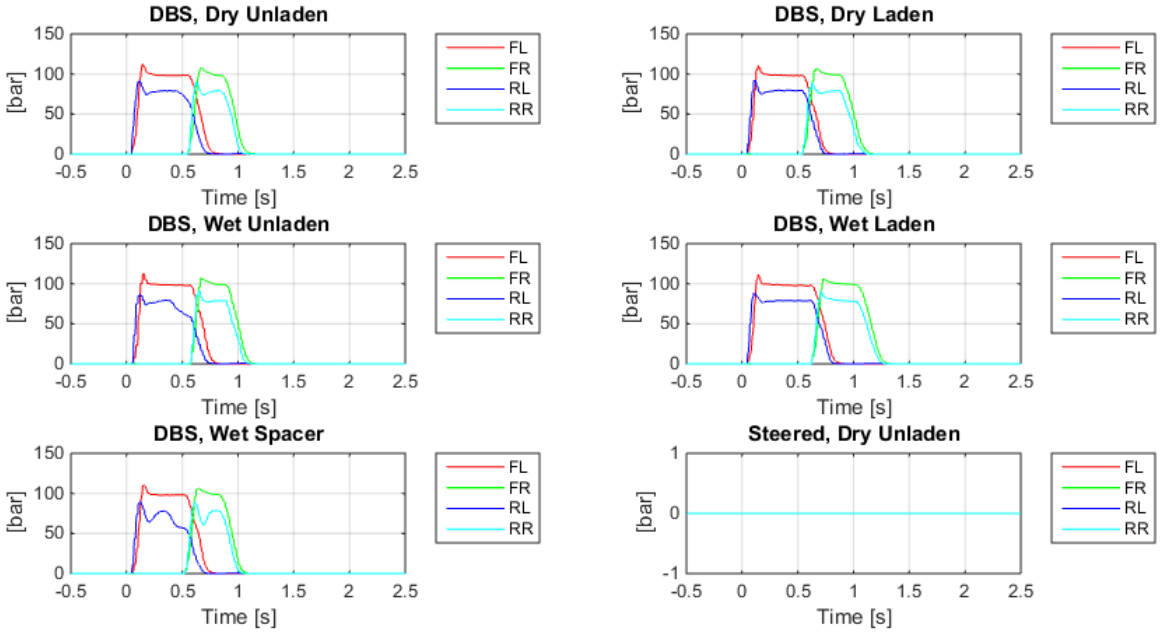

Figure G.14: *Brake pressure comparison*

G.3 0.5m, 120km/h Avoidance Maneuver

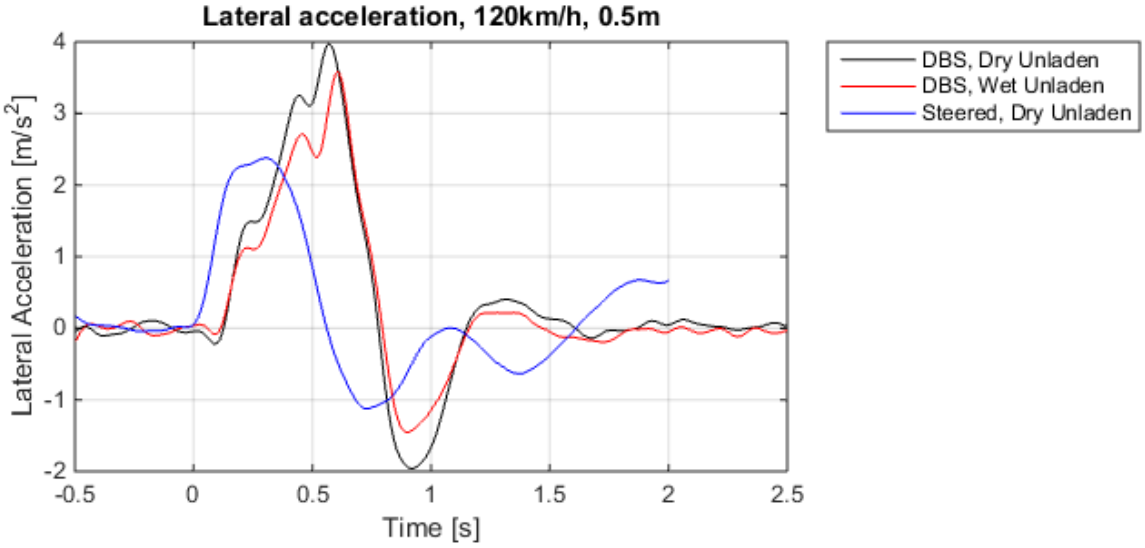

Figure G.15: *Lateral acceleration comparison*

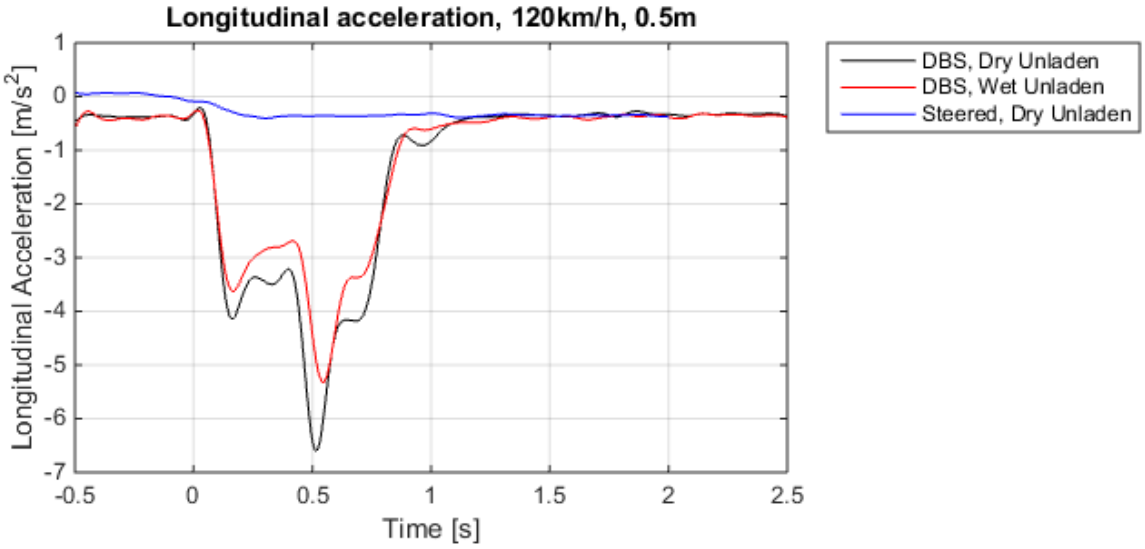

Figure G.16: *Longitudinal acceleration comparison*

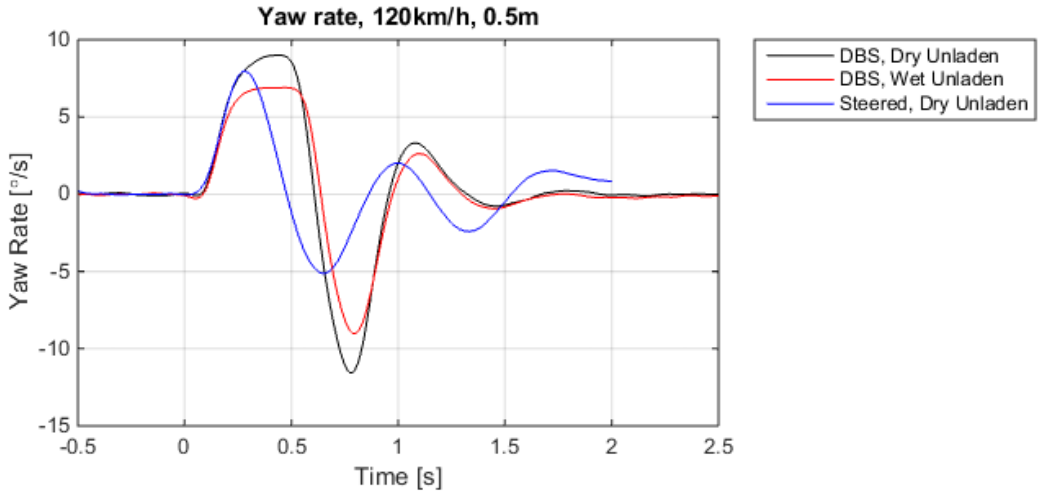

Figure G.17: *Yaw rate comparison*

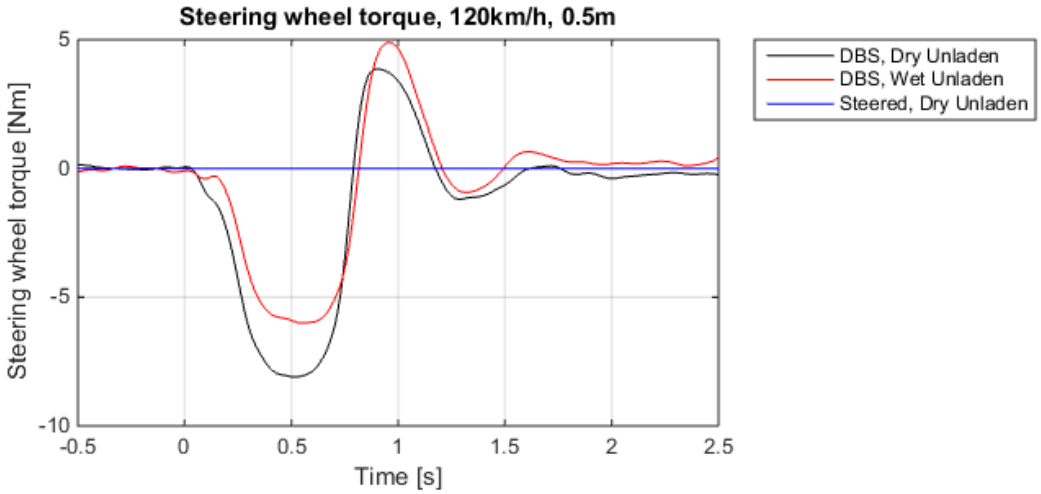

Figure G.18: *Steering wheel torque comparison (steered maneuver not logged)*

Figure G.19: *Steering wheel angle*

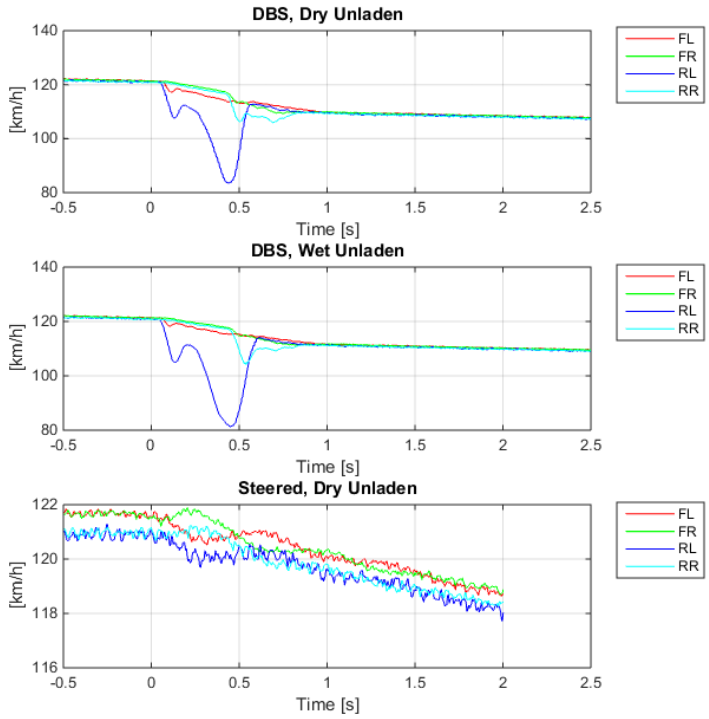

Figure G.20: *Wheel speed comparison*

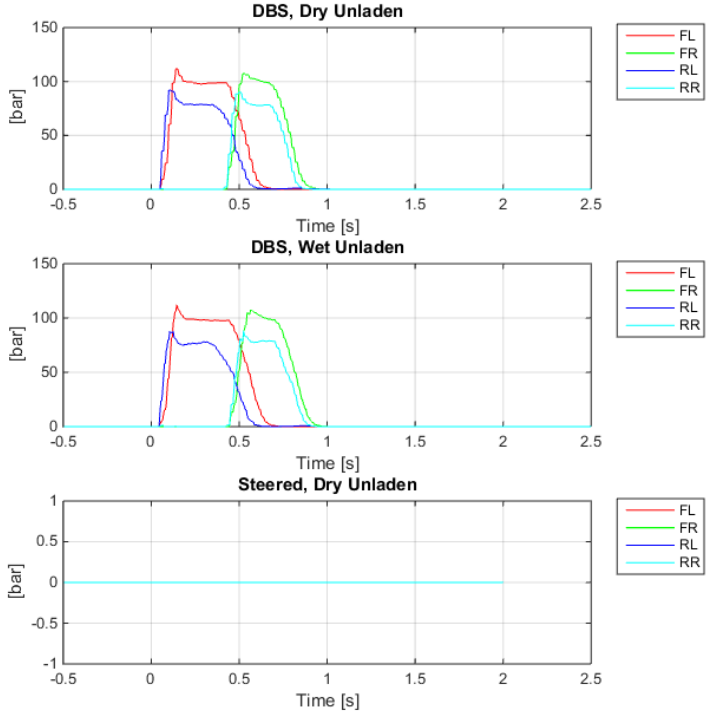

Figure G.21: *Brake pressure comparison*

G.4 1m, 50km/h Avoidance Maneuver

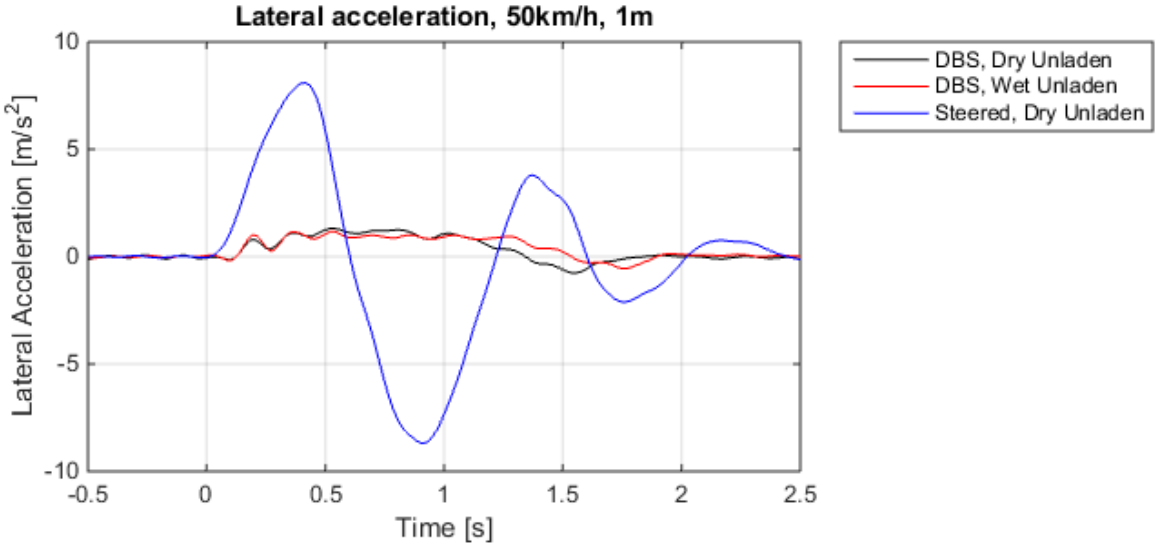

Figure G.22: *Lateral acceleration comparison*

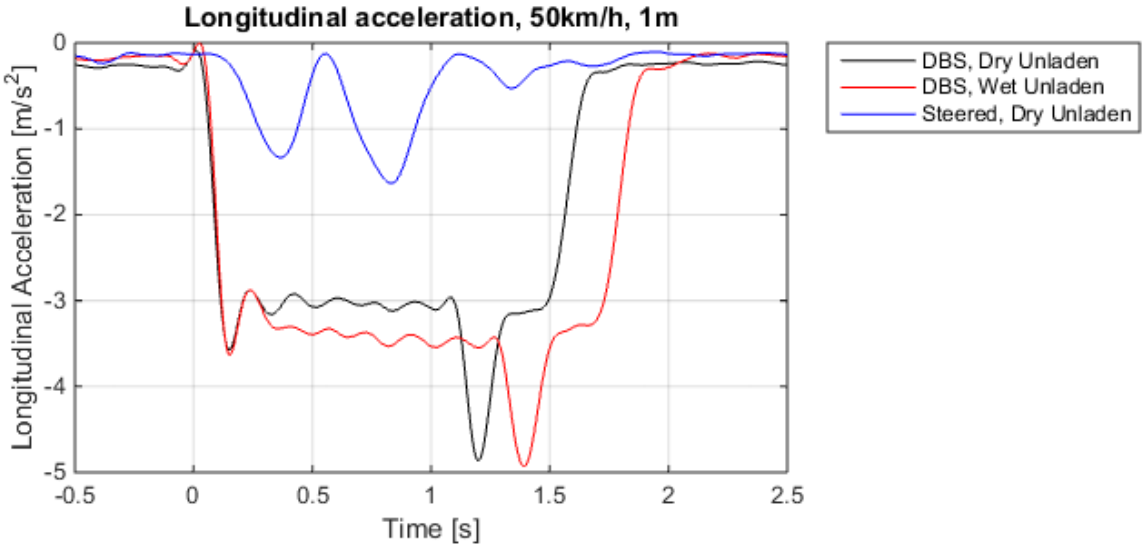

Figure G.23: *Longitudinal acceleration comparison*

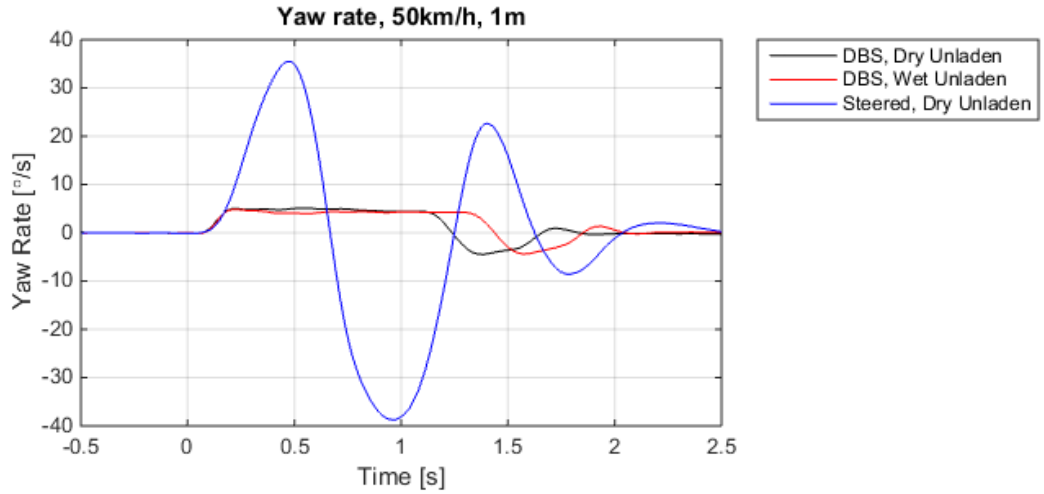

Figure G.24: *Yaw rate comparison*

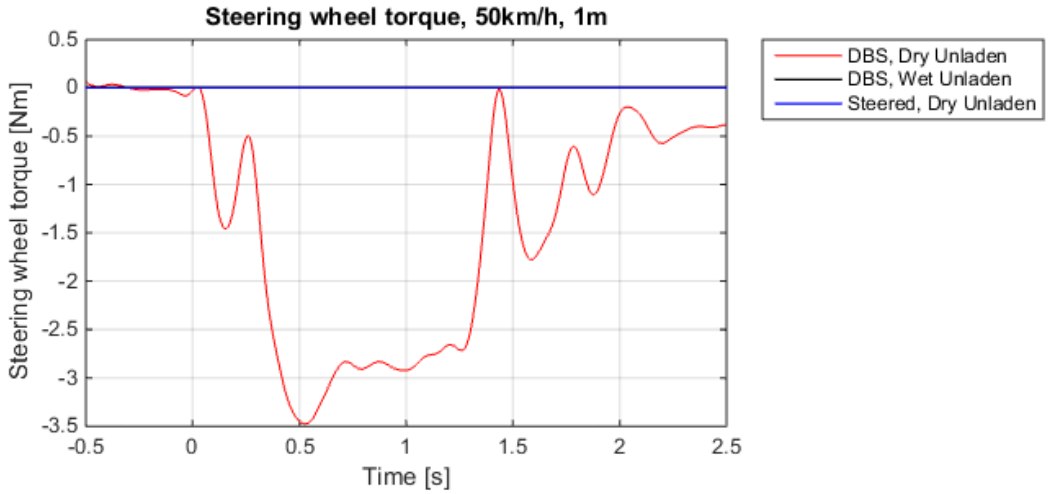

Figure G.25: *Steering wheel torque (steered maneuver and wet test not logged)*

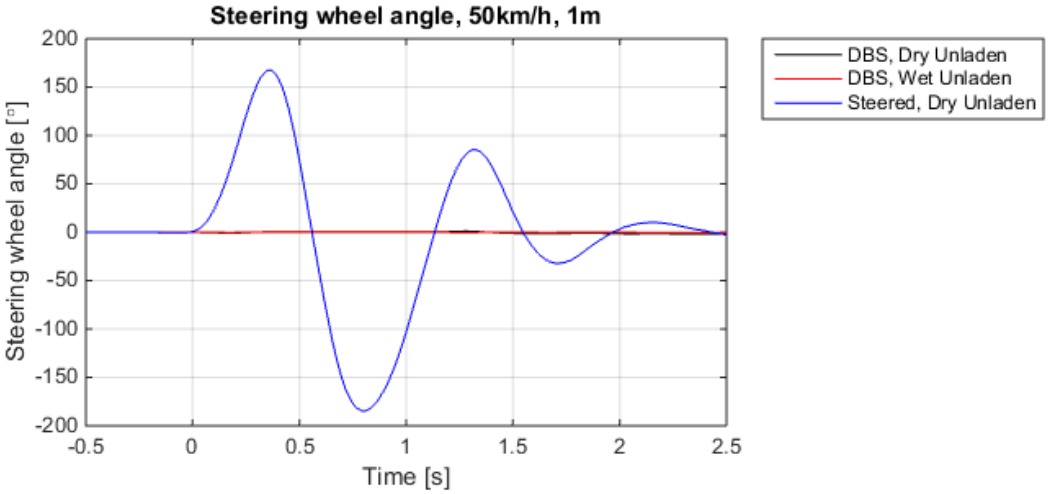

Figure G.26: *Steering wheel angle*

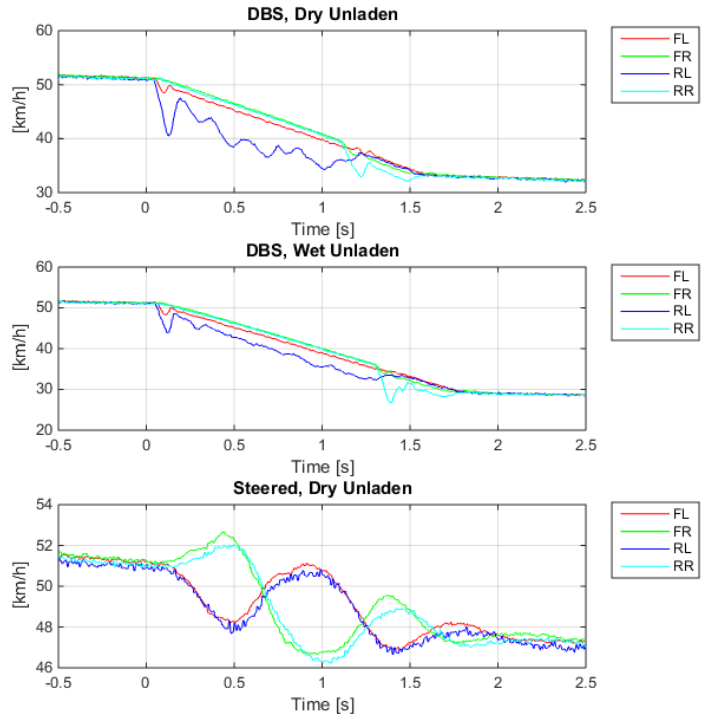

Figure G.27: *Wheel speed comparison*

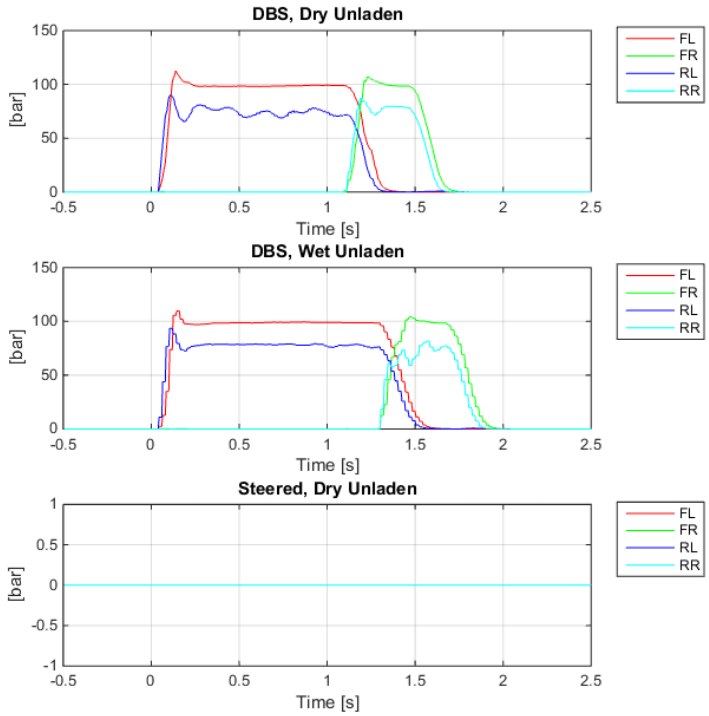

Figure G.28: *Brake pressure comparison*

G.5 1m, 80km/h Avoidance Maneuver

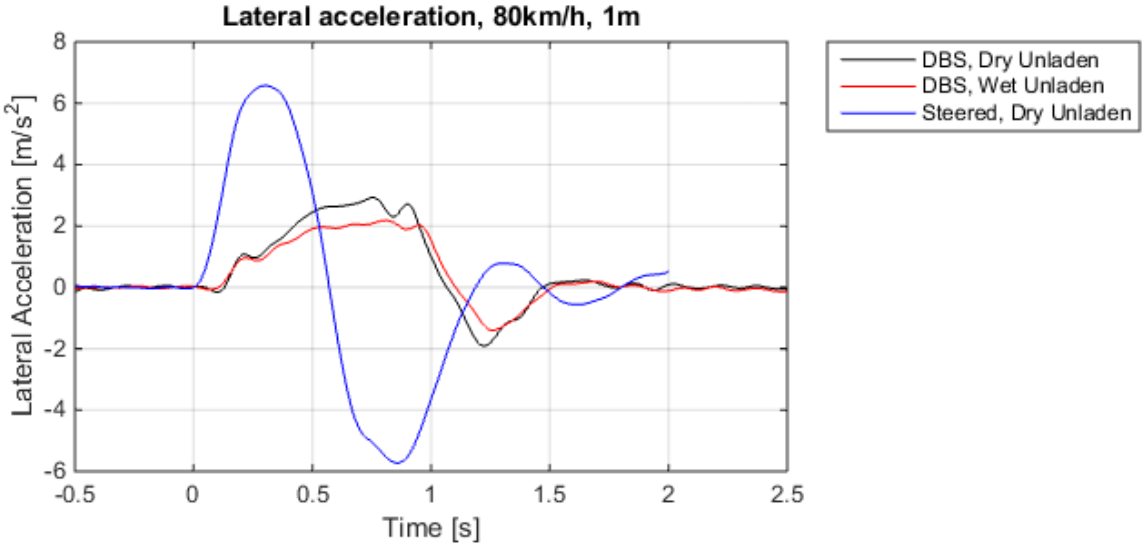

Figure G.29: *Lateral acceleration comparison*

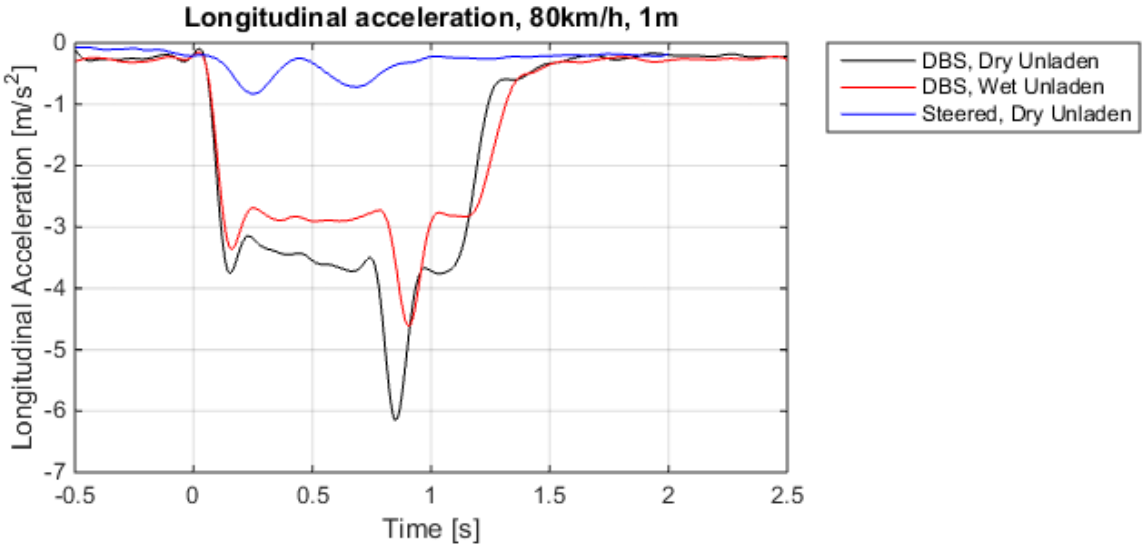

Figure G.30: *Longitudinal acceleration comparison*

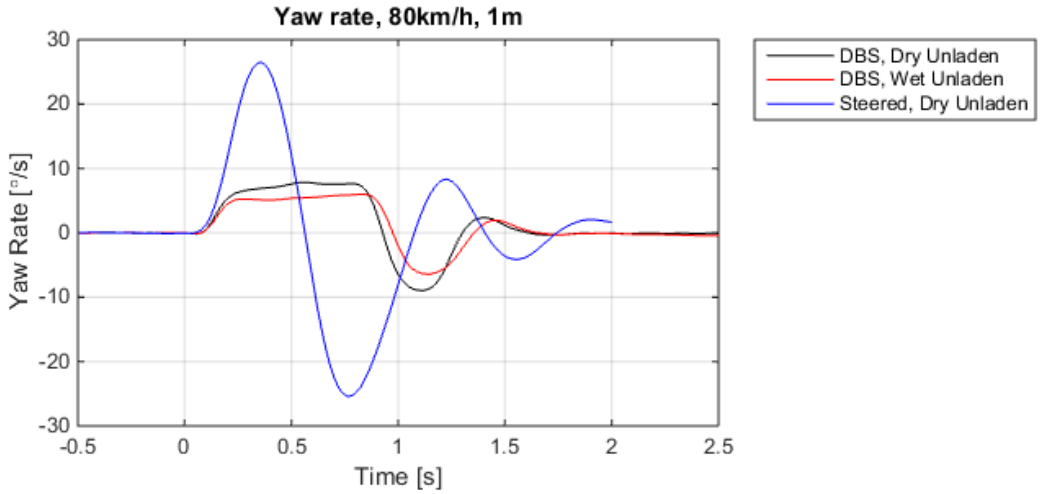

Figure G.31: *Yaw rate comparison*

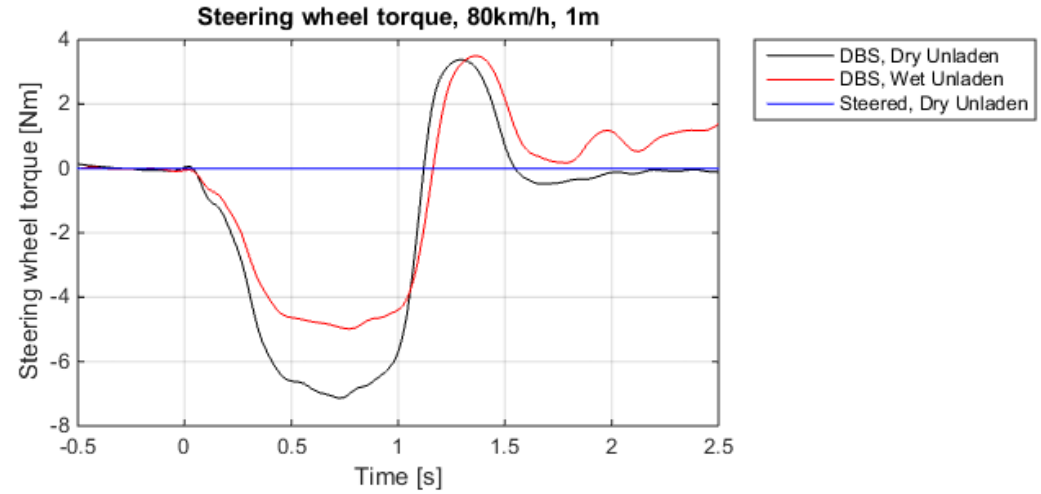

Figure G.32: *Steering wheel torque (steered maneuver not logged)*

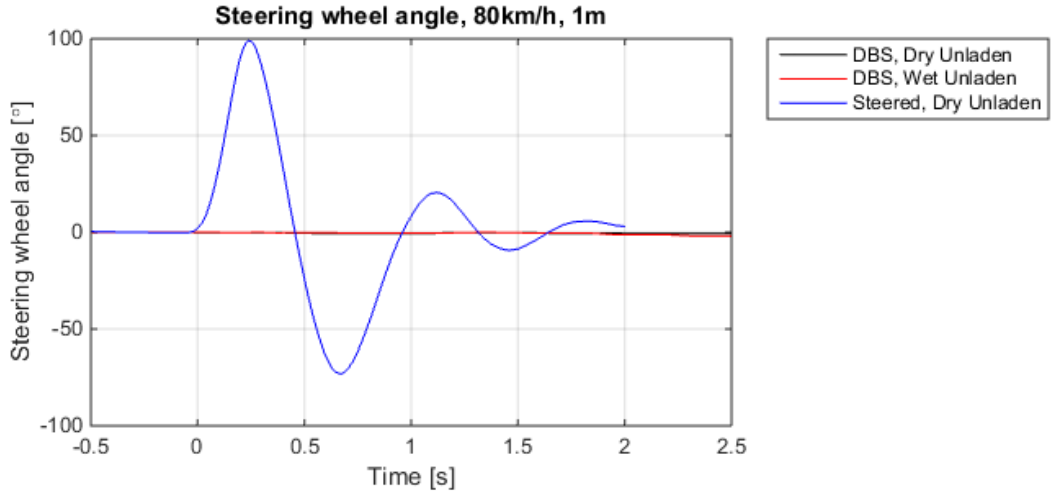

Figure G.33: *Steering wheel angle*

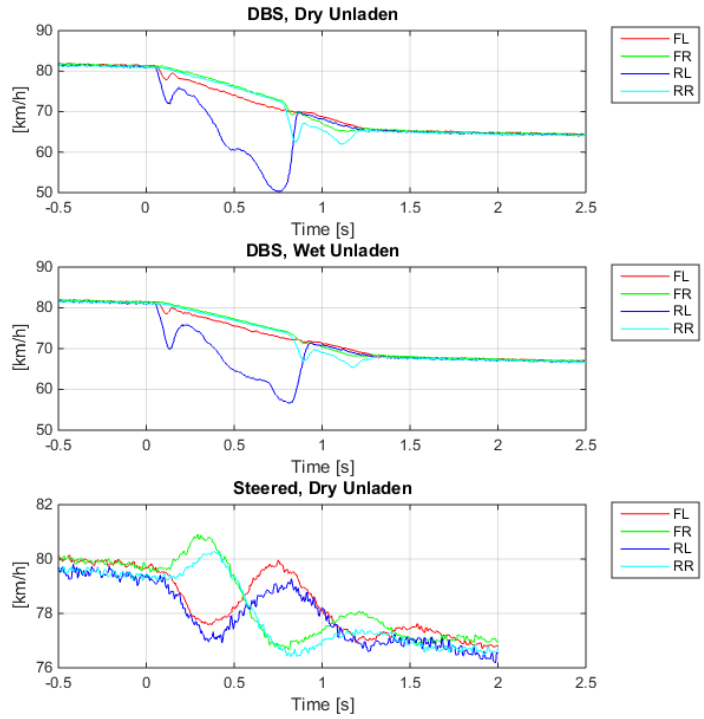

Figure G.34: *Wheel speed comparison*

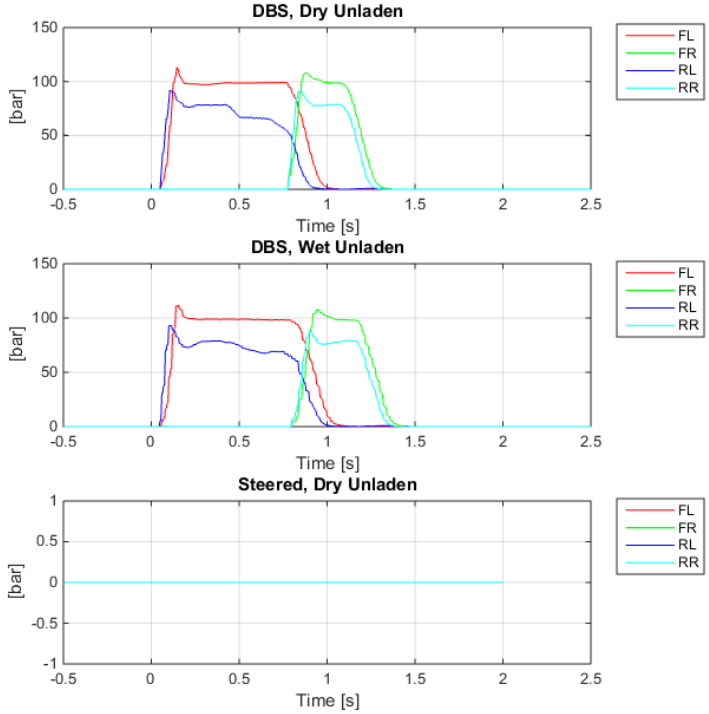

Figure G.35: *Brake pressure comparison*

G.6 1m, 120km/h Avoidance Maneuver

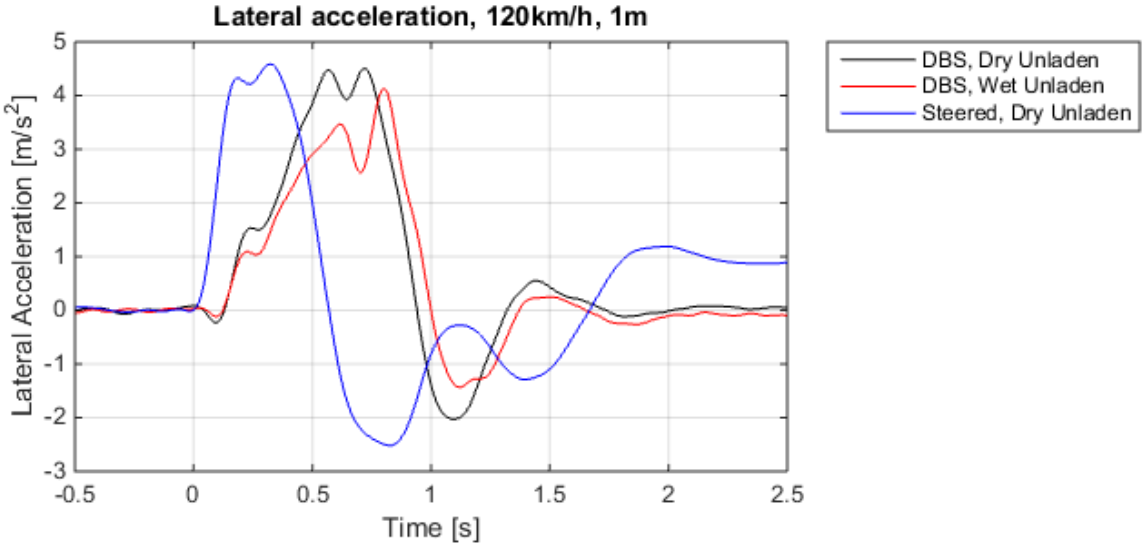

Figure G.36: *Lateral acceleration comparison*

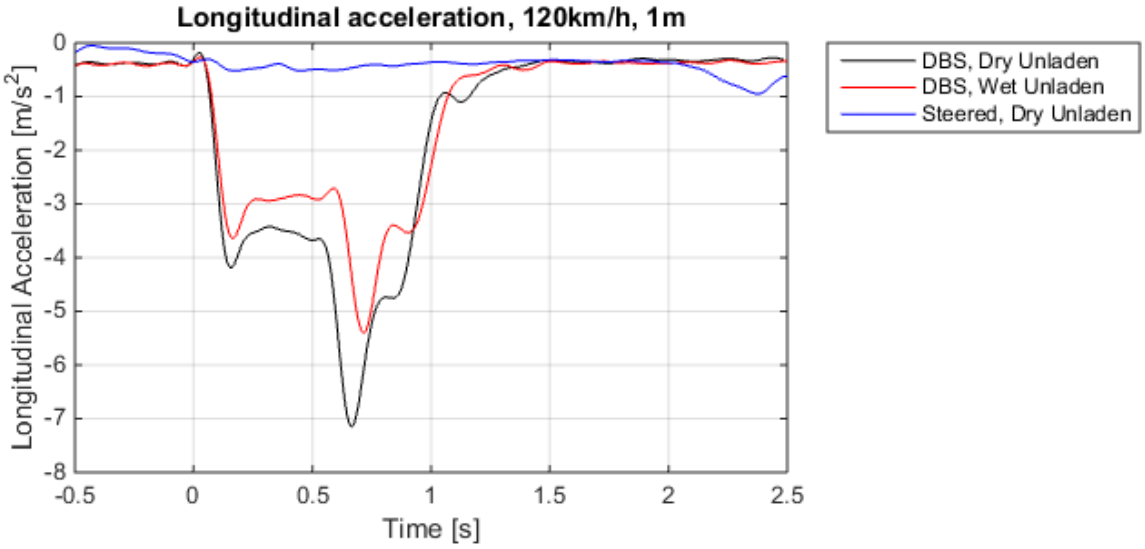

Figure G.37: *Longitudinal acceleration comparison*

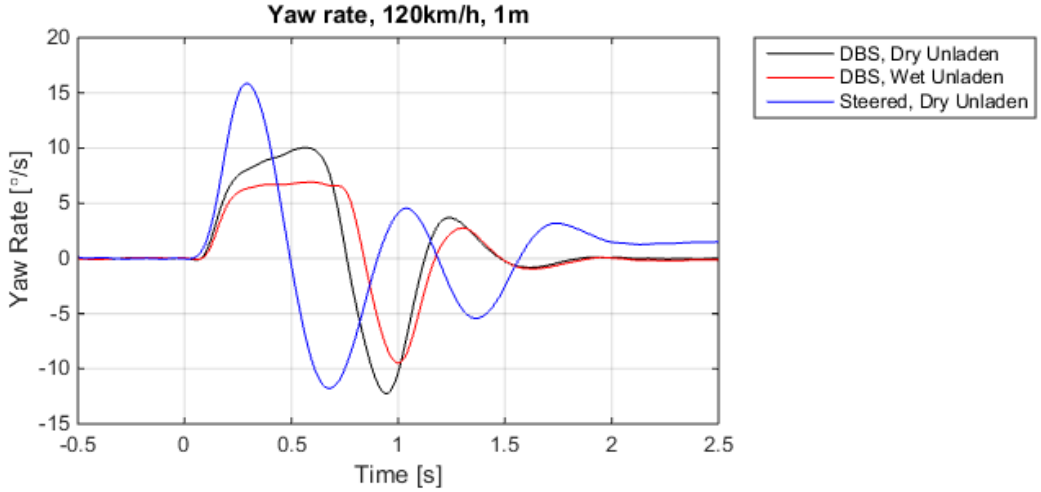

Figure G.38: *Yaw rate comparison*

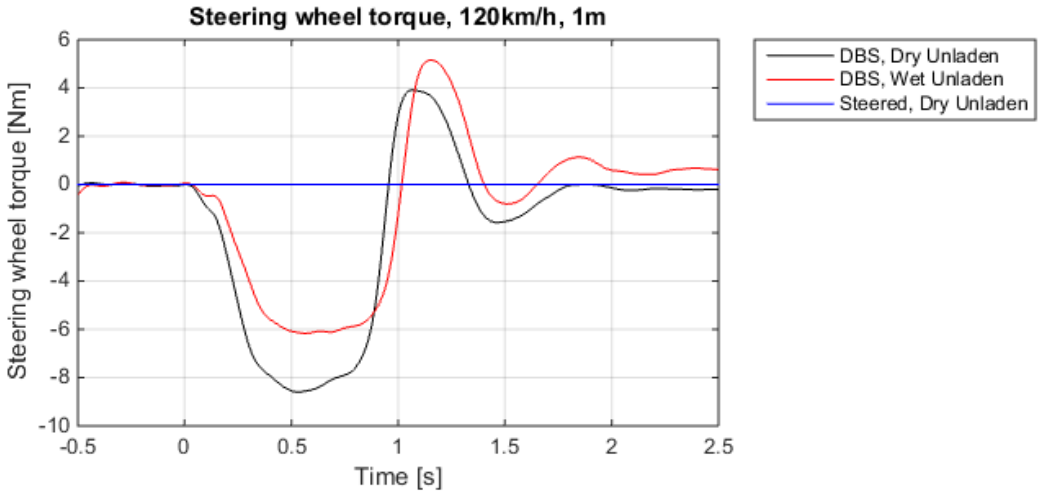

Figure G.39: *Steering wheel torque (steered maneuver not logged)*

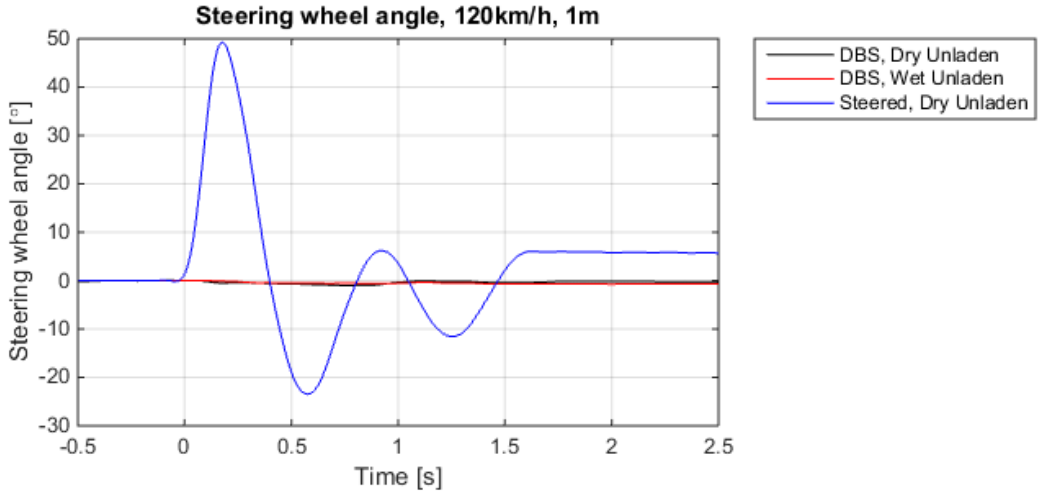

Figure G.40: *Steering wheel angle*

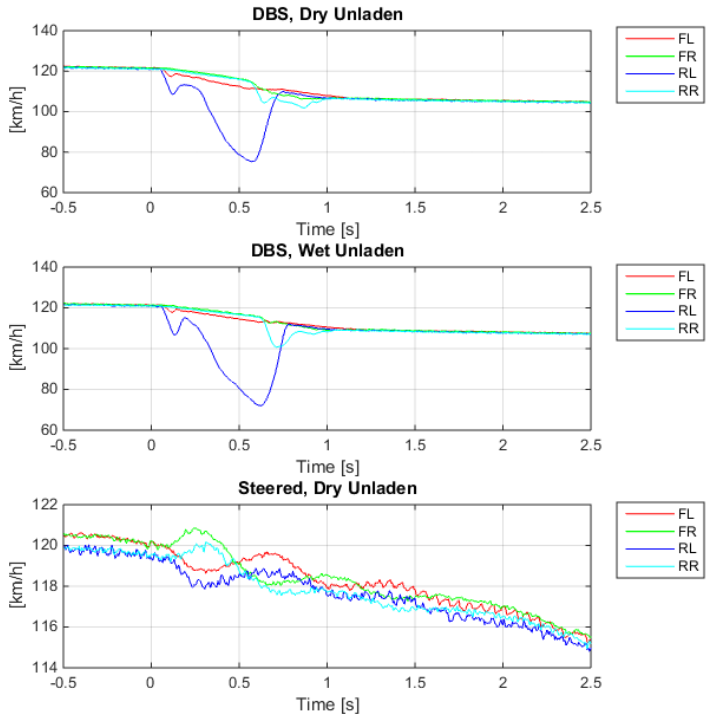

Figure G.41: *Wheel speed comparison between DBS and steered maneuver*

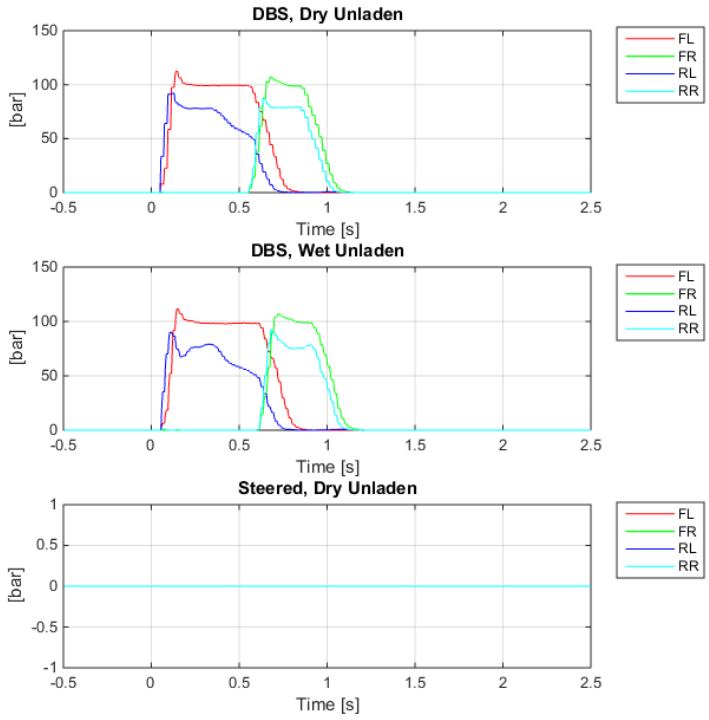

Figure G.42: *Brake pressure comparison between DBS and steered maneuver*

G.7 Step Brake vs. Step Steer Performance Test

A step brake and step steer test was conducted in order to determine the vehicle response from a maximum pressure step brake input compared to a step steer input. The step brake input was applied to the left side wheels at a constant brake pressure of 100bar in the front and 80bar in the rear. The step steer input was a 45° left turn at a rise time of $350°/s$.

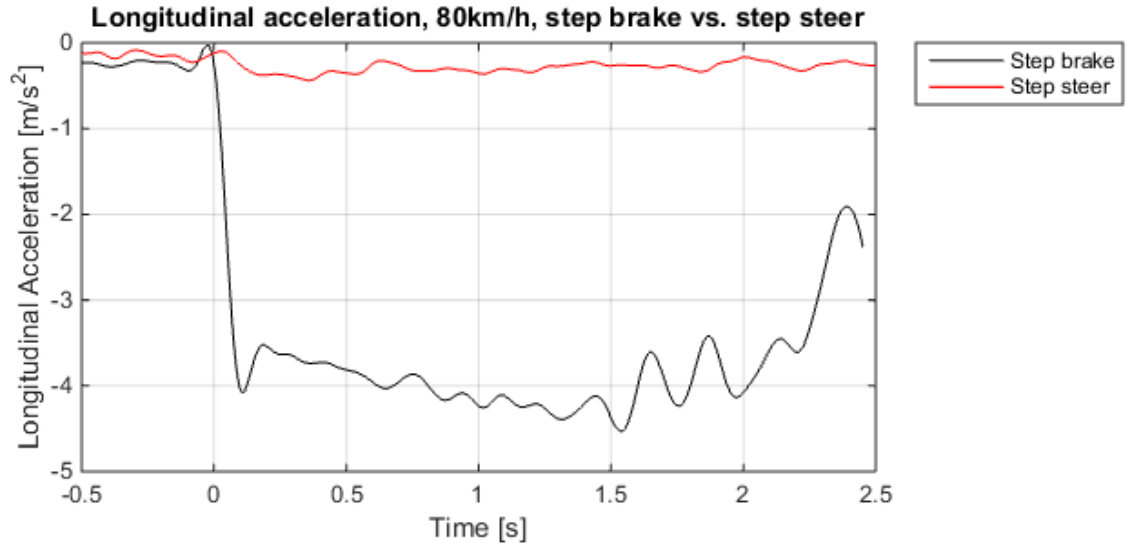

Figure G.43: *Longitudinal acceleration achieved from step brake input on left side wheels vs.* 45° *step steer input*

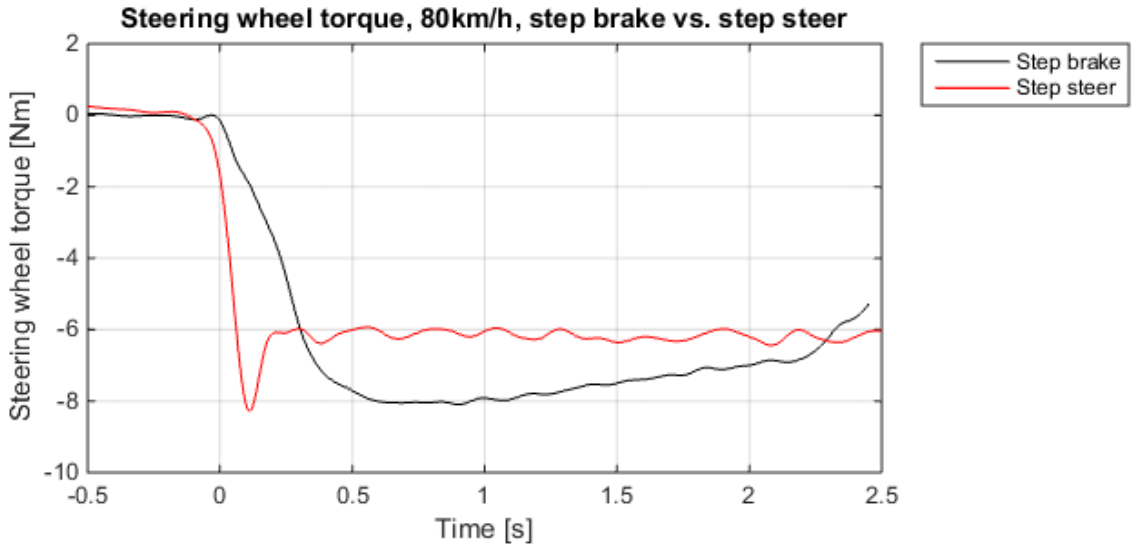

Figure G.44: *Steering wheel torque achieved from step brake input on left side wheels vs.* 45° *step steer input*

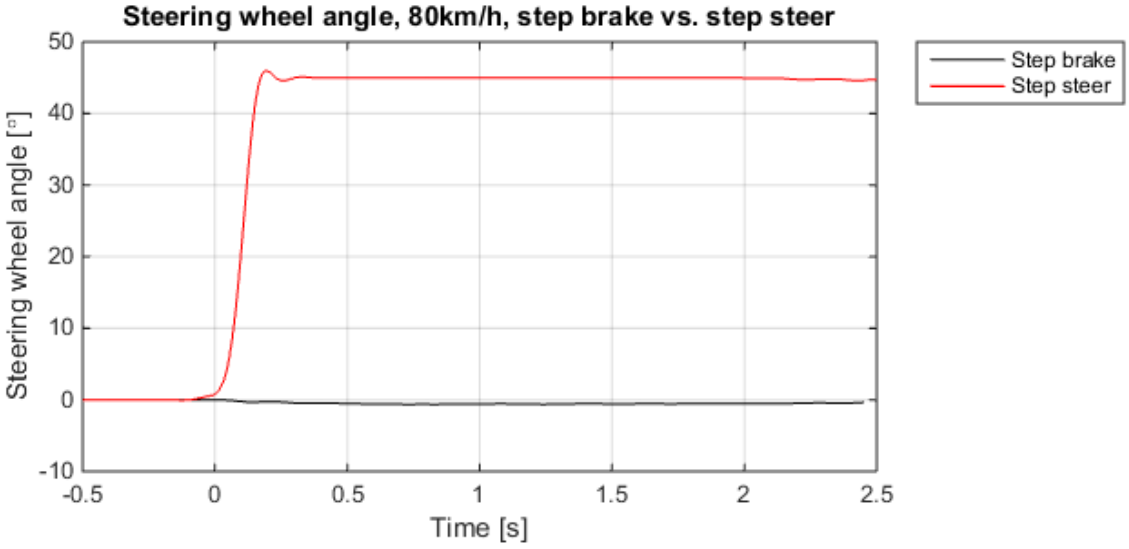

Figure G.45: *Steering wheel angle*

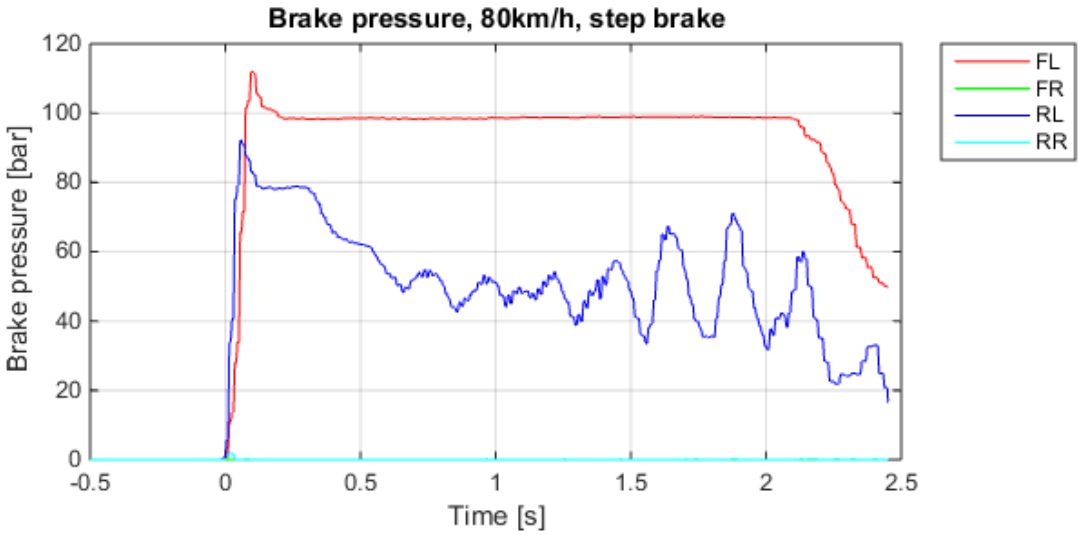

Figure G.46: *Resulting brake pressure from step brake input on left side wheels*

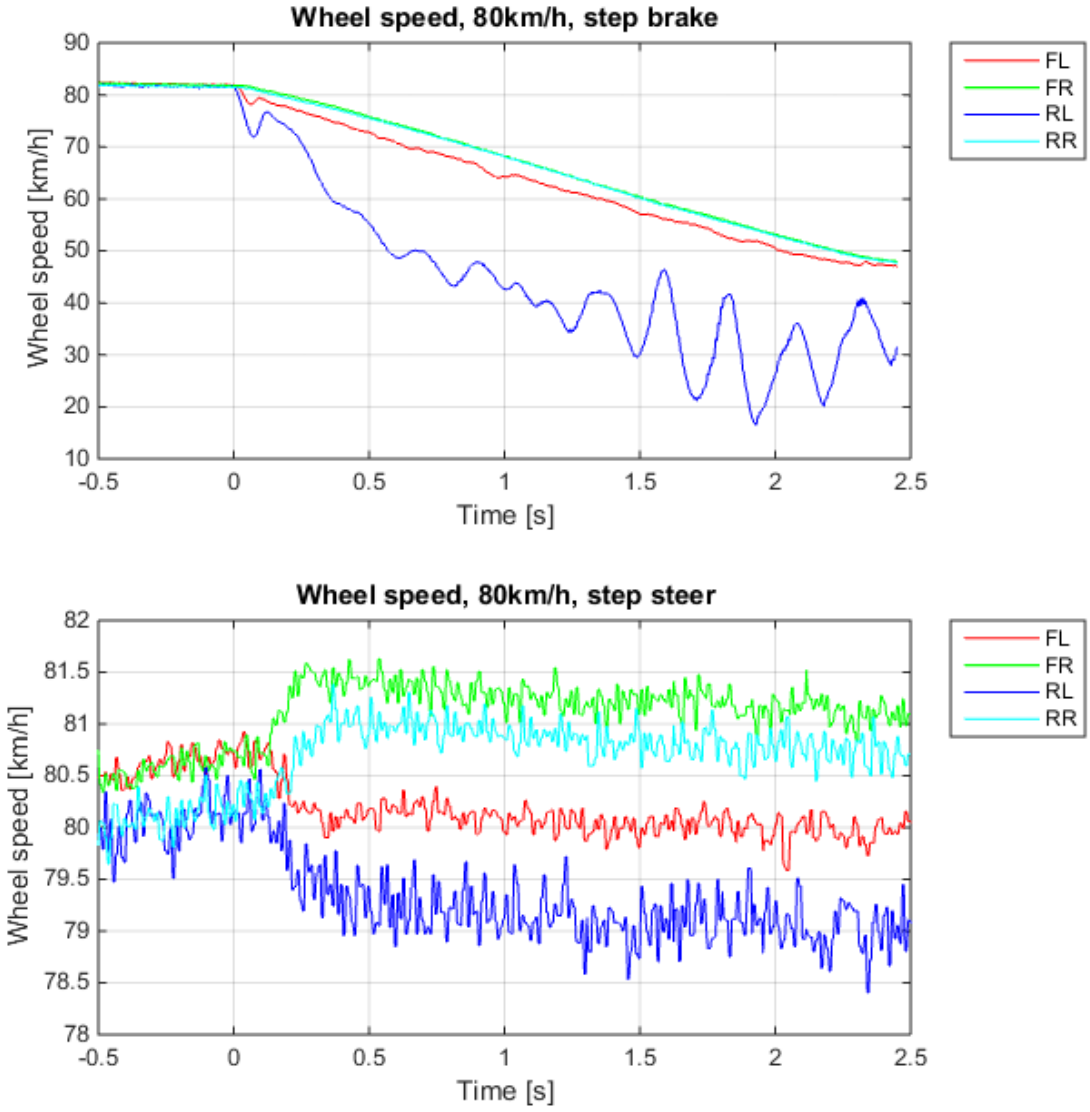

Figure G.47: *Individual wheel speed from step brake input on left side wheels (top) and* 45° *step steer input (bottom)*